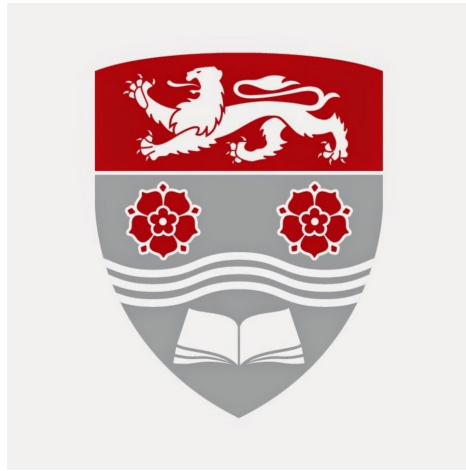


On the Efficiency of Dynamic Licenced Shared Access for 5G/6G Wireless Communications



Samuel Olusayo Onidare

School of Computing and Communications
Lancaster University

A thesis submitted in partial fulfillment for the degree of
Doctor of Philosophy

June 2021

I would like to dedicate this thesis to my loving mum, the most special woman on planet earth . . .

Declaration

I hereby declare that except where specific reference is made to the work of others, the contents of this dissertation are original and have not been submitted in whole or in part for consideration for any other degree or qualification in this, or any other university. This dissertation is my own work and contains nothing which is the outcome of work done in collaboration with others, except as specified in the text and Acknowledgements.

Samuel Olusayo Onidare

June 2021

Acknowledgements

I would like to acknowledge my two supervisors. First of all, I have to express my very deep appreciation to Dr. Keivan Navaie not only for his excellent supervision but also for his all-encompassing support and very genuine care, his guidance, and motivation all through my Ph.D. In my academic journey, you are unparalleled. Secondly, I will like to thank Professor Qiang Ni, for the Ph.D. studentship position. I consider it a great privilege to study at Lancaster University. This would have been impossible if not for the opportunity you gave me.

I would like to express my sincere gratitude to my examiners, Dr. Reza Nakhai and Dr. Richard Jiang. Our interaction was four hours short but very insightful. My sincere thanks also go to the friends I have made here in the School of Computing and Communications (SCC), who in one way or the other have contributed positively to my stay here and the successful completion of my Ph.D.: Ibrahim Ethem Bagci, Yusuf Sani, Hamed Balogun and his family, Marvin Ramokapane and Farid Bello. I will also like to acknowledge Dr. Benachour, Dr. Bran Knowles, and Dr. Ezeani.

I must also express my appreciation to Prof A. A. Ayeni, for his inspiration and mentorship. I also like to acknowledge Mayomi Alege and Olulanu Durosinmi-Etti, you are more than friends to me. Special thanks to a special person, my very good friend of about two decades, Adebimpe Sami Adebajo. More importantly are my two angels, Ire-Oluwa, and Oluwaseteminire Onidare. Although it has not been easy without you for the past five years, I always thank God for the priceless jewel you both are. The last, but not in any way the least, is my sweet Mum. I pray that your sweetness continues to exist for a very very long time to come. My greatest thanks go to the almighty God, to whom I owe every step of this journey from the beginning to the very end.

Abstract

The licensed shared access (LSA) is a spectrum licensing scheme authorizing additional new users (the licensees) to dynamically share the same spectrum with the old users (the incumbents). Contained in the terms of the spectrum usage authorization is a set of strict protective measures for the incumbent system which introduce extra restrictions on the licensee operations. Such measures imply that the licensee's access to the spectrum can be revoked or restricted at any time which may result in the degradation of critical performance metrics of the latter. Addressing this issue and the accompanying challenges as we enter the 5G zettabytes era motivates the research problems addressed in this thesis.

A vertical LSA spectrum sharing involving a mobile network operator (MNO) as the licensee and two categories of incumbent including the aeronautical telemetry, and a group of terrestrial public and ancillary wireless services is adopted in this thesis. Firstly, an analytical examination of the uplink and downlink licensee's transmit power, when its spectrum access right is revoked (i.e., the limited transmit power) is done. Then a power allocation scheme that maximizes the energy efficiency (EE) of the licensee when it is operating with limited transmit power is proposed. Simulation results reveal the impact of the LSA spectrum access revocation on the allowable transmit power of the licensee as a function of the effect of different interference propagation path and the transmission direction. A comparison of the proposed optimal power allocation method with the equal power allocation (EPA) method further shows considerable improvement in the achievable EE of the licensee.

Furthermore, in the LSA, the achievable spectrum efficiency (SE) of the licensee is limited by the interference threshold constraint set by the incumbent's protective measures. Consequent on this, we propose an SE maximization of the licensee's system subject to the incumbent interference threshold constraint. Furthermore, the LSA band spectral utilization was characterised as a function of the licensee's achievable SE and the statistics of the LSA spectrum availability. The obtained results provide quantitative insights for practical system design and deployment of the LSA system, especially when compared to the results obtained in the maximization of the EE. In particular, the effect of variations in critical operational parameters throws up interesting network design trade-off challenge, worthy of consideration. This informs the subsequent multi objective optimization of the EE-SE trade-

off investigated next. Interestingly, the obtained results indicate that with careful selection of the licensee eNodeB coverage radius, transmit power, and number of user equipment per eNodeB coverage area, one can engineer the best possible trade-off between the spectrum and energy efficiency in practical LSA deployment.

A major LSA feature is guaranteeing predictable quality of service (QoS) for both the incumbent and the licensee systems. In terrestrial implementation, the reduction in the achievable data rate caused by the incumbents' protective measures, may violate guaranteed QoS in the licensee system. To address this issue, we propose a LSA - based hybrid aerial-terrestrial system with drone base station (D-BS). Simulation results show that using the proposed scheme, the licensee, when operating under the incumbents' imposed restrictions, is able to achieve the QoS data rate requirements of the users on its network. In conclusion, the findings in this research indicates that the dynamic LSA is a practically viable solution to the spectrum management requirements of the emerging vertical wireless technologies in 5G and beyond.

Table of contents

List of figures	xv
List of tables	xix
Acronyms	xxi
1 Introduction	1
1.1 Research Problem	3
1.2 Research Motivation	5
1.3 Thesis Structure	6
1.4 Contributions	8
1.5 List of Publications	9
2 Licensed Shared Access (LSA) - The Future of Spectrum Access?	11
2.1 The Evolution of the Licensed Shared Access	11
2.1.1 The Dynamic Licensed Shared Access	13
2.1.2 The Evolved Licensed Shared Access (eLSA)	15
2.2 Flexible Spectrum Management With LSA	16
2.2.1 Market Based Auction of LSA Spectrum	17
2.2.2 Game Theory Approach to LSA Spectrum Allocation	18
2.2.3 Fairness Based LSA Spectrum Allocation	19
2.2.4 Ranking Based LSA Spectrum Allocation	20
2.3 Experimental Verification of the LSA Viability	21
2.4 The LSA Service Availability	22
2.5 Challenges and Gaps in the LSA Research	25
2.6 Chapter Summary	27
3 System Model	29
3.1 The Aeronautical Telemetry Incumbent	29

3.1.1	Incumbent's Received Interference	30
3.1.2	The Interference Propagation Path	39
3.1.3	UE Mobility Model	42
3.2	PMSE and PPDR Incumbent	43
3.2.1	Spatial Distribution of UEs	44
3.2.2	Capacity Demand Variation	45
3.3	Chapter Summary	46
3.4	Conclusion	46
4	Spectral - Energy Efficiency and QoS Guarantee in Dynamic Licensed Shared Access	49
4.1	Energy Efficiency Under the Limited Power Regime	49
4.1.1	The Limited Transmit Power	50
4.1.2	The Licensee Energy Efficiency	52
4.1.3	Energy Efficient Limited Power Allocation	53
4.2	Spectral Efficiency of Dynamic Licensed Shared Access	57
4.2.1	Licensee System Spectrum Efficiency	58
4.2.2	Maximizing the Licensee Spectrum Efficiency	58
4.2.3	Efficiency of Spectrum Utilization Under LSA	63
4.3	The Energy and Spectrum Efficiency of the Dynamic LSA	66
4.3.1	Interference Threshold	67
4.3.2	Energy and Spectrum Efficiency	68
4.3.3	SE-EE Trade-off Optimal Power Allocation	68
4.4	Quality of Service Guarantee in Drone Assisted LSA	72
4.4.1	Dynamic D-BS Positioning	73
4.5	Chapter Summary	75
4.6	Conclusion	78
5	Implementation Set-up.	81
5.1	The Licensee Network	81
5.1.1	UE Distributions in a Circular eNodeB Coverage Area	81
5.1.2	The Propagation Paths	82
5.1.3	Evaluation of the Proposed Methods for Licensee Optimal Efficiency	83
5.1.4	Drone BS Simulation, Assumptions and Justifications	84
5.1.5	QoS Provisioning in Aerial-LSA	85
5.2	Incumbent's Interference Threshold Measurement	86

6	Results Analysis and Discussions	87
6.1	Energy Efficiency of the Dynamic LSA Under Limited Power	87
6.1.1	Effect of Spectrum Access Revocation on Transmit Power	89
6.1.2	Impact of Different UE Propagation Paths	90
6.1.3	Performance Evaluation of the Proposed Method	90
6.1.4	Summary of Results	98
6.2	Spectra Efficiency Results and Analysis	98
6.2.1	Efficiency of the LSA Spectrum Utilization	101
6.2.2	Summary of Results	106
6.3	EE-SE Optimization- Results Discussion and Analysis	108
6.3.1	Effect of Importance Weight on the EE-SE Trade-Off	112
6.3.2	Effect of Circuit Power on the EE-SE Trade-Off	115
6.3.3	Summary of Results	119
6.4	Drone-BS Assisted LSA Simulation Results	121
6.4.1	Summary of Results	130
6.5	Chapter Summary	131
6.6	Conclusion	132
7	Conclusion and Future Work	133
7.1	Summary of the Thesis	133
7.2	Future Work	138
	References	143

List of figures

1.1	The United States Spectrum allocation Chart (2016) [1]	2
2.1	The LSA Architecture and Sharing Framework [2]	12
2.2	The Functional Blocks of the ADEL Dynamic LSA Architecture. [3]	14
2.3	The schematic of LSA spectrum availability state space.	23
2.4	The schematic of service unavailability in LSA [4].	24
3.1	A schematic of the considered system: Incumbent’s transmission shadow only crosses licensee cell C, while cells A, B, D, and E are outside the transmission shadow.	31
3.2	A schematic of the considered aerial-terrestrial LSA system.	44
5.1	UE in the eNodeB coverage area.	83
6.1	Downlink and uplink limit power, interference power, and power differential for selected values of P_{\max}	89
6.2	Upper and Lower bounds for the Uplink limit power, interference, and power differential.	91
6.3	Downlink EE vs. transmit power.	92
6.4	Uplink EE vs. transmit power.	92
6.5	Uplink EE vs. transmit power for limited and maximum power.	94
6.6	EE vs. maximum transmit power for the optimal limited power, EPA and maximum power spectrum in the downlink.	94
6.7	Effect of eNodeB coverage radius on the EE gain by the proposed method. .	95
6.8	Downlink interference and P_{Δ} for different radius.	96
6.9	Effect of circuit power on the EE gain by the proposed method.	97
6.10	Comparison of the SE in optimized and the non-optimized systems vs. total transmit power.	100
6.11	Downlink SE gain vs. transmit power.	101

6.12	Downlink SE gain vs. transmit power for various eNodeB radius and number of users.	102
6.13	Uplink SE gain vs. transmit power for various number of users, where $R = 250$ m.	102
6.14	Downlink Interference power for different eNodeB.	104
6.15	BP ratio, v_q , for different eNodeB.	105
6.16	Uplink SE, interference power and v_q for eNodeBs across different separation distance.	106
6.17	Uplink interference to ATC tower.	107
6.18	SE, EE, and the Trade-off curves.	109
6.19	Effect of UE movement on the SE, EE, and the Trade-off curves.	109
6.20	Effect of I_{th} on EE vs. Transmit power for different user number.	110
6.21	Effect of I_{th} on SE vs. Transmit power for different user number.	110
6.22	Effect of I_{th} on EE vs. Transmit power for different eNodeB coverage radius.	111
6.23	Effect of I_{th} on SE vs. Transmit power for different eNodeB coverage radius.	112
6.24	Effect of w on SE-EE Trade-off vs. Transmit power for different user number.	113
6.25	Effect of w on SE-EE Trade-off vs. Transmit power for different eNodeB coverage radius.	114
6.26	Comparison of free and idle spectrum SE vs. Transmit power at different values of w	114
6.27	Comparison of free and idle spectrum EE vs. Transmit power at different values of w	116
6.28	Effect of different values of P_c on the trade-off function at different w	117
6.29	Effect of P_c on the trade-off function for different user number.	117
6.30	Effect of P_c on the trade-off function for different radius.	118
6.31	Comparison of free and idle spectrum SE vs. Transmit power at different values of P_c	118
6.32	Comparison of free and idle spectrum EE vs. Transmit power at different values of P_c	119
6.33	EE vs. SE for different P_c and users number.	120
6.34	LSA Drone-BS positioning in the idle incumbent mode.	122
6.35	Incumbent received interference vs. transmit power.	122
6.36	LSA Drone-BS positioning in the active incumbent mode.	123
6.37	Original UE distribution between the aerial-BS and terrestrial eNodeB.	124
6.38	Spatial spectral efficiency in the active incumbent mode.	124
6.39	EE vs. transmit power.	125

6.40	Variation in mark distribution in the idle incumbent mode.	126
6.41	Target and achieved data rate in the active incumbent mode.	127
6.42	ASE for different $Z(V)$ in idle incumbent mode.	127
6.43	Spatial spectral and energy efficiency for different $Z(V)$ in active incumbent mode.	128
6.44	Different incumbent position in the coverage area.	129
6.45	Achievement level of surplus capacity requirement at different incumbent's position.	130

List of tables

3.1	List of Parameters.	32
3.2	List of Parameters Continues	33
3.3	Parameters for $\Pr\{\text{LoS}, \theta\}$ in (3.26) [5].	40
5.1	Computation of Incumbent's I_{th}	86
6.1	Simulation Parameters for the LSA EE.	88
6.2	SE Simulation Parameters.	99
6.3	Simulation Parameters for the EE-SE Trade-Off.	108
6.4	D-BS LSA Simulation Parameters.	121

Acronyms

3GPP	3rd Generation Partnership Project
4G	Fourth Generation
5G	Fifth Generation
ASA	Authorised Shared Access
ATC	Air Traffic Control
ATG	Air- to -Ground channel
CAGR	Compound Annual Growth Rate
CO ₂ e	Carbon Dioxide equivalent
CR	Cognitive Radio
CSI	Channel State Information
DSA	Dynamic Spectrum Access
DSS	Dynamic Spectrum Sharing
ECC	European Communication Commission
EE	Energy Efficiency
EIRP	Effective Isotropic Radiated Power
ETSI	European Telecommunications Standards Institute
EU-RSPG	European Union Radio Spectrum Policy Group
FDD	Frequency Division Duplexing

GHG	Greenhouse Gas
ICT	Information and Communication Technology
ITU-R	International Telecommunication Union- Radiocommunication sector
KKT	Karush-Kuhn- Tucker
LHQWN	Local High Quality Wireless Networks
LoS	Line of Sight
LSA	Licensed Shared Access
LTE	Long Term Evolution
MINLP	Mixed Integer Non-Linear Problem
MNO	Mobile Network Operator
MOP	Multi-objective Optimization Problem
NLoS	Non-Line of Sight
NOMA	Non Orthogonal Multiple Access
NRA	National Regulatory Authority
NTIA	National Telecommunication and Information Administration
Ofcom	Office of Communications
PMSE	Programme Making and Special Events
PPDR	Public Protection and Disaster Relief
QoS	Quality of Service
RAN	Radio Access Network
REM	Radio Environment Map
RF	Radio Frequency
SE	Spectrum Efficiency
SINR	Signal -to- Noise and Interference Ratio

SNR Signal -to- Noise Ratio

TDD Time Division Duplexing

UE User Equipment

WCDMA Wideband Code Division Multiple Access

Chapter 1

Introduction

Ever since the invention of wireless communication, sufficient availability of the radio spectrum has been a recurrent challenge. This has been largely driven by the appeal of the wireless communication that has accounted for the unexpectedly high rate of its growth. In fact, the growth rate of global broadband traffic over the last decade has consistently exceeded the hitherto high expectations. For example the mobile data growth rate (excluding fixed wireless access) was forecasted to be thirty nine percent compound annual growth rate (39% CAGR) between the year 2017 and 2023 [6]. However, in reality, the same report shows that the actual growth between the first quarter of 2017 and 2018 was actually 54% CAGR while [7] shows an even higher rate of 79% between the third quarter of 2017 and 2018.

Historical fragmentation of the spectrum has come handy in addressing this ever increasing spectrum need of the wireless communication technology. However, in recent times, it has been observed that practically all usable portion of the sub-6 GHz radio spectrum has been allocated to one wireless service or application (Fig. 1.1). Conversely, the need for more spectrum keeps growing and it is even expected to grow more as the predominant services of the 5G technology space take centre stage of wireless mobile communication [6, 8].

In spite of the above mentioned realities, researches have established that a substantial portion of the radio spectrum is grossly under-utilized by the respective systems licensed to use them [9]. Several spectrum occupancy measurements conducted around the world testify to the under-utilization level of various portion of the radio spectrum [10–12]. This is due to the exclusivity of usage right granted to spectrum license holder under the traditional approach of frequency assignment. This inadequacy of the static spectrum allocation coupled with the challenges posed by the ever increasing demand for wireless broadband services led to a new paradigm in spectrum access, dynamic spectrum sharing/access (DSS/DSA).

DSS/DSA schemes are geared towards increasing the efficiency of spectrum utilization by ensuring that the unused portion (whether spatial or temporal) of the spectrum are dynamically

UNITED STATES FREQUENCY ALLOCATIONS

THE RADIO SPECTRUM

RADIO SERVICES COLOR LEGEND

■ AERIAL TELEVISION	■ AIR SERVICE	■ AIRSOUNDING
■ AERIAL TELEVISION SATELLITE	■ AIR SERVICE SATELLITE	■ AIRSOUNDING SATELLITE
■ AERIAL TELEVISION SATELLITE	■ AIR SERVICE SATELLITE	■ AIRSOUNDING SATELLITE
■ AERIAL TELEVISION SATELLITE	■ AIR SERVICE SATELLITE	■ AIRSOUNDING SATELLITE
■ AERIAL TELEVISION SATELLITE	■ AIR SERVICE SATELLITE	■ AIRSOUNDING SATELLITE
■ AERIAL TELEVISION SATELLITE	■ AIR SERVICE SATELLITE	■ AIRSOUNDING SATELLITE
■ AERIAL TELEVISION SATELLITE	■ AIR SERVICE SATELLITE	■ AIRSOUNDING SATELLITE
■ AERIAL TELEVISION SATELLITE	■ AIR SERVICE SATELLITE	■ AIRSOUNDING SATELLITE
■ AERIAL TELEVISION SATELLITE	■ AIR SERVICE SATELLITE	■ AIRSOUNDING SATELLITE
■ AERIAL TELEVISION SATELLITE	■ AIR SERVICE SATELLITE	■ AIRSOUNDING SATELLITE
■ AERIAL TELEVISION SATELLITE	■ AIR SERVICE SATELLITE	■ AIRSOUNDING SATELLITE
■ AERIAL TELEVISION SATELLITE	■ AIR SERVICE SATELLITE	■ AIRSOUNDING SATELLITE
■ AERIAL TELEVISION SATELLITE	■ AIR SERVICE SATELLITE	■ AIRSOUNDING SATELLITE
■ AERIAL TELEVISION SATELLITE	■ AIR SERVICE SATELLITE	■ AIRSOUNDING SATELLITE
■ AERIAL TELEVISION SATELLITE	■ AIR SERVICE SATELLITE	■ AIRSOUNDING SATELLITE
■ AERIAL TELEVISION SATELLITE	■ AIR SERVICE SATELLITE	■ AIRSOUNDING SATELLITE
■ AERIAL TELEVISION SATELLITE	■ AIR SERVICE SATELLITE	■ AIRSOUNDING SATELLITE
■ AERIAL TELEVISION SATELLITE	■ AIR SERVICE SATELLITE	■ AIRSOUNDING SATELLITE
■ AERIAL TELEVISION SATELLITE	■ AIR SERVICE SATELLITE	■ AIRSOUNDING SATELLITE
■ AERIAL TELEVISION SATELLITE	■ AIR SERVICE SATELLITE	■ AIRSOUNDING SATELLITE
■ AERIAL TELEVISION SATELLITE	■ AIR SERVICE SATELLITE	■ AIRSOUNDING SATELLITE

ACTIVITY CODE

■ EXCLUSIVE USE	■ EXCLUSIVE USE
■ EXCLUSIVE USE	■ EXCLUSIVE USE

ALLOCATION USAGE DESIGNATION

■ PRIMARY	■ SECONDARY	■ SHARED
■ PRIMARY	■ SECONDARY	■ SHARED
■ PRIMARY	■ SECONDARY	■ SHARED
■ PRIMARY	■ SECONDARY	■ SHARED
■ PRIMARY	■ SECONDARY	■ SHARED
■ PRIMARY	■ SECONDARY	■ SHARED
■ PRIMARY	■ SECONDARY	■ SHARED
■ PRIMARY	■ SECONDARY	■ SHARED
■ PRIMARY	■ SECONDARY	■ SHARED
■ PRIMARY	■ SECONDARY	■ SHARED

U.S. DEPARTMENT OF COMMERCE
NATIONAL TELECOMMUNICATIONS AND INFORMATION ADMINISTRATION
 October 2016

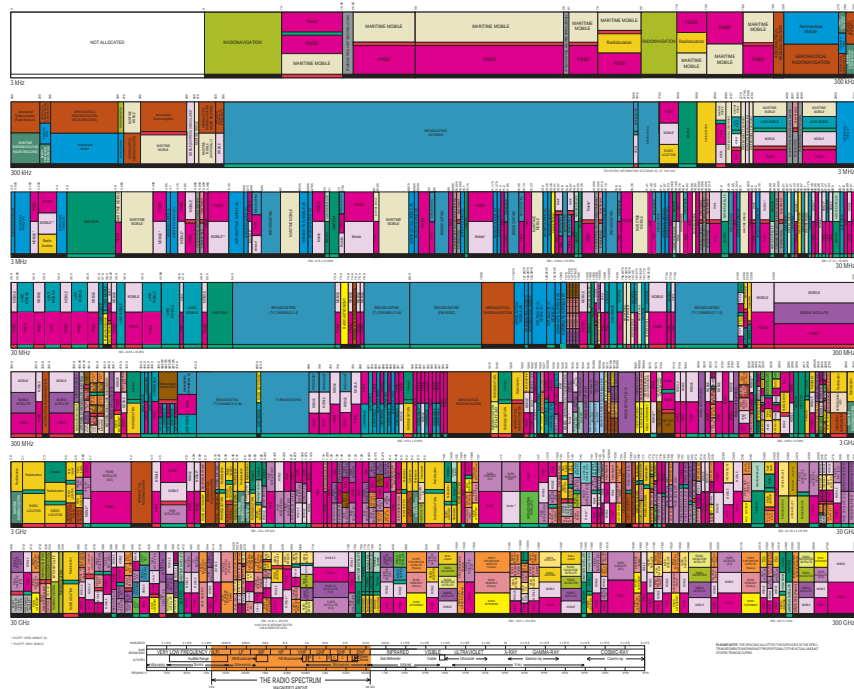


Fig. 1.1 The United States Spectrum allocation Chart (2016) [1]

accessed by other users apart from the original, hitherto exclusive, owners. Cognitive radio (CR) was one of the early candidate technology proposed for DSS. Under the CR DSS scheme, an unlicensed secondary user takes advantage of the unused portion of the spectrum (otherwise known as spectrum holes or white spaces) by the primary user or licensed owner in either time or space domain, provided the operation of the primary user is not adversely affected. There are however, a couple of limitations and challenges that plague the CR driven spectrum sharing network.

Firstly, the opportunistic nature of the CR technology has a major drawback on the different players on the two divide of the DSS scheme [2]. For the quality of service (QoS) of the primary network (the original exclusive owner of the spectrum) to be guaranteed, the interference protection margin must be excessively provided for. This could lead to spectra inefficiency and sub-optimal spectrum utilization, problems that DSS is meant to address. More importantly, due to the uncertainty and randomness in the dynamism of the spectrum availability, the secondary network (the opportunistic CR driven user, taking advantage of the holes in the primary spectrum utilization) cannot provide guaranteed QoS for the users of its network.

Secondly, to prevent harmful interference from secondary user to the primary user, a critical technology for the operation of cognitive radio is RF sensing. In the TV white space

technology trial conducted in the USA, it was categorically stated that there were doubts on the ability of sensing to protect primary systems from harmful interference [13]. Similarly, Ofcom in the UK noted that the granularity of sensing needed to prevent harmful interference could be expensive or not achievable [13]. Beacon transmission, another technology for protecting primary systems from harmful interference, has been noted for its prohibitive infrastructural cost and inefficient transmission within the permitted spectrum [13]. Although the geo-location database technique seems not to be plagued with the challenges of the other two techniques, the CR driven DSS, still exists on opportunistic spectrum access for the secondary users.

1.1 Research Problem

Today, every discussion in virtually all spheres of human lives and endeavours is centred on the sustainability paradigm. As a result, terms such as, environment friendly, green technologies, conservation biology, renewable energy, ecovillages, eco-municipalities, green building, and green computing are common place. In conformity with the global trend, the fifth generation (5G) wireless communications system can be appropriately termed the green communication generation (GCG). In fact, a key requirement of 5G includes, a hundred times (100x) energy efficiency (EE) more than the fourth generation (4G) wireless communication standard [14, 15]. In the light of the existing facts and figures this requirement is not just a performance improvement/enhancement issue but a necessity.

Recent studies show that the energy consumption of the information and communication technology (ICT) sector is on the increase [16, 17]. As a result of this the projected carbon dioxide equivalent (CO₂e) emission, when combined with those of non-ICT has resulted in a faster than expected growth of greenhouse gas (GHG) emission [18]. For example, the study in [16] revealed that the ICT sector alone consumed 670 Terra Watt-hour (TWh) in 2007, and about 930 TWh in 2012, an average of 6.6% annual increase in the energy consumption. At this rate, the fraction of ICT to the global energy consumption was projected to increase from 8% in 2008 to 14% in 2020 [17]. This corresponds to an estimated 1.43 billion tonnes (Gt) carbon dioxide equivalent (CO₂e) emissions in 2020, up from 0.53 GtCO₂e in 2002.

Apart from the global warming concerns, continual growth of GHG emission, if unchecked is a threat to the global economy. It was estimated that 5⁰C of global warming is equivalent to a reduction of welfare by approximately 5% of global GDP [19]. Not to be discounted is the implication of increased energy consumption on the operating expenditure of ICT service providers. Furthermore, the improvement in battery power, has been found to be at a significant lower rate to the increase in energy consumption of ICT systems especially the

wireless mobile broadband devices. The projected improvement in battery power put at five to ten percent (5 – 10%) CAGR is significantly lower than expected growth rate of energy consumption in microprocessors[20].

These challenges are further exacerbated by the direct relationship between energy consumption and the expected exponential growth in the demand and services accompanying the improvement of the wireless broadband technology. Reports show that the growth rate of global broadband traffic over the last decade has consistently increased [6, 7]. Furthermore, since 5G is also expected to facilitate a more diverse set of services, higher user density (about 1 million devices/km²) with significantly higher data rates (about 100× user experienced data rate) more than the 4G [14], it is evident that the trend in global broadband traffic will continue. In fact, the global mobile traffic is forecasted to grow ten -to- one hundred times (10 – 100×) from 2020 to 2030 [8]. Similarly, [21] forecasted the annual global IP traffic to reach 3.3 Zettabytes by the year 2021. These and the key requirement of, three times (3×) spectrum efficiency (SE)[14, 15], of the 5G, implies that researches in SE and EE optimization will continue to be a main part of the discussion in the foreseeable future.

The implication of the expected continuous exponential growth in wireless traffic, is a corresponding increase in bandwidth requirements of the 5G networks. The radio spectrum, the resource to meet this increased bandwidth requirement is finite and does not grow in the same manner. Although it could be argued that with the advent of millimeter-waves and tetra hertz frequency communication, the apparent spectrum shortage of the sub -6 GHz is more than adequately compensated for, yet the need for more spectrum in the sub -6 GHz frequency range still persist for several reasons. Chief among those, is the significantly greater attenuation of these higher frequency wireless communication systems which makes them less suitable at large distances [22]. As a direct consequence of this, there are other challenges [22–27] which suggests that communication in the sub -6GHz will still be an important player in the 5G technology space in the foreseeable future.

In the light of the above mentioned reasons, it became necessary to provide spectrum access in the microwave bands, to meet the SE and EE requirements of 5G and bandwidth demands resulting from the continuous explosive growth of mobile traffic. As mentioned earlier, because of the traditional static allocation of frequency, current bandwidth demands is already stretching the spectrum in the sub -6 GHz to its limit. It thus become imperative to leverage on the alternatives provided by DSS schemes in order to meet the 5G goals and future needs. However, the CR driven opportunistic DSS is riddled with challenges such as lack of QoS guarantee, reliable RF sensing viability and the high infrastructural cost of beacon transmission, amongst others [13]. Furthermore, the lack of co-ordination between

the different parties sharing the spectrum also makes its practicability in the 5G space a daunting challenge.

1.2 Research Motivation

The opportunistic nature of the CR DSS implies, the secondary network has no access authorization to the primary spectrum, hence it can't offer its users a guaranteed or predictable QoS. For the emerging generation of network, the 5G, this pose a major challenge in meeting the design standards. Inspired by this and the challenges mentioned earlier, licensed shared access (LSA) was developed as a spectrum sharing scheme under a licensing regime [2]. LSA, the regulatory spectrum sharing scheme is a coordinated arrangement with rights of spectrum access, hence predictable QoS for all parties, and interference protection for the initial owner of the spectrum [28].

Different experimental trials [29–37] has demonstrated the practical viability of the LSA as well as confirmed the encouraging results of compatibility studies in [28, 38]. Despite that, the non-availability of the LSA spectrum, where and when, the original license holder is active on its spectrum, poses significant threat to guaranteed and predictable QoS, spectrum and energy efficiency (SE and EE) for the new spectrum sharers, and the overall spectrum utilization efficiency. As a matter of fact, researches have established that the non-availability of the LSA spectrum results in a significant spatial spectrum hole [39, 40, 38]. To address this, the dynamic form of the LSA was proposed in the form of imposition of certain restrictions rather than total suspension of the new sharers transmission when the spectrum becomes non-available. Nevertheless, it has been reported in the literature that this results in a significant reduction in the new user's achievable data rate [41].

Motivated by these, as well as the key 5G goals of $100\times$ users' experienced data rate and EE [14], this research aims to explore how to model the operation of the LSA during the period of the LSA's spectrum non-availability for 5G compliant EE-SE performance. This is more so considering the fact that, the 'LTEband 40', initially designated for LSA operation by the European union regulatory body [28] is utilised by systems of critical national importance such as the aeronautic telemetry and public safety systems. Achieving optimal SE and EE and guaranteed QoS for the new users of the LSA spectrum is at the risk of radiating harmful interference into these safety critical systems. On one hand, in order to achieve spectral-energy efficient 5G complaint spectrum utilization, we aim to maximise the achievable EE and SE of the LSA new sharers when the spectrum is not available. On the other hand, in the design of such LSA system, there is the challenge of ensuring that interference threshold of critical safety systems is not exceeded.

In the light of the exceedingly high data demand of the 5G, the resulting reduced achievable data rate when the spectrum is not available poses a great risk to achieving guaranteed QoS for the new users of the LSA band. This is not a desirable outcome because, a main feature of the LSA is the advantage of QoS guarantee it has over opportunistic cognitive radio network. To this end, this research work aim to investigate and explore the possibility of leveraging on the agility and mobility of the drone or unmanned aerial vehicle assisted wireless communication to compensate for the expected data rate reduction and achieve optimal QoS guarantee.

1.3 Thesis Structure

The research work presented in this thesis focusses on the 2.3 GHz -2.4 GHz or the ‘LTE band 40’ as it is called by the 3rd Generation Partnership Project (3GPP). The thesis is organised into six different chapters as highlighted below.

Following this chapter, **Chapter 2**, will provide a detailed description of the licensed shared access framework as a regulatory paradigm shift to ensure more efficient utilization of the ‘scarce sub -6 GHz radio spectrum’. The chapter will discuss the motivation behind the LSA initiative and how it progressively evolved in response to the demand of emerging mobile broadband network. The various flexibility options for spectrum management that the LSA offers as against the traditional static spectrum assignment is also explained from both the technical point and the regulatory or administrative perspective. Interestingly there are have been several experimental field trials that puts the LSA at a remarkable advantage over opportunistic cognitive ratio driven dynamic spectrum sharing. In addition to this, the chapter discusses the distribution of the LSA band availability. The identified gaps in existing LSA research which forms the basis of this thesis concludes the chapter.

In **Chapter 3**, the considered system models and assumptions will be described in detail. The several incumbents hitherto occupying the LTE band 40 are categorised into two in the system model presentation. The first system model presented assumed a vertical spectrum sharing between an aeronautical telemetry incumbent and the mobile network operator (MNO). The terrestrial incumbent types of the public protection and disaster relief (PPDR), and programme making and special events (PMSE) are grouped together in the second system model described. The scenario also assumed spectrum sharing with a MNO. For each of the system models, the propagation path, interference, and mobility models used are described.

The contents of **Chapter 4** is exclusively devoted to examining the effect of the original exclusive owner of the LSA band invoking its priority of spectrum access right and the mathematical formulations of the proposed improved LSA resource allocation schemes.

The uncertainty in the availability of the LSA spectrum leads to significant performance degradation especially for the MNO, even while implementing the dynamic form of the LSA. Therefore, this chapter will present evaluation of the performance of the dynamic LSA under the limited power. Furthermore, optimization schemes and algorithms to improve the EE, SE and the EE-SE trade-off of the MNO when the LSA spectrum becomes unavailable will be presented.

An obvious effect of the limited transmit power is a reduction in the achievable data rate of individual users in the MNO network. This threatens predictable and guaranteed QoS, a main distinguishing feature of the LSA when compared to the opportunistic CR driven DSA. **Chapter 4** also presents a hybrid aerial-terrestrial LSA system intended to improve the ability of the LSA to achieve guaranteed QoS which is practically impossible in a conventional terrestrial cellular network. The proposed network configuration assumes a drone Base station operating in the LSA band co-exists with a terrestrial eNodeB operating on the legacy cellular band in a hybrid aerial terrestrial network. Thus, by taking advantage of the mobility and flexibility in configuration of the drone base station it is assumed that the QoS degrading effect of the limited operating power can be adequately compensated for. In order to appropriately quantify the overall spectrum utilization efficiency of the LSA, a new utility function is also presented in this chapter.

Chapter 5 discusses the results of the simulated implementation of the system models and the proposed solutions presented in **Chapter 4**. Results and findings on the LSA licensee's EE, SE, spectrum utilization efficiency, the SE-EE maximization and trade-off as well as the QoS improvement provided by the proposed D-BS assisted LSA system will be presented. Adopting typical values of practical system parameters for a commercial MNO, the evaluation of the proposed methods' performance vis -a- vis critical operational parameters of a conventional MNO system, will be analysed and discussed in this chapter. For each of the results, the implication for practical implementation of the LSA for mobile broadband wireless networks in the 5G space will also be discussed.

Chapter 6, the last chapter, presents the conclusion of this research work by reviewing the contributions of the proposed methods and discussing the practical implications for an efficient implementation of the LSA scheme on a commercial scale in the 5G technology space. Future research directions on implementation of the evolved LSA in view of emerging technologies of mobile wireless broadband and vertical services, that are the defining characteristics of the 5G networks, are also discussed.

1.4 Contributions

- An expression for the power differential (i.e., the power adjustment required to guarantee that the incumbent victim receivers do not suffer from excessive harmful interference) is derived as a function of the incumbent's interference threshold and the respective received interference from the licensee's downlink and uplink transmitters. On the basis of this, the limited transmit power equation in **Section 4.1.1** is formulated for when the spectrum access right is revoked. This part of the thesis is also published in part in [128].
- Then in **Section 4.1.3**, an optimal power allocation technique for optimization of the licensee EE when it is operating with the limited transmit power is proposed. The analysis (in **Section 6.1**) of the performance of the proposed method using critical network parameters such as the eNodeB coverage radius and circuit power, provides practical network design insights for energy efficient operation of the licensee under the limited transmit power regime. These results is also part of the contribution published in [128].
- In **Section 3.1.1** an expression is formulated for the interference received by the incumbent from the licensee's transmission both in the uplink and downlink while also proving the validity of the Poisson network interference distribution for the air-to-ground channel between the licensee UE and the incumbent airborne victim receiver in **Proposition 3.2**. These mathematical formulations are published in [129] and [130] respectively.
- Furthermore, in place of the conventional metric for spectrum utilization, i.e., the simple percentage duty cycle, a novel metric, an utility function of the achievable SE and busy period ratio of each service layer (eNodeB coverage area) within the tandem queue, i.e., the protection radius was proposed for adequately quantifying the LSA spectrum utilization efficiency. This is shown in **Section 4.2.3**. This is also published in part in [129].
- In **Section 6.2** a novel performance measure, "decibel capacity gain" was introduced to quantify the improvement obtained by the proposed power allocation technique. Using the metric we further investigate the SE gain pattern which shed light on the relation of SE to the number of UEs and transmit power adjustment. This is also published in [129].

- An expression for the probability of the maximum tolerable interference of the LSA incumbent is derived in **Section 4.3.1**, and from this an optimal power allocation technique for joint optimization of both EE and SE is proposed in **Section 4.3.3**. This is part of the contribution published in [130].
- The effect of various operational parameters, (e.g., number of channels in the LSA cells, the cell radius and eNodeB transmit power) on these two performance metrics are examined, while further investigating the effect of circuit power and the design priority (the weight parameter) on the joint optimization problem in **Section 6.3**. This is also part of the contribution published in [130].
- Finally in **Section 6.3**, it is established that the simultaneous maximization of the two conflicting objectives of EE and SE is possible by smartly setting network design parameters and configuration goals to take advantage of the bounds and limits of the relationship between the investigated operational parameters and the two efficiency metrics. This is also part of the contribution published in [130].
- The revocation of the licensee's spectrum access during the time the incumbent is busy on the LSA spectrum poses a serious challenge to the actualization of predictable QoS for users on the licensee network. **Section 4.4** an aerial-LSA licensee scheme is proposed as a possible solution to this challenge.
- The results in **Section 6.4**, demonstrated that the flexibility in positioning offered by the proposed aerial-LSA licensee is robust enough to ensure the predictable QoS feature of the LSA scheme is achieved when the licensee spectrum access right is revoked. This is a remarkable result, considering the fact that in the traditional terrestrial network, the desired QoS of each UE in the licensee system suffers as a result of the reduction in transmit power when the licensee spectrum access right is revoked

1.5 List of Publications

S. Onidare, K. Navaie, and Q. Ni, "Spectral Efficiency of Dynamic Licensed Shared Access," in *IEEE Transactions on Vehicular Technology*, vol. 69, no.12, pp.15148-15161, December 2020. doi: 10.1109/TVT.2020.3036113.

S. Onidare, K. Navaie, and Q. Ni, "On the Achievable Energy Efficiency in Dynamic Licensed Shared Access," *2019 IEEE Globecom Workshops (GC Wkshps)*, Waikoloa, HI,

USA, 2019, pp. 1-6.

S. Onidare, K. Navaie, and Q. Ni, "On the Spectrum and Energy Efficiency in Dynamic Licensed Shared Access Systems: A Multiobjective Optimization Approach," in *IEEE Access*, vol. 7, pp. 164517-164532, October, 2019.

S. Onidare, K. Navaie, and Q. Ni, "Maximum Achievable Sum Rate in Highly Dynamic Licensed Shared Access," *2019 IEEE 89th Vehicular Technology Conference (VTC2019-Spring)*, Kuala Lumpur, Malaysia, April 28- May 1, 2019 pp. 1-5.

Chapter 2

Licensed Shared Access (LSA) - The Future of Spectrum Access?

The Licensed Shared Access (LSA) is a regulatory spectrum management shift from single ownership of a frequency band to multi-tenancy of the same portion of the spectrum. It replaces exclusive usage rights of the incumbent of a particular portion of the spectrum with the sharing of usage rights by several licensees and the incumbent. Instead of having just a single entity authorised to use the spectrum at all times, it ensures co-existence of several authorised entities to utilize the spectrum on a non-interfering, and non-disruptive basis. The framework for the LSA in [28] specifically requires protection of both the incumbent and licensee from harmful emissions and interference. In [2], it was categorically stated that: "the LSA does not include concepts such as "opportunistic spectrum access", "secondary use" or "secondary service" in which case the new systems in the spectrum are not protected from the initial occupant".

2.1 The Evolution of the Licensed Shared Access

The original framework of the LSA was based on a similar industry initiative called the Authorised Shared Access (ASA) [13]. It is an EU-RSPG (European Union radio spectrum policy group) regulatory formalization and extension of the ASA spectrum sharing beyonds the IMT bands identified by the industry consortium. The stake holders in the sharing architecture, as shown in Fig. 2.1, include:

- The Incumbent: the original occupier of the spectrum with exclusive usage rights at all times and geographical location as approved by the national regulatory agency (NRA) of the country. Traditionally the LSA envisaged a vertical sharing between such

incumbents as aeronautical and terrestrial telemetry, portable cameras, programme making and special events (PMSE), military applications, satellites and any system that have been assigned the frequency between 2.3 GHz - 2.4 GHz as well as 3.8 GHz [42].

- The Licensee(s): limited number of new users given authorization to share the usage rights to the spectrum, or a portion of it, with the original/old user at some time and/or place by the NRA. Mainly, the providers of mobile broadband services such as mobile network operators (MNOs) are the original intended LSA licensee.
- The National Regulatory Authority (NRA): arbitrates between the incumbent(s) and the licensee(s) on the definition of the sharing framework; namely on the frequency, spatial, and temporal availability of the spectrum, terms of the utilization granted and operations modality of all stake holders. It also issues individual license to each of the licensees on the basis of the agreed framework.

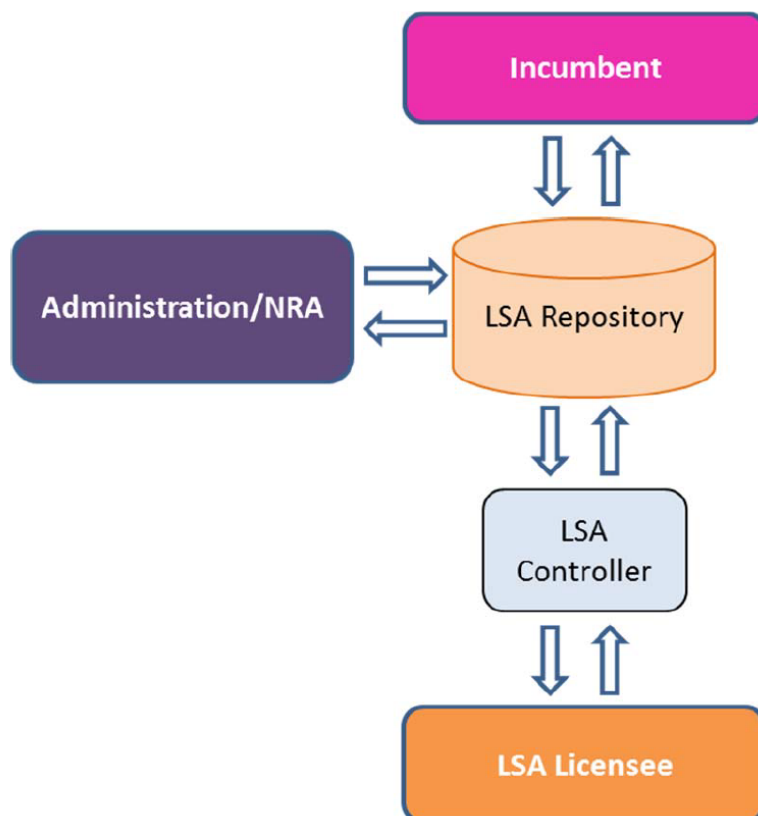


Fig. 2.1 The LSA Architecture and Sharing Framework [2]

The LSA repository and LSA controller in Fig. 2.1 ensures a harmonious co-existence of both parties in a non-disrupting way, such that both can provide predictable quality of service to their users. The LSA repository stores information on the available spectrum for LSA sharing and the conditions associated with its availability while the controller, on the basis of earlier defined rules, provides spectrum access rights to and/or revokes the same from the licensee[2]. The imposition of constraints on the licensee operations to protect the incumbent from harmful interference inspires creation of protection, restriction and exclusion zones [43]. These geographical areas, where the licensee operations are either curtailed or restricted as defined in the initial framework could be significantly large. Hence raising the question of inefficiency in the LSA's ability to achieve its original goal of better utilization efficiency. According to [39], for an airport incumbent, the exclusion zone could be as large as 25 Km radius, while [40] indicates it could be up to an area excluding more than half of the United states population if the incumbent is a naval radar system.

2.1.1 The Dynamic Licensed Shared Access

To address this spatial spectrum hole inherent in the static LSA, the EU funded ADEL (Advanced Dynamic spectrum 5G mobile networks Employing Licensed shared access) project proposed *dynamic zones* as one of the several extensions to the LSA in [3]. The motivation behind this is the constant changing or variations in the availability of the LSA frequency bands as a result of the turnover in the operations of the incumbents. For instance, in [39], it was argued that for a small airports with a relatively low air traffic, it will be rather inefficient to adopt the static exclusion zone of 25 Km radius. In such cases, it is reasonable to assume that an airplane incumbent will not receive interference in all places within the exclusion zone but rather in a very small portion of it at different time instance, i.e., precisely where and when the licensee transmission is within the shadow radius.

Another notable extension geared towards making the scheme more dynamic was incorporation of sensing capabilities to enhance the system's radio resource management. As shown in Fig. 2.2 this proposition calls for additional functional blocks to the LSA architecture as depicted in Fig. 2.1. From the architecture in Fig. 2.2, two functional blocks enhance the dynamism in the sharing; (1) the Radio Coverage Map, which provides on the spot information on the radio environment, from information obtained from the LSA repository; and (2) the sensing reasoning and its constituents sensing networks blocks.

There have been several proposed implementations of the dynamic LSA scheme. One of such is the work in [44] which proposed a Kalman filter based method for detecting the specific area where the incumbent is actively operating at a particular time instant. The rationale behind their work is that the exclusion, protection and restriction zones in the static

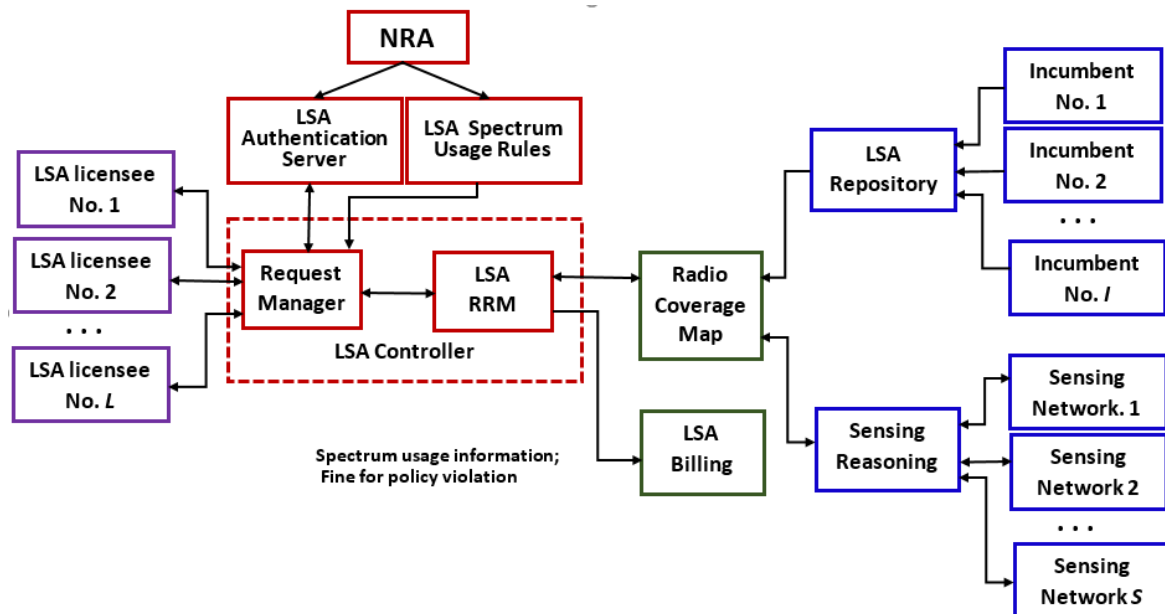


Fig. 2.2 The Functional Blocks of the ADEL Dynamic LSA Architecture. [3]

LSA scheme is created in line with the long term sharing contract (several months or years) between the stakeholders. In practice however, the cycle of the incumbent's operations is in the order of shorter timing (hours, minutes or even seconds) and of a smaller coverage area. Using a combination of received signal strength (RSS) measurements by the user equipment (UE), and the information on the location of the incumbent contained in the LSA repository, a radio environment map (REM) was constructed to determine the geographical coverage of the incumbents transmission at every specific time instant. By so doing, the licensee transmitter can dynamically adjust its operation at each instants of time to prevent disruption of the incumbents system. With this method of determining the effective coverage area of the incumbent at a particular time, it is possible to utilize the spectrum in other areas within the *zones*, thereby reducing the spatial waste that could occur with the static *zones*. Also because the REM is constantly updated, the area marked out for the *zones* changes with the incumbent's activities.

Considering an LSA sharing between an air traffic control (ATC) incumbent system and mobile network operator (MNO) licensee system, the authors of [39] proposed another possible implementation of the dynamic LSA scheme. Their proposition is based on the fact that the airport only uses the LSA spectrum during the time it has to track incoming or outgoing aircraft(s), at other times the spectrum is unused by the ATC. It is also assumed that the eNodeB of the MNO licensee is directed down towards the UEs and hence has a clear isolation from the aircraft(s) in the sky and thus doesn't cause interference to it. Furthermore,

since the aircraft will be at a relatively smaller portion of the exclusive zone, which could be as much as 25 Km radius, it cannot be susceptible to interference in the entire area, but in area within its shadow radius as it ascends. Thus, instead of the licensee not been able to access the LSA spectrum in the entire area of the exclusion zone, especially during the times when the ATC is operational, three policies were proposed. Among the three proposed policies, the limited power policy, requires the UEs in the licensee network to reduce their transmit power when in the shadow radius of the aircraft, while other UEs can operate at the maximum transmit power. Mathematical formulation of this limited power as a function of the projection of the airplane-eNodeB distance and radio shadow was provided in [45].

2.1.2 The Evolved Licensed Shared Access (eLSA)

The LSA as described in the previous section is designed for a long term shared individual licensing, for typically an MNO, as the licensee over a wide coverage area, possibly a national coverage. However, the 5G communication network is expected to feature multiple and usually vertical technologies in an heterogeneous ecosystem. While most of these technologies such as wireless industrial automation, e-Health, public protection disaster relief and PMSE usually have localized coverage, they are expected to provide predictable QoS, and thus can not rely on unlicensed spectrum. With the difficulty in finding new dedicated spectrum, the LSA as a licensed sharing scheme becomes a viable solution. To this end, the original LSA scheme has to be extended to include multiple licenses involving such local vertical service providers who needs spectrum for a short period, probably in the order of hours or days. The eLSA includes such local high quality wireless networks (LHQWN) as licensees for either short or long term spectrum usage within a more localised or smaller area relative to the coverage area of the MNO licensee [46].

Thus the eLSA accommodates multiple licensees that includes MNO(s) and LHQWN(s) sharing the LSA band with the incumbent(s). There are three functional sharing scenarios that has been identified by the ETSI (European Telecommunications Standards Institute) [47]. The first is a situation where an MNO licensee provide spectrum access as a service to a LHQWN licensee. In this instance the MNO either uses its infrastructure to provide service to the users of the LHQWN system on its frequency for a predetermined period, in which case the LHQWN exists as a slice of the MNO network; or the MNO expands its infrastructures to cater for service demands of the LHQWN. The second scenario, has the MNO acting as a lessor of spectrum to the LHQWN. In this case, portions of the LSA spectrum of the MNO is sub-leased to the LHQWN who owns and manage its private network separately from the MNO. The third one is a situation where the LHQWN is given individual license to portion of the spectrum from the spectrum resource repository to operate as a stand alone network.

In this case, the MNO is not involved. The LHQWN obtains a shared spectrum local license for a predetermined period on its own.

To support these additional players in the eLSA architecture, it is imperative to factor their protection and possible impact on others into the sharing framework. This calls for the creation of the *allowance zone*. According to [47], the allowance zone, are geographical area where the LHQWN licensee is permitted to operate on its assigned spectrum and provide its users predictable QoS under the condition that its neighbours and incumbent(s) will be protected against harmful interference. This allowance zone is usually defined within a predetermined *allowance time*. Within the allowance zone, there could also be a restriction zone, in which case the licensee's operation is subject to further restrictions other than radio conditions defined in the lease or license agreement for the entire allowance zone. Consequently, the existing LSA functional entities such as the LSA repository and controller need to be enhanced to support additional multiple eLSA licensee, additional sharing techniques such as leasing and subleasing, managing different roles of the system, and the allowance zones for each vertical operator.

2.2 Flexible Spectrum Management With LSA

The LSA is complementary to the conventional spectrum management [2]. The implication of this is that the NRA(s) does not have the legal power to mandate the incumbent to partake in LSA. That is to say, the LSA licensing can not replace or supersedes the original license by which the incumbent hold the spectrum access rights. Thus a prerequisite to introducing the LSA in a band is a tri-lateral dialogue and negotiation among the NRA, the incumbent and possible licensees [43]. In fact, in countries, where there is no legal framework for the tri-lateral agreement, the actual negotiation is between the prospective licensee(s) and a *willing* incumbent. The NRA only comes in as an arbitrator or a moderator, suggests technical solutions and administer the issuing of licensing on the basis of the agreement already reached by the two negotiators. Therefore, spectrum allocation technique and approach for the LSA must be geared towards providing attractive incentives to encourage incumbents' participation.

The most important concern of an incumbent is the protection of its right of access under the exclusive licensing it holds. As a result, a key incentive to participate in sharing this access right with others will be to have control of or at least "a say" in how the spectrum is assigned to the new entities. Moreover, while the corresponding financial or economic benefits is always attractive, an incumbent will be more willing to lease its spectrum, if it can easily retrieve it when needed. Another important consideration of the incumbent will

be measures to be put in place to ensure that no licensee violates the terms of its spectrum use to its own advantage. If such a violation happens, there must be mechanism to ensure the impact is mitigated on its system and the erring entity is penalized appropriately. In the literature, some of the common approaches to allocation of the LSA shared spectrum are auction based [48–52], based on game theory, and fairness driven [53, 42], ranking based [42, 52].

2.2.1 Market Based Auction of LSA Spectrum

This approach models the granting of spectrum license to the interested entities as an asset auctioning process. The sellers are the incumbents, the buyers are the LSA licensees, while the NRA or a third party serves as the moderator. The process usually begins with the moderator announcing the opening of the auction. The seller then supplies information of the spectrum it has on offer while the buyer sends a notification of its demand. This model has been reported to be very flexible in terms of the granularity of duration of the licensee granted. It could be a short term [48], appropriate for a LHQWN or a long term arrangement for a typical MNO licensee. Another interesting incentive is the inherent ability of the incumbent to choose from several available options, e.g., the one that simultaneously maximizes its revenue and protect its interests. Furthermore, the mechanism could be designed to enable the incumbent offer its spectrum to different operators at the same time, enabling it to optimize possible conflicting interest of revenue and interference management. Negotiating features of bidding licensees includes favourable: (to the incumbent) (i) geographical coverage [51], (ii) transmit power [49], (iii) level of interference [50] as well as a higher spatial efficiency of spectrum utilization and revenue generated by the incumbent. A review of some literatures on LSA spectrum auctioning mechanism is presented in the following.

The authors of [48] presented an online platform for LSA spectrum allocation. To incentivize incumbents, they propose a short term spectrum allocation modelled as a market based auction. The algorithm for the auction involves an auctioneer that arbitrates between the participating incumbents and licensees. The auctioneer announces the auction to all participating parties. The main advantage of this solution is that it ensures a competitive market environment for spectrum sub-leasing. The incumbents have the choice of offering their spectrum for the most attractive offer while the licensees also have different variations of the offer to pick from. Similarly, the work in [49] proposed an auction based algorithm for the spectrum sharing under the LSA system. Two key features of the auction mechanism are flexibility in transmit power that can be submitted in the bids, and the fact that bidding entities are operators' base stations (BSs). The incentive for the incumbents in this auction mechanism is the ability to choose a group of BSs that maximizes the revenue acquired

irrespective of which operator owns each of them. An analysis of the auction method indicates improvement in licensee satisfaction and incumbent incentives in comparison with the conventional fixed transmit power auction mechanisms.

In an earlier work, the authors of [50] proposed an auction mechanism based on mixed interference graph of bidding BSs in different MNOs. The essence of the mixed graph is to manage inter MNO interference while coordinating the auction process. The resulting higher spatial efficiency leads to a better pay-off to the sellers (the incumbents) as well as a higher satisfaction for the buyers (the licensees). On the basis of the fact that the emerging network topology is very heterogeneous, bidding BSs are given the opportunity to negotiate by submitting different preference of coverage area in their bids in [51]. As a result, the determination of the winning bids is based on both the spectrum efficiency per unit space, and the coverage area of the bidding BS. This ensures the incumbents maximize their revenue by being able to compare different attractive bids and choosing the best. Moreover, it also encourages level playing ground for smaller operators BSs and ensure improved spatial efficiency especially if users on the network are concentrated in a relatively small area. The work in [52] similarly proposed a spectrum auction algorithm for LSA spectrum allocation. It used a ranking method to determine the best set of BSs that maximizes the incumbent's revenue from the auction.

2.2.2 Game Theory Approach to LSA Spectrum Allocation

Game theory is a mathematical tool that has been used to analyse, describe and model a very diverse range of physical every-day phenomenon, [54]. It's applicable to situations where the decision(s) to be made or objective(s) to be optimized is(are) influenced by the action of other parties in the activity space. A game involves a set of players with a set of strategic actions (restricted by some constraints and notably the activities of other players in the game) taken with the ultimate aim of achieving a set of expected optimal outcomes. As a result game theory has been applied extensively to different scenarios in wireless communication where there are usually multiple entities cooperating or competing to utilize shared resources. It has been proposed for joint channel and transmit power allocation in CR systems [55], for sharing interference channel [56, 57] and medium access control [58, 59].

The appeal of this approach to spectrum allocation is its dynamism and flexibility to realise different interests of the stakeholders in an LSA system. It can be configured to simultaneously maximize revenue for the incumbents while ensuring fairness and optimal pay-off for the licensees, e.g., in a two-tier evolutionary game [60], or just focussed on protecting the over riding interest of just one of the stakeholders [61]. In the case of the incumbent, it can take advantage of the inherent changing dynamics as in a game to adjust

the price of its spectrum as well as other parameters based on inferred market realities from previous rounds of the game. By doing so, it can maximize its revenue over time. Mathematically, this is expressed as a pay-off utility function defined as [60]:

$$\text{Ipf}_m = \sigma_I \log(\Upsilon_I b_m t_m) + \Phi_I \rho_{m,r} d^{(a)} n_m^{(a)}, \quad (2.1)$$

where Ipf_m is the m^{th} incumbent pay-off function, b_m and t_m , the offered bandwidth and coefficient of time availability by the m^{th} incumbent, $\rho_{m,r}$ is the adjusted bandwidth price at the r^{th} round of the game. In (2.1) it is assumed there are many groups of licensees each containing N number of licensees, a is the index for the group, n for the licensees in each group. In this formulation $d^{(a)}$ is the percentage discount given to a specific a^{th} licensee group as specified in the LSA agreement, while $n_m^{(a)}$ is the the number of licensees in the a^{th} group utilizing the spectrum block offered by the m^{th} incumbent. In (2.1) σ_I , Υ_I and Φ_I are empirical values derived by the incumbent.

From the licensees' perspective, it seeks to get a fair share of the spectrum allocation as the game unfolds. This is done by comparing the net pay-off of each licensee, at each round of the game, to the average pay-off. This informs the decision of the licensee in the succeeding round of the game. The licensee pay-off function is defined as:

$$\text{Lpf}_n^a = \sigma_L \log \left(\Upsilon_L \frac{b_m t_m g_i}{n_m^{(a)}} \right) - \Phi_L \rho_{m,r} d^{(a)}, \quad (2.2)$$

where g_i is the grant factor determined by the licensee at the i^{th} round of the game where the licensee calculate its pay-off to be equal to the overall average. The other parameters are the licensee equivalent of the definition for the incumbents in (2.1), and g_i is a function of the allocated spectrum to the demanded bandwidth. Thus, as it is seen in (2.2), it is a measure of the level of the licensee's satisfaction by the spectrum allocation mechanism. The higher the value of Lpf_n^a , the higher is the satisfaction level.

2.2.3 Fairness Based LSA Spectrum Allocation

For the incumbents, this approach to spectrum allocation is only desirable for the penalty to those licensees that violate the terms of the spectrum access given to it. The main objective is to prevent skewness of the spectrum allocation in favour of some licensees over the others. Moreover, unlike the auction approach which is rather a policy mechanism, it is more of a technical approach to a methodical and coordinated assignment of the LSA spectrum [42]. The main metric used for determining the amount of spectrum to be allocated to a particular

licensee is the *priority index* (PI) which is defined as

$$\text{PI}_n = \lim_{W \rightarrow \infty} \frac{\sum_{w=1}^W B_n^a(w)}{\sum_{j=w}^W B(w)}, \quad (2.3)$$

where $B(w) = \sum_{N=1}^n B_n^a(w)$, $B(w)$ is the total LSA spectrum made available by the incumbent at the w^{th} round of allocation, $B_n^a(w)$ is the fraction of the LSA spectrum allocated to a licensee, w is the index for different round of allocations, n is the index for the number of licensees requesting for the LSA spectrum, and W is the window size of the allocation rounds. At each succeeding round, the amount of spectrum allocated to a licensee, n , is inversely proportional to its PI from the preceding round as follows:

$$B_n^a(w) = B(w) \left(\frac{1 - \text{PI}_n}{\sum_{n=1}^N (1 - \text{PI}_n)} \right). \quad (2.4)$$

The idea behind (2.4) is to ensure that licensees with smaller allocated bandwidth in the previous round are compensated in the next round, thereby ensuring all licensee gets fair proportion of spectrum access in the long term. In [53] defines a penalty index (PeI) to form the basis for determining the magnitude of spectrum access violation and to apportion the appropriate penalty as:

$$\text{PeI}_n = \lim_{W \rightarrow \infty} \frac{\sum_{w=1}^W I(V_n(w))}{\sum_{w=1}^W I(B_n^a(w))}, \quad (2.5)$$

where $I(\cdot) \in \{0, 1\}$ is the indicator function and V_n is the violating licensee.

2.2.4 Ranking Based LSA Spectrum Allocation

Similar to the fairness based LSA spectrum allocation, the ranking based is a technical framework that aims to penalise violators and reward compliance with the spectrum sharing terms and condition. In [42], the ranking metric is defined as:

$$R_n = \sum_{k=0}^K \varepsilon_{n,k} \cdot \exp \left(-\frac{t-t_k}{\Lambda_{n,k}} \right), \quad (2.6)$$

where R_n is the rank of a licensee, n , ε is the extent of the violation, Λ is the temporal effect of the violation, k is the index for different occurrence of violations while t is the time a particular violation occurred. The ranking mechanism should also factor the availability or otherwise of spectrum in a particular area into consideration for ranking licensees [42]. The

higher the rank of a licensee, the higher the willingness of the incumbent and the larger the spectrum block allocated to the licensee.

It is worth mentioning that the ranking based and the fairness based approaches offer the scalability for effective resource allocation under the eLSA. More specifically, in the use cases where an MNO subleases the spectrum to a number of LHQWN, these methods could be easily deployed to provide a technical framework for equitable distribution of the spectrum by all parties. Another possible way to envisage the attraction of these two methods is as a complement to a policy or regulatory focused allocation technique such as the auction based in an eLSA ecosystem. For instance, at the interface between the MNO and the incumbent, the auction based allocation could be employed, then between the MNO and the LHQWN, either the ranking, or the fairness based method is used.

2.3 Experimental Verification of the LSA Viability

For the LSA to progress from a theoretical concept to a real life spectrum access technology, it has to be experimentally shown that it is able to meet the requirements set out in the regulatory frameworks [2]. On the basis of compatibility reports such as in [46, 38], there have been several research works done in a couple of countries to verify the practicability of the LSA. The results of the experimental trials have been encouraging largely due to the fact, that the ASA on which the LSA sharing is based does not require technologies such as sensing that has proven to be challenging and costly [13]. The obtained results from such experimentation have indicated a successful co-existence of the licensee with the incumbent with regards to the key requirement of the LSA; predictable QoS for the licensee and interference protection for the incumbent.

One of the early reports of the experimental validation of the LSA is the work by the authors of [29]. The experimentation environment includes a live LTE (long term evolution) testbed which was deployed in 2.3 - 2.4 GHz band to demonstrate LSA sharing between an MNO and a PMSE. The results of the experiment show that the MNO was able to provide predictable QoS to the users in its network by transferring those users to other networks when it was requested to evacuate the LSA spectrum by the incumbent. The recorded evaluation and handing over time were both within values that do not affect the licensee QoS delivery or disrupt the incumbent's operation. A similar study [30] used a FDD-LTE on the cellular band, a WCDMA and WiFi as alternative networks for the LSA licensee to evacuate its users upon demand by the incumbent. The obtained results show that with a minimal addition to the existing LTE-TDD network, the dynamic LSA can be implemented in a non-interfering manner with the incumbent and a predictable QoS provision for the licensee's end users.

In [31], the authors presented a proof of concept of the LSA scheme using a 3GPP release 8 compliant LTE radio network. The authors extended the trial in [30] by considering different use cases of the incumbent and how the sharing scheme performs under different conditions. The evacuation time to an alternate network was shown to be reasonably good so as not to affect the QoS of the users on the licensee's network. This further confirms that under different deployment conditions, the LSA is easily implementable. The field trial went a step further by integrating a tracking algorithm into the LSA controller to determine the location of an incumbent system in [35]. This is necessary for estimating the interference from the licensee dynamically and ensuring adequate protection of the incumbent system. By fully integrating the LSA controller into the MNO network management, the trial was able to implement LTE resource optimization algorithms to further maximize availability of resources for the licensee.

Further to this, the authors of [36] conducted empirical measurements to verify the specifications of the regulatory compatibility studies in [38]. The obtained results of the interference measurements of a real LTE network and a portable camera system indicates that the regulatory specifications were considerably stricter than the reality. A more comprehensive demonstration of the feasibility of the LSA is presented in [62]. The work in [62], unlike the others considered not just a single incumbent but several incumbents of the 2.3 GHz to 2.4 GHz band including the Telemetry system. Furthermore different LTE optimization features were tested in an architecture using real LTE networks across three different European countries. The results verify the feasibility of the LSA to provide a predictable QoS for both parties and also demonstrated that the regulatory requirements can be easily met with regards to different incumbent's protection zones.

2.4 The LSA Service Availability

The dynamic nature of the LSA spectrum's availability is analogous to a birth-death process that is best described by a queuing system [4, 63, 41] with an unreliable server. The first state, describes the cases where the spectrum is not being used by the incumbent, and hence is available for the unconstrained utilisation by the licensee(s). The second state is when the spectrum is being used by the incumbent system. In this state, the spectrum is referred to as busy or unavailable.

For example, assuming an LSA sharing arrangement between an ATC incumbent and an MNO licensee[4, 63, 41], the spectrum availability can be characterised by the following parameters:

- γ^{-1} : interval between successive flight take-off or landing(s), i.e., a cycle of the birth death process,
- μ^{-1} : time of ATC communication with an aircraft, i.e, duration of the spectrum occupancy(s) also referred to as busy period (BP),
- τ^{-1} : duration of the spectrum vacancy(s), i.e., idle period (IP),
- s : LSA spectrum status given as $s \in \{0, 1\}$,
- J : number of aircraft landings at or take-offs from the airport (service request) at different times with an exponential arriving rate, γ , and service rate, μ .

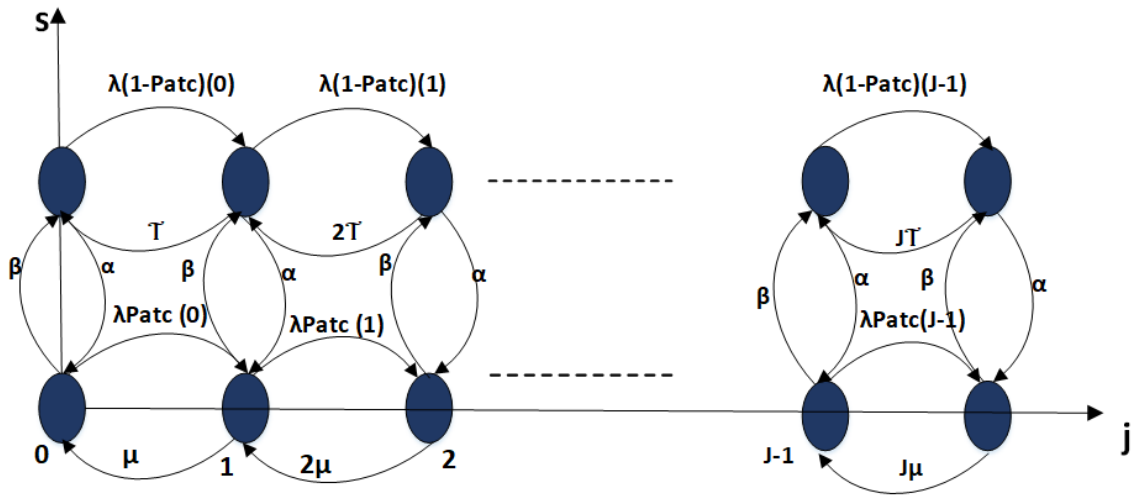


Fig. 2.3 The schematic of LSA spectrum availability state space.

Fig. 2.3 shows the state space diagram of the LSA system. P_{ATC} is the probability of ATC transmission occurring during the interval between successive flight take-offs or landings, i.e, the probability of the LSA spectrum busy period. The converse $(1 - P_{ATC})$ holds for when the spectrum is not being used by the incumbent, β is the birth – to – death transition rate and α the death – to – birth rate, where $\alpha + \beta = 1$.

As a consequence of the incumbent revoking the LSA band, the service unavailability time of the users on the licensee network is composed of the waiting time, such as in the case of congestion, before the users request is serviced, and the service disruption time when the spectrum is revoked.

Fig. 2.4 is a graphic illustration of the service unavailability time. In the figure, when the service request arrives, all the licensee’s resources are under use, hence it has to wait for a

free resource to be available. Then during the servicing of the request, the LSA band became unavailable twice, thus causing interruption in the service. This phenomenon affects the key QoS defining metrics of the LSA namely: the request blocking probability, the mean data rate, and the mean number of users suffering service interruption. Assuming, the licensee server has a total capacity of C_T and the capacity of the buffer for storing service requests is R_{bf} , the following probabilities define the system's characteristics:

$$P_{Av} = \sum_{u=1}^{R_{bf}} \Pr\{u, 0\}, \quad (2.7)$$

$$\mathbb{E}(N_u) = \sum_{u=1}^{R_{bf}-C_T} u \cdot \Pr\{u, C_T\} + \sum_{u=1}^{R_{bf}} u \cdot \Pr\{u, 0\}, \quad (2.8)$$

$$P_B = \Pr\{R_{bf} - C_T, C_T\} + \Pr\{R_{bf}, 0\}, \quad (2.9)$$

where P_{Av} is the probability that the LSA band is not available, u is the index for users in the licensee system, $\mathbb{E}(N_u)$ is the mean number of users suffering from service unavailability, and P_B is service blocking probability. The first expression on the right hand side of (2.8) indicates the expected number of users waiting for their service to start while the second expression describes the expected number of users whose service are interrupted as a result of the unavailability of the LSA band [4]. Bounds for these limiting probabilistic characteristics were modelled by authors of the work [64].

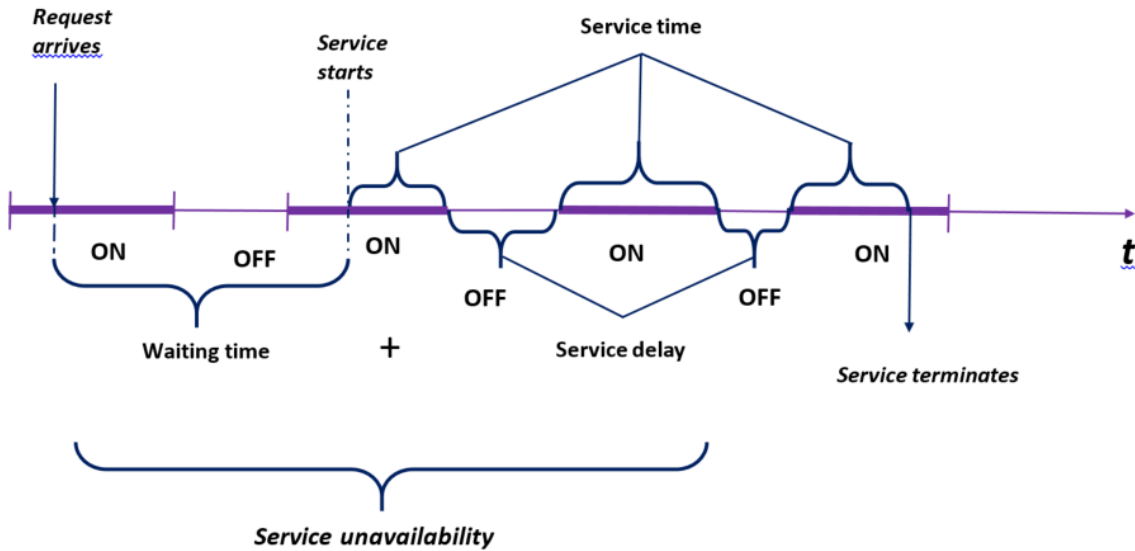


Fig. 2.4 The schematic of service unavailability in LSA [4].

2.5 Challenges and Gaps in the LSA Research

As noted in the previous section, the availability or otherwise of the LSA band affects various performance metrics of the licensee system. An effect of the spectrum revocation by the incumbent is seen in spatial limitation on the utilization of the spectrum. Improving the spectrum spatial utilization efficiency when the incumbent is busy in its spectrum is the focus of the works in [65, 66, 44]. For different types of incumbent system, the authors of [65] investigated means of reducing the region or area covered by the licensee interfering signals. They basically employed two methods, antenna down-tilting and reduction in eNodeB transmit power. The idea is to improve on the number of eNodeBs that can be turned on while incumbent system is active around the licensee's coverage area.

Similarly, the work in [66] proposed a system of heterogeneous cellular networks aimed at reducing the geographical separation distance between the licensee and incumbent. The analysis also investigated different antenna orientation to achieve the same aim of minimizing the interference area around the incumbent system. A similar idea was investigated with the use of REM in [44] while the authors of the work in [67] propose different scenarios and application of the use of smart antennas to optimize the spectrum utilization and throughput of the LSA system.

Several research works have evaluated performance metrics such as the interruption, and blocking probability, average number of connected users, service failure, mean bit rate, etc of the LSA. [63, 41, 64, 4, 68]. The authors of [69, 70] identify its suitability for high density machine type communication and as a viable back up solution to unexpected network down-time especially for public safety purposes during disaster outbreaks and for rescue operations. Different scenarios where the LSA can be deployed for capacity increase in the 5G technology space as well as a new architecture and enabling technologies were presented in [71]. The work in [72] focuses on the enforcement of compliance, by all parties in the LSA sharing arrangement, to the sharing rules. In [73], the authors examined a spectrum sharing arrangement between terrestrial satellite system and a cellular network.

However there are still key research problems critical to the performance of the LSA that have not been addressed in the literature. These impacts negatively, on the QoS of users on the licensee network when the spectrum is revoked by the incumbent. This is inconsistent with the key requirement of guaranteed and predictable QoS for the licensee system under the LSA scheme. Critical to any 5G technology are the following:

- The importance of the LSA licensee's *energy efficiency* (EE) can not be over-emphasized in the light of the 5G key technology goals; a hundred times ($100\times$) energy efficiency and/or 90% reduction in energy consumption. This has become a much discussed issue

in the research world because of the ecological concerns posed by the information and communication technology (ICT) carbon footprint [17] as well as the economic implications [19, 74]. Added to these, and several other important reasons, motivate the investigation of an energy efficient LSA architecture in this research work. The *energy efficiency of the LSA* is made more challenging by the necessity of imposing restrictions on the licensee system to prevent harmful interference to the incumbent system.

- The challenge of energy efficient LSA system is further exacerbated by the direct relationship between energy consumption and the expected growth of the global mobile broadband traffic [8]. Even though, the limited power technique ensures that the licensee system is not switched off when the band is revoked, there is still a degradation in the achieved data rate [41]. These coupled with the challenge of spectrum scarcity and achieving the 5G goal of about $100\times$ user experienced data rate more than the 4G [14], underscores the need to optimize the *spectrum efficiency (SE) of the LSA licensee*, especially when the LSA band is deemed not available due to the incumbent's occupation of its spectrum. In sharing network, the interference threshold constraint of the primary service plays a major role in the achievable capacity of the secondary service [75]. Thus, the strict interference threshold of the incumbent makes maximizing the SE of the licensee in an LSA system non-trivial.
- To a large degree, EE and SE are conflicting objectives and thus cannot be maximized at the same time. Increasing achievable data rate comes at the cost of increased transmission power requirement [76] which in turn result in a reduced EE. On the other hand, increasing the transmission bandwidth, improves EE but at the cost of degraded system spectrum efficiency (SE) [77, 78]. Thus, finding the right *trade-off between EE and SE* is a challenging issue in designing wireless communications systems. This work examined the optimal EE and SE trade-off of the LSA licensee under the constraints of the incumbent's interference threshold.
- Furthermore due to its ease of deployment [79–81], flexibility in positioning [82–86], wide application scenarios [87–90] and relatively cheaper implementation [91, 92], the drone base station (D-BS) or aerial relay has received attention in the literature. For example the authors of [93] proposed it for congestion handling in cellular networks, as a critical component of the 5G heterogeneous network architecture [94], as a viable alternative for public safety operations in [95], and for improving reliability and systems performance of cellular networks [96]. These, as well as the better signal propagation path [97–101], inspired the motivation to *leverage the D-BS agility to*

compensate for the QoS degrading effect of the reduced achievable data rate of the limited transmit power regime when the LSA band is revoked by the incumbent.

2.6 Chapter Summary

In this chapter, a systematic review of the existing work on the LSA spectrum sharing scheme has been provided. A detailed description of the original LSA framework as a regulatory paradigm shift for a more efficient utilization of the spectrum and its limitation was followed by a description of the dynamic LSA, which in addition to addressing the limitations of the static LSA, also includes further extensions to ensure an improved spectrum utilization efficiency by the LSA. Several aspects of the LSA that has been addressed in the literature, such as the different approaches to spectrum management it offers, the experimental field trials as proof of concepts for its practical deployment, and the dynamics of the LSA spectrum availability was discussed. Finally, the contributions of this thesis, i.e., the identified gaps in existing research, which is the impact of the licensee's spectrum access revocation on the efficiency of the dynamic form of LSA scheme was discussed. On the basis of the system model and mathematical formulations of **section 3.1**, a resource allocation optimization method to improve the EE of the licensee when its spectrum access is revoked was proposed in section 4.1. Specifically **section 4.1** contains the mathematical formulation while the simulation results of the proposed method was analysed in **section 6.1**. Similarly, **section 4.2** shows the mathematical formulations and model for the SE maximization of the licensee while the results were analysed in **section 6.2**. The trade-off between the SE and EE was formulated in **section 4.3** and the analysis of the findings are presented **section 6.3**. Then using the system model in **section 3.2**, **section 4.4** presents the mathematical formulations for leveraging the D-BS agility to compensate for the QoS degrading effect of the reduced achievable data rate of the limited transmit power regime, while the results of the proposition was presented in **section 6.4**.

Chapter 3

System Model

The licensed shared access (LSA) can facilitate authorised or licensed spectrum sharing, either horizontally or vertically between the incumbent(s) and licensee(s). Horizontal LSA spectrum sharing involves incumbents and licensees with similar or the same communication technology, such as two or more mobile network operators (MNOs) sharing the same frequency band [102, 103, 40]. However, the work presented in this thesis is strictly for the more sensitive and significant spectrum sharing between systems of vertical technologies as contained in the original LSA framework [2]. As mentioned in **Chapter 2**, there are several incumbents operating in the initial frequency band proposed for the LSA under the European communication commission (ECC) harmonization, the 2.3 GHz- 2.4 GHz. Therefore, this chapter presents the system models adopted in this thesis in two categories to account for the different incumbents.

3.1 The Aeronautical Telemetry Incumbent

In this section, the considered system includes an LSA arrangement between an airport incumbent and an MNO cellular network as the LSA licensee. Each of the incumbent and licensee systems perform based on their own standards and the coordination among the nodes in each of the systems remains the same as it was without using LSA.

Assuming a circular area with a radius similar to the exclusion zone radius for an airport incumbent, the LSA licensee, a MNO, has multiple cells of radius R within the considered geographical radius (Fig. 3.1). The airport telemetry system uses the spectrum specifically for air traffic control (ATC) i.e., for communication between the ATC tower and aircraft(s) during and shortly after take-off as well as before landing. It is at this period when the incumbent utilizes its spectrum that it revokes the right of access granted to the licensee. In

this time period, the LSA spectrum is considered as busy or unavailable. The rest of the time, the spectrum is referred to as free and available for the MNO unrestricted access.

However, as earlier mentioned, under the dynamic LSA implementation recommended in [39], the revocation of the licensee's spectrum access is an imposition of constraints on the transmission power, rather than an outright vacation of the spectrum. During this period, the licensee transmit power must be set at a level such that the interference received by the incumbent does not exceed its maximum tolerable interference power, i.e., the incumbent's interference threshold.

It is also assumed that a LTE system is deployed by the MNO licensee. The channel gain vector for k UE (where $k = 1, 2, \dots, K$) is represented as $\mathbf{g} = [g_1, \dots, g_K]$. For easy reference, the parameters used in this chapter are also presented in Table 3.1 and 3.2. Similar to the ATC communication system, the licensee uses a time division duplexing (TDD) system. Furthermore, it is also assumed that the transmission link from the ATC tower to the aircraft uses the same channel as the MNO uplink transmission and equivalently the reverse link, i.e., from the aircraft to the ATC tower, uses the same channel as the MNO downlink.

In practice, the justification for using LSA sharing between a MNO licensee and the aeronautical telemetry system as the incumbent is made for small airports with a rather low air traffic. In such cases, under the dynamic LSA, one may consider the fact that an airplane will not receive interference in all places within the exclusion zone but rather in just a very small portion of it, i.e., precisely where the licensee transmission is within the shadow radius, [39, 45]. Furthermore, the requirements set by the LSA framework ensure the incumbent system is protected from harmful interference hence its reliability is not compromised. Based on the LSA, the incumbent and licensee are expected to have agreed on the specifications of their communications systems to ensure safe operation for the incumbent. In addition, the ATC interference threshold and the interference probability are designed conservatively enough to ensure the reliability of the ATC.

3.1.1 Incumbent's Received Interference

In this section, the interference that could impair the ATC transmission to the flying aircraft during the take-off or landing is examined. Here two cases are considered. The first case corresponds to the eNodeB coverage, see eNodeB coverage area A in Fig. 3.1, where the interference to the incumbent's system comprises of rather strong interference signals from eNodeBs and less strong but multiple interfering signals originating from the UEs. We consider the effect of this interference on the ATC tower and the aircraft with the assumption that there is perfect co-operation and synchronization between the licensee and the incumbent operation that ensures no cross-slot interference.

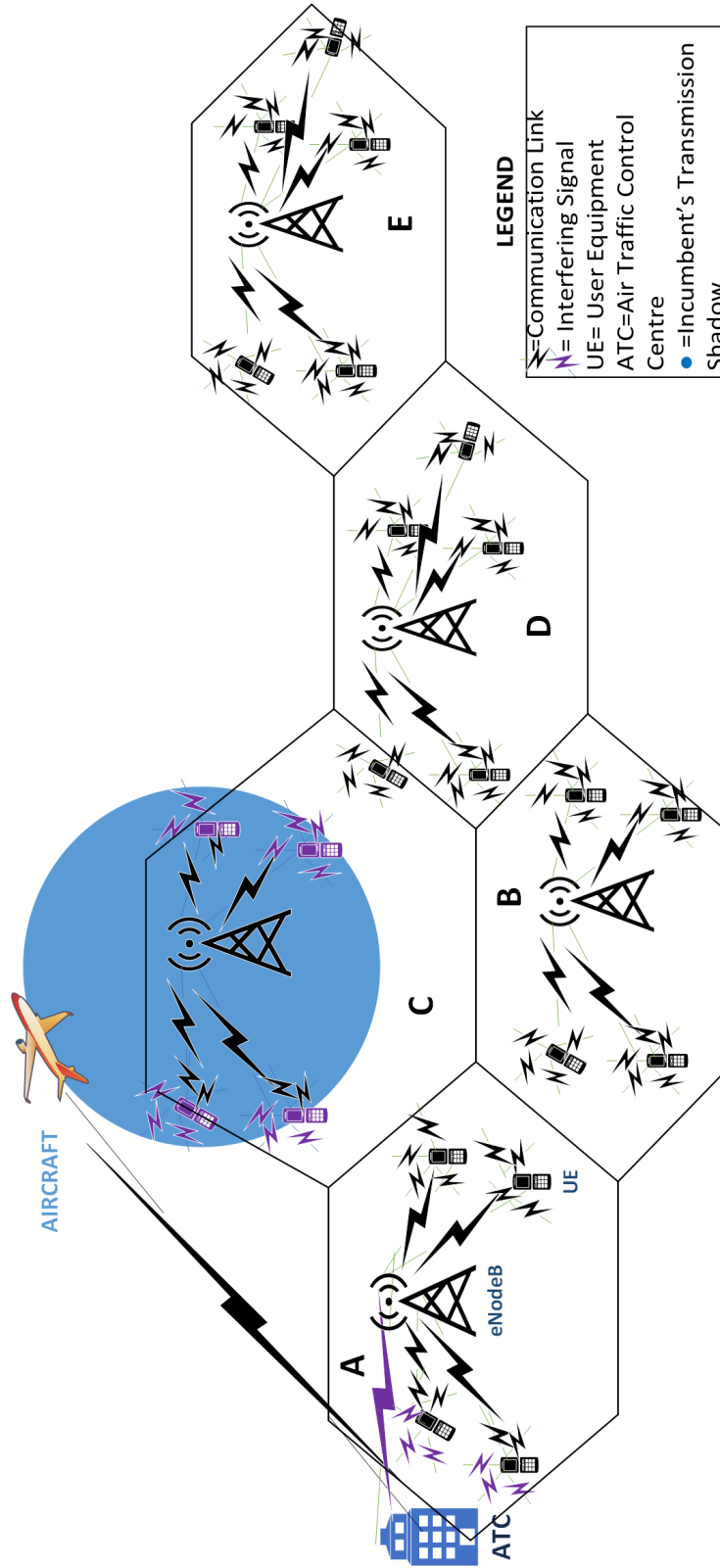


Fig. 3.1 A schematic of the considered system: Incumbent's transmission shadow only crosses licensee cell C, while cells A, B, D, and E are outside the transmission shadow.

Table 3.1 List of Parameters.

Parameter	Description
φ	UE Poisson Point Process
I_φ	Received interference point process
k	Individual UE
y_k	Location of individual UE
y_a	Location of aircraft
Q	Number of tandem queue service layers
γ^{-1}	Time between successive flight take-off or landing(s)
μ^{-1}	Time of ATC communication with an aircraft
τ^{-1}	Duration of the spectrum vacancy(s)
s	LSA spectrum status
J	Number of aircraft landings at or take-offs
n	Path loss exponent
P_k	Transmission power
l	Distance related power loss
r	Distance between the ATC transceiver and the MNO interferer
F	Fading co-efficient
g_d	Ground/horizontal distance between the aircraft and a user equipment
v_d	Vertical distance/height between the aircraft and a user equipment
D	Radius of the interference circular area
ζ	Maximum interference probability
I_{th}	Incumbent interference threshold
G	Propagation constant
P_s	Total dissipated power
\mathbf{g}_k	Channel gain vector
\mathbf{P}	transmit power vector
η_{EE}	Energy efficiency
η_{SE}	Spectrum efficiency
\mathcal{L}, χ, u, v	Lagrange multipliers

Table 3.2 List of Parameters Continues . . .

Parameter	Description
r_c	eNodeB cell radius
n_{UE}	No. of user equipment
λ	Density of UE per unit area
N	Noise power
N_0	Noise power density
P_c	Circuit power
P_{LT}	Limited transmit power
P_B	eNodeB transmit power
B	Individual eNodeB
ε	Amplifier efficiency
T	UE total movement time
T_p	Pause time
t	Index of different UE movement time
M	UE destination point at a specific t^{th} time
V	UE movement speed
ξ	point process UE mark
$Z(V)$	UE mark distribution
λ	Density of UE per unit area
R_k	UE data rate
R_T	Total network traffic requirement
R_{TG}	Excess traffic requirement
R_{NL}	Normal network traffic load
S_{UE}	Excess traffic UE set
K	Total UE set
BW	Transmission Bandwidth
PL	Path loss
ρ	ATG propagation group
θ	ATG elevation angle

The second case is where the incumbents' interference is only comprised of signals from the UEs. It is reasonable to assume that a critical network design consideration of an LSA licensee is to ensure that the eNodeB antenna height is sufficiently low relative to the ATC tower with a directional pattern (directed downwards to the UEs). Hence, omni-directional transmissions of UEs becomes the main components of the interfering signal [39]. Moreover, for distant licensee cells, i.e., where the ATC tower is outside the eNodeB coverage area, the incumbents received interference only includes UEs' signals within the incumbent's transmission shadow radius. This is shown in eNodeB coverage area C of Fig. 3.1.

3.1.1.1 Interference from the Licensee eNodeB

It is assumed here that the licensee's eNodeB is at least of a comparable height and possibly on the same horizon with the ATC tower. Although careful network design should ensure that the likelihood of this scenario playing out is very low but it is a possibility that is worth considering. Thus, the interference from a licensee's eNodeB located at a distance r to the ATC tower is [104]:

$$I_B = P_B F_B l(r), \quad (3.1)$$

where, I_B is the licensee eNodeB interference power, P_B, F_B , is the eNodeB transmit power and fading component respectively, $l(r)$ is the path loss as a result of the separation distance d between the eNodeB and the ATC tower and is given by $l(r) = \|r\|^{-n}$, n is the path loss exponent.

In cases where there are more than one eNodeB within interfering range of the ATC tower, the aggregate interference from multiple eNodeBs is:

$$I_{AGB} = 10 \log \left[\sum_{B=1}^{N_B} I_B \right] + 30, \quad (3.2)$$

where I_{AGB} is the aggregate interference to the ATC tower from multiple eNodeBs in dBm (hence adding 30 in the above), N_B is the number of interfering eNodeBs, and I_B is the individual eNodeB interference power in Watts.

3.1.1.2 Interference from Licensee UE

Another, more likely, source of interference to the incumbent system is the omni directional transmission in the uplink direction of the licensee system. The interference from this source comprises of interfering signals from the UEs to both the uplink (airplane receiver) and the downlink (ATC tower receiver) of the incumbent system, in contrast to the interference signal

from the eNodeB which only affects the downlink transmission of the aeronautic telemetry system. This is based on the assumption that the eNodeB uses antennas with directional radiation pattern directed downwards to the mobile stations [39]. For this scenario, K UEs are considered, each independently and randomly located at location x within the coverage area of eNodeB. The spatial distribution of the UEs in the coverage area of the eNodeB can then be characterised by a Poisson point process as the following:

$$\varphi = \{x_1, x_2, \dots, x_K\}. \quad (3.3)$$

Therefore, the cumulative interference to the incumbent system at a point y as a result of the licensee UEs transmission is:

$$I_K = \sum_{k \in \varphi} P_k F_k l(\|y_a - x_k\|), \quad k = \{1, 2, \dots, K\} \quad (3.4)$$

where P_k , the UE transmission power, is Bernoulli distributed with parameter $p = \Pr\{P_k = 1\}$ as the probability that each of the expected K UEs is transmitting, F_k , the fading coefficient, is an exponential random variable. In practice, the PHY and MAC layers of LTE try to avoid all simultaneous transmissions from UEs connected to a single eNodeB. Therefore it can be assumed that even though there could be many UEs per eNodeB, there is no more than one UE per eNodeB transmitting simultaneously.

Then the distance between the aircraft and a node, $\{\|y_a - y_k\|, \{y_k \in \varphi\}\}$ is defined as $\|r\| \leq D$ and the intervening area between them can then be represented as a sphere $b(y, D)$, centred at y with a radius of D . Therefore, we can define an interference PPP, $\varphi_I = \varphi \cap b(y, D)$, similar to the inner city model of the Cox process [105], where φ_I , and φ are Poisson processes with density λ_I , and λ , respectively, and $\lambda_I = \lambda c_d d r^{d-1}$, where, $c_d = \|b(0, 1)\|$ is the volume of d -dimensional unit hyper - ball. Based on the above, the interference received at the aircraft from UE located within distance D of the aircraft is

$$I_D = \sum_{r \in \varphi_I} l(r). \quad (3.5)$$

The following proposition gives the probability density function (pdf) of I_D .

Proposition 3.1: The pdf of the received interference is [106]

$$\begin{aligned}
 f_I(i; \theta) &= \frac{1}{\pi i} \sum_{k=1}^{\infty} \frac{\Gamma(\theta k + 1)}{k!} \left(\frac{\lambda_I \pi \Gamma(1 - \theta)}{i^\theta} \right)^k \sin k\pi(1 - \theta), \\
 &= \frac{1}{\pi i} \sum_{k=1}^{\infty} \frac{\Gamma(\theta k + 1)}{k!} \left(\frac{\rho}{i^\theta} \right)^k \sin k\pi(1 - \theta),
 \end{aligned} \tag{3.6}$$

where $\theta = \frac{2}{n}$, $\Gamma(\cdot)$ is the gamma function, $\rho = \lambda_I \pi \Gamma(1 - \theta)$, and $\lim_{r \rightarrow 0} l(r) = \infty$, and $\lim_{r \rightarrow \infty} l(r) = 0$.

Proof: For I_D we write,

$$\mathcal{F}I_D(\omega) = \mathbb{E}\{\exp^{j\omega I_D}\}, \tag{3.7}$$

where $\mathcal{F}(\cdot)$ and $\mathbb{E}\{\cdot\}$ are Fourier transform, and expectation operator, respectively. We then write $\mathcal{F}I_D(\omega)$ as the following:

$$\begin{aligned}
 \mathcal{F}I_D(\omega) &= \mathbb{E}\{\mathbb{E}\{\exp^{j\omega I_D} | k\}\} \\
 &= \sum_{k=0}^{\infty} \frac{\exp^{-\lambda_I \pi D^2} (\lambda_I \pi D^2)^k}{k!} \mathbb{E}\{\exp^{j\omega I_D} | k\}.
 \end{aligned} \tag{3.8}$$

The first expectation operator in (3.8) defines the characteristic function, (i.e. the Fourier transform) $\mathcal{F}I_D(\omega)$, of the received interference I_D . Since I_D is conditioned on the presence of K UEs within radius D , the second expectation operator defines that conditional probability.

Locations of the UE within $b(y, D)$ are random variables determined by the direction and speed of movement of users from their previous location. It is assumed that the initial distribution of the UE before movement follow a radial density as follows:

$$f_R(r) = \begin{cases} \frac{2r}{D^2} & 0 \leq r \leq D, \\ 0 & \text{otherwise.} \end{cases} \tag{3.9}$$

The interference, I_D , is the summation of independent random variables, therefore, $\mathbb{E}\{\exp^{j\omega I_D} | k\}$ is

$$\begin{aligned}
 \mathbb{E}\{\exp^{j\omega I_D} | k\} &= \left(\mathbb{E}\{\exp^{j\omega l(r)}\} \right)^k, \\
 &= \left(\int_0^D \frac{2r}{D^2} \exp^{j\omega l(r)} dr \right)^k.
 \end{aligned} \tag{3.10}$$

Combining (3.7), (3.8), and (3.10) yields:

$$\begin{aligned} \mathcal{F}I_D(\omega) &= \exp\left(\lambda_I \pi D^2 \left(-1 + \int_0^D \frac{2r}{D^2} \exp^{j\omega l(r)} dr\right)\right). \end{aligned} \quad (3.11)$$

Setting $D \rightarrow \infty$, $r(x) = l^{-1}(x)$, followed by straightforward manipulations, it is then easy to show that

$$\begin{aligned} \lim_{D \rightarrow \infty} \mathcal{F}I_D(\omega) &= \lim_{D \rightarrow \infty} D^2 \left(-1 + \int_0^D \frac{2r}{D^2} \exp^{j\omega l(r)} dr\right), \\ &= \int_0^\infty (l^{-1}(x))^2 j\omega \exp^{j\omega x} dx. \end{aligned} \quad (3.12)$$

Therefore,

$$\mathcal{F}_I(\omega) = \exp\left(j\lambda_I \pi \omega \int_0^\infty (l^{-1}(x))^2 \exp^{j\omega x} dx\right). \quad (3.13)$$

Applying the standard path-loss model, $l(r) = r^{-n}$, (3.13) is then reduced to:

$$\mathcal{F}_I(\omega) = \exp\left(j\lambda_I \pi \omega \int_0^\infty x^{-\frac{2}{n}} \exp^{j\omega x} dx\right). \quad (3.14)$$

The transmission path between the UE interferers and the aircraft is characterised by the ground- aerial channel model. Hence

$$r = \sqrt{g_d^2 + v_d^2}, \quad (3.15)$$

where r is the distance between the UE and the aircraft, g_d and v_d are the horizontal distance and height between the UE and aircraft. If $n \leq 2$, the integral in (3.14) diverges hence, the interference is infinite [105]. However, when $n > 2$, then, $0 < \frac{2}{n} < 1$ and (3.14) is further simplified to

$$\mathcal{F}_I(\omega) = \exp\left(-\lambda_I \pi \Gamma(1 - \theta) \exp^{-\frac{\pi\theta}{2}} \omega^\theta\right), \quad \omega \geq 0, \quad (3.16)$$

where $\theta = \frac{2}{n}$, and $\mathcal{F}_I^*(-\omega) = \mathcal{F}_I(\omega)$.

The following proposition proof that $n > 2$.

Proposition 3.2: The air- to -ground (ATG) channel path loss (PL_{ATG}) between the licensee UE and the aircraft is equivalent to $r^{-(2+\delta)}$, $\delta > 0$.

Proof: We first show that the ATG channel can be approximated by the standard path-loss model, $l(r) = r^{-n}$ and then it is shown that $n > 2$. The ATG path - loss in dB is [80]:

$$PL_{ATG}(\text{dB}) = \text{FSPL} + \Delta_{\rho}, \quad (3.17)$$

where FSPL is the free space path-loss, Δ is the excessive path-loss which depends on the propagation group $\rho \in \{\text{LoS}, \text{NLoS}\}$. Thus:

$$PL_{ATG} = \begin{cases} \text{FSPL} + \Delta_{\text{LoS}} & \rho = \text{LoS}, \\ \text{FSPL} + \Delta_{\text{NLoS}} & \rho = \text{NLoS}. \end{cases} \quad (3.18)$$

The spatial expectation of the path-loss between the aircraft and all UE can thus be expressed as:

$$\mathbb{E}\{PL_{ATG}(\text{dB})\} = \sum_{\rho} PL_{\rho} \Pr\{\rho\}, \quad (3.19)$$

where $\Pr\{\cdot\}$ is the probability of occurrence of line of sight (LoS) or non-line of sight (NLoS) propagation which is linked by the expression

$$\Pr\{\text{LoS}\} = 1 - \Pr\{\text{NLoS}\}. \quad (3.20)$$

By the virtue of (3.20), there are two extremes: (i) when the $\Pr\{\text{LoS}\} = 1$, which implies only LoS propagation and (ii) when $\Pr\{\text{LoS}\} = 0$, which is when only NLoS propagation exists between all the UE and the aircraft. Thus assuming only LoS propagation, (3.17) in watts is:

$$PL_{\text{LoS}(w)} = 10^{\left(\frac{\text{FSPL}}{20} + \frac{\Delta_{\text{LoS}}}{10}\right)}, \quad (3.21)$$

From (3.21) and applying the standard distance - path loss relation, $PL \propto r^{-n}$, we can write

$$r^{-n} = r^{-(2+\delta)}, \quad \delta > 0, \quad (3.22)$$

where the index '2' is the path loss exponent for FSPL and δ is the exponent of the excessive path loss. Since path-loss exponent n for NLoS is shown to be greater than 2, and $\Delta_{\text{NLoS}} \gg \Delta_{\text{LoS}}$, hence it can be concluded that $n > 2$. ■

Following the same line of argument as in [106], the pdf of (3.16) is then estimated as an infinite series. Applying to it inverse Fourier transform, we then obtain

$$\begin{aligned} f_I(i; \theta) &= \frac{1}{\pi i} \sum_{k=1}^{\infty} \frac{\Gamma(\theta k + 1)}{k!} \left(\frac{\lambda_I \pi \Gamma(1 - \theta)}{i^\theta} \right)^k \sin k\pi(1 - \theta) \\ &= \frac{1}{\pi i} \sum_{k=1}^{\infty} \frac{\Gamma(\theta k + 1)}{k!} \left(\frac{\rho}{i^\theta} \right)^k \sin k\pi(1 - \theta), \end{aligned} \quad (3.23)$$

where $\rho = \lambda_I \pi \Gamma(1 - \theta)$, and $f_I(i; \theta)$ is the pdf of the received interference. ■

By implication (3.23) indicates that for very large numbers of UEs, i.e., as $k \rightarrow \infty$, the interference distribution can be accurately approximated by $f_I(i; \theta)$. However for small number of UEs, the expression might not adequately describe the interference distribution.

3.1.2 The Interference Propagation Path

Following the same line of argument as in 3.1.1, the propagation path for the interference due to the UEs as well as the interference due to the eNodeB is characterized as the air-to-ground path loss model and the extended Hata model respectively.

3.1.2.1 Air-to- Ground Pathloss Model

The path between the UE interferers and the flying aircraft is analogous to the air to ground channel model. According to [80], the transmitter–receiver path/air to ground channel (ATG) can be characterised as:

$$PL = \sum_{\rho} PL_{\rho} \Pr\{\rho, \theta\}, \quad (3.24)$$

where PL, stands for the path loss between the aircraft and the ground receivers or UEs, $g \in \{\text{LoS}, \text{NLoS}\}$, is the propagation group, where LoS and NLoS are the line of sight and non line of sight propagation respectively. In (3.24), $\Pr\{\rho, \theta\}$ is the probability of LOS and NLOS, θ is the elevation angle between a ground UE and the aircraft, and

$$PL_{\rho} = \text{FSPL} + \xi_{\rho}. \quad (3.25)$$

In (3.25) FSPL is the free space path loss and ξ is the excessive path loss, which is, propagation group (LOS or NLOS) and environment dependent. Note that ξ_{LoS} , can be approximated by a log-normal distributed with location variability parameter ζ_{LoS} [107], while for the

Table 3.3 Parameters for $\Pr\{\text{LoS}, \theta\}$ in (3.26) [5].

Environment	a	b	c	d	e
Suburban	101.6	0	0	3.25	1.241
Urban	120.0	0	0	24.30	1.229
Dense Urban	187.3	0	0	82.10	1.478
Urban High-Rise	352.0	-1.37	-53	173.80	4.670

ξ_{nLoS} , an additional building roof top diffraction loss l_b [5] is factored into the equation, i.e., $\xi_{\text{nLoS}} = \zeta_{\text{nLoS}} + l_b$.

Using the ITU-R recommendations P-1410 [108], $\Pr\{\rho, \theta\}$ for LoS propagation is obtained in [5] as:

$$\Pr\{\text{LoS}, \theta\} = a - \frac{a-b}{1 + \left(\frac{\theta-c}{d}\right)^e}, \quad (3.26)$$

where a, b, c, d , and e , are parameters obtained from extensive simulations and presented in ITU-R recommendations P-140 [108] and experimentally validated in [5]. Table 3.3 presents the values obtained from the experiment

Substituting FSPL, (3.25), (3.26) into (3.24) and noting that transmitter-to-receiver distance is $r = \sqrt{v_d^2 + g_d^2}$, the path loss is then expressed as a function of elevation angle:

$$\begin{aligned} \text{PL}(\theta) = & 20\log(g_d) + 10\log\left(1 + (\tan\theta)^2\right) + k + \zeta_{\text{nLoS}} + l_b \\ & + A \left[a - \frac{a-b}{1 + \left(\frac{\theta-c}{d}\right)^e} \right], \quad \text{if } g_d > v_d, \end{aligned} \quad (3.27a)$$

$$\begin{aligned} \text{PL}(\theta) = & 20\log(v_d) + 10\log\left(1 + \frac{1}{(\tan\theta)^2}\right) + k + \zeta_{\text{nLoS}} + l_b \\ & + A \left[a - \frac{a-b}{1 + \left(\frac{\theta-c}{d}\right)^e} \right], \quad \text{if } g_d \leq v_d, \end{aligned} \quad (3.27b)$$

or as a function of the aircraft altitude and the ground/horizontal distance of the UEs:

$$\begin{aligned} \text{PL}(v_d, g_d) = & 20\log(g_d) + 10\log\left(1 + \frac{v_d^2}{g_d^2}\right) + k + \zeta_{\text{nLoS}} + l_b \\ & + A \left[a - \frac{a-b}{1 + \left(\frac{\tan^{-1}\left(\frac{v_d}{g_d}\right) - c}{d}\right)^e} \right], \quad \text{if } g_d > v_d, \end{aligned} \quad (3.28a)$$

$$\begin{aligned}
\text{PL}(v_d, g_d) &= 20 \log(v_d) + 10 \log \left(1 + \frac{g_d^2}{v_d^2} \right) + k + \zeta_{\text{nLoS}} + l_b \\
&+ A \left[a - \frac{a-b}{1 + \left(\frac{\tan^{-1}(\frac{v_d}{g_d}) - c}{d} \right)^e} \right], \quad \text{if } g_d \leq v_d,
\end{aligned} \tag{3.28b}$$

where g_d is the horizontal distance of the UEs in Km, v_d , is the altitude of the aircraft also in Km, $k = 20 \log(f) + 92.4$, f is the carrier frequency in GHz, and $A = \xi_{\text{LoS}} - \xi_{\text{nLoS}}$.

3.1.2.2 Extended Hata Model

In line with the recommendation contained in the report by the U. S. department of commerce, National Telecommunication and Information Administration (NTIA) in [109], the extended Hata model (eHata) is adopted for the signal attenuation along the path between the licensee interferers (both the UE and the eNodeB) and the ATC tower. The model is valid for frequency range from 1500–3000 MHz, distance of 1–100 Km, transmitter and receiver height of 30–200 m and 1–10 m respectively.

Therefore, the eHata point to point median basic transmission loss for an urban outdoor environment is:

$$\begin{aligned}
\text{PL}_{\text{eH}}(f, r, h_B, h_R) &= L_{\text{bm}}(f, R_{\text{bp}}) + 10n \log \left(\frac{r}{R_{\text{bp}}} \right) + 13.82 \log \left(\frac{200}{h_B} \right) \\
&+ v(3) - v(h_R) + \text{PL}_{\text{fs}}(f, R(r, h_B, h_R)),
\end{aligned} \tag{3.29a}$$

$$\begin{aligned}
L_{\text{bm}}(f, R_{\text{bp}}) &= 30.52 - 16.81 \log f \\
&+ 4.45(\log f)^2 + (24.9 - 6.55 \log h_B) \log R_{\text{bp}},
\end{aligned} \tag{3.29b}$$

$$v(h_R) = (1.1 \log f - 0.7)h_R - 1.56 \log f + 0.8, \tag{3.29c}$$

$$R_{\text{fs}}(r, h_B, h_R) = \sqrt{(r \times 10^3)^2 + (h_B - h_R)^2}, \tag{3.29d}$$

$$R_{\text{bp}} = \left(10^{2n_h} \frac{l_{\text{bm}}(f, 1)}{l_{\text{bm}}(f, 100)} \right)^{\frac{1}{(n_h - n_l)}}, \tag{3.29e}$$

$$n = \begin{cases} 0.1(24.9 - 6.55 \log h_B) & \text{for } 1\text{km} \leq r \leq R_{\text{bp}}, \\ 2(3.27 \log h_B - 0.67(\log h_B)^2 - 1.75)d, & \text{for } R_{\text{bp}} \leq r \leq 100\text{km}, \end{cases} \tag{3.29f}$$

and L_{bm} is the basic median attenuation relative to free space, r is the transmitter-receiver separation distance, R_{bp} is the breakpoint distance, h_B and h_R is the transmitter and receiver

antenna height respectively, $v(h_R)$ is the receiver's reference height correction factor, PL_{fs} is the free space path loss at distance R_{fs} , f represents the transmission frequency, n_h and n_l are the transmitter's effective height dependence of the higher and lower distance path loss exponent of the median attenuation relative to free space respectively, and l_{bm} is the frequency extrapolated basic median transmission relative to free space. For a suburban outdoor environment the eHata Pathloss model is,

$$PL_{eHs} = PL_{eH} - (54.19 - 33.30 \log f + 6.25(\log f)^2), \quad (3.30)$$

where PL_{eHs} is the eHata Path loss model for the suburban environment and PL_{eH} is its urban equivalent presented in (3.29a)- (3.29f).

3.1.3 UE Mobility Model

Before moving, the UE are initially placed randomly in the eNodeB coverage area of radius R with a radial density according to (3.9). To characterize the possible mobility of the UE in the eNodeB coverage area, the random waypoint mobility model is adopted in this thesis. Let T represent the total travel time and t the index of different travel times either side of the pause time T_p . If the randomly selected speed of movement of the UE is denoted by V and their corresponding destination is represented by \mathbf{M} , the UE mobility process can then be characterised as [110]

$$\{\mathbf{M}_t, T_{p,t}, V_t\} = \{\mathbf{M}_1, T_{p,1}, V_1, \dots, \mathbf{M}_N, T_{p,N}, V_N\} \quad \forall t = 1, \dots, N, \quad (3.31)$$

where \mathbf{M}_t is the destination point of a UE at a specific t^{th} travel time, with $\mathbf{M}_t \ni \{X_t, Y_t\}$, $T_{p,t}$, is the pause time at \mathbf{M}_t and V_t is the velocity of the UE during the t^{th} travel time.

For the circular eNodeB coverage area of radius R , the random destination points $\mathbf{M}_j \ni \{X_j, Y_j\} = \mathbf{M}_t \ni \{p_t, \vartheta_t\}$ in polar coordinates has their pdf given as [111]

$$f_{\mathbf{M}}(p; \vartheta) = \frac{1}{\pi R^2} \quad \text{for } 0 \leq p \leq R, \text{ and } 0 \leq \vartheta \leq 2\pi. \quad (3.32)$$

The pdf of the distance between two consecutive points, i.e., the spatial length during a unit movement period, $Lm_t = \mathbf{M}_t - \mathbf{M}_{t-1}$ [112] of a circular plane is given as [111],

$$f_{Lm}(lm) = \begin{cases} \frac{8}{\pi R^2} \frac{lm}{2R} \left(\arccos \frac{lm}{2R} - \frac{lm}{2R} \sqrt{1 - \left(\frac{lm}{2R}\right)^2} \right) & 0 \leq lm \leq 2R, \\ 0 & \text{otherwise.} \end{cases} \quad (3.33)$$

The expected value of Lm is:

$$\mathbb{E}\{Lm\} = \int_0^{2R} lm f(lm) dl \quad (3.34)$$

Similarly, the probability density for the distribution of T is given as

$$f_T(t) = \int_0^\infty \vartheta f_L(\vartheta t) f_V(\vartheta) d\vartheta \quad \text{for } t \geq 0. \quad (3.35)$$

Factoring the pause time T_p into the equation (3.35) becomes:

$$f_{T'}(t') = \int_0^{t'} f_T(t) f_{T_p}(t' - t) dt \quad \text{for } t' \geq 0, \quad (3.36)$$

and its expectation is

$$\mathbb{E}(T') = \mathbb{E}(T) + \mathbb{E}(T_p), \quad (3.37)$$

where $T' = T + T_p$, V_j is randomly and uniformly chosen from $[V_{\min}, V_{\max}]$ under the assumption that $V_{\min} > 0$ and $T_{p,\min} \geq 0$ [110], T_p is chosen from the interval $[T_{p,\min}, T_{p,\max}]$ with an arbitrary pdf and expected value $\mathbb{E}\{T_p\}$.

The first category of the incumbents in the 2.3 GHz-2.4 GHz, i.e., the aeronautical telemetry is described in this section. It should be noted that the air-to-ground interference path in addition to the usual terrestrial path between the incumbent airborne victim receiver and the licensee interfering transmitter adds an extra dimension to the interference threshold requirement that the licensee's system must factor into its operation. This is because the better LoS in the air-to-ground path results in stronger interference signal and thus more adjustment in the transmit power of the licensee is needed. The system model and scenarios described in this section (i.e., **section 3.1**) is adopted for the works presented in the first three sections of **chapter 4**. The next section describes the second category of incumbents which does not have to contend with the peculiarity of the air-to-ground interference path.

3.2 PMSE and PPDR Incumbent

The system model presented in this section, considers a vertical LSA spectrum sharing between a mobile network operator (MNO), as the licensee, and services and applications deployed under the public protection and disaster relief (PPDR) such as the police, emergency health service, fire fighting service, as well as the programme making and special events (PMSE) applications such as the cordless camera, portable video link, mobile video link, etc.



Fig. 3.2 A schematic of the considered aerial-terrestrial LSA system.

as the incumbent systems. Also assuming a circular coverage area of radius R , comprising the main MNO system: a terrestrial eNodeB operating at the legacy cellular spectrum bands, and the LSA licensee system: a D-BS borrowing the incumbent's spectrum to cater for surplus traffic above the capacity of the terrestrial eNodeB. Within the coverage area are K randomly located user equipment (UEs) (Fig. 3.2). The D-BS becomes operational only when the terrestrial eNodeB couldn't meet the traffic demand within its coverage area.

The transmission link from the transmitter in the incumbent system to the receiving devices uses the same channel as the licensee downlink. The reverse transmission link between the ground user transmitters to the incumbent receiver uses the same channel as the licensee uplink. Since, the transceiver at the incumbent's core network is presumed to be far from the field and the licensee UEs' operating power is relatively small, the interference caused to the incumbent system by transmissions in the uplink is negligible.

3.2.1 Spatial Distribution of UEs

Assuming there are K UE in the eNodeB coverage area of an MNO, the UE distribution is modelled as a bivariate marked Poisson Point Process [113]:

$$\varphi = \{[y_1; \xi_1], [y_2; \xi_2], \dots, [y_K; \xi_K]\}, \quad (3.38)$$

where y_k is the location of individual UE in the eNodeB coverage area, $\xi \in \{V, eB\}$ marks the UE as belonging to either the set of users that constitutes the surplus traffic requirement of the system or otherwise, V is the mark for the UE served by the D-BS, while eB is the mark for UE served by the terrestrial eNodeB. Subsequently, the mark distribution of the Poisson process is given by $Z(V) = \frac{\lambda_U}{\lambda}$, where λ and λ_U are the density of all UEs, and the UEs belonging to the surplus traffic set S , respectively.

3.2.2 Capacity Demand Variation

Since the D-BS and the LSA concept are meant to complement the existing terrestrial systems, the proposed architecture is meant to adapt to the excess capacity demand resulting from the variations in wireless traffic and/or service demand. We begin by defining R_k as the minimum data rate demand for user k in the coverage area, thus total traffic requirement, \mathbf{R}_T , is

$$\begin{aligned} \mathbf{R}_T &= \sum_{k \in \varphi} R_k = \sum_{k=1}^{S_{UE} \subset K} R_k^V + \sum_{k=1}^{K \setminus S_{UE}} R_k^{eB} \\ &= \text{BW} \log_2 \prod_{k=1}^K \left(1 + \frac{P_k}{\text{PL}_k(v_d, g_d) N} \right), \end{aligned} \quad (3.39)$$

where $S_{UE} \subset K$ is the group of k UE that constitutes excess capacity need of the network, $K \setminus S_{UE}$ is the group of k UE that makes up the normal load of the network, BW , P_k , $\text{PL}_k(v_d, g_d)$ and N are the transmission bandwidth, transmit power allocated to user k , the path loss between the eNodeB (aerial or terrestrial) and user k , and the respective noise power.

The individual user k rate requirement is met, if $\gamma_k \geq \gamma_{\text{th}}$, and

$$\gamma_k = \frac{P_k}{\text{PL}_k(v_d, g_d) N}, \quad (3.40)$$

is the signal-to-noise ratio (SNR) of a user, where γ_{th} is a threshold which indicates the minimum SNR for the user's capacity need to be satisfied. By substituting $\mathbf{R}_{\text{TG}} = \sum_{k=1}^{S_{UE} \subset K} R_k^V$, $\mathbf{R}_{\text{NL}} = \sum_{k=1}^{K \setminus S_{UE}} R_k^{eB}$ and assuming a mean rate \bar{R}_k , (2.2) simplifies to

$$\mathbf{R}_T = \mathbf{R}_{\text{NL}} + \frac{Z(V)}{1 - Z(V)} \mathbf{R}_{\text{NL}}, \quad (3.41)$$

where \mathbf{R}_{TG} and \mathbf{R}_{NL} are the excess capacity demand and the normal traffic load of the network respectively. It goes without saying that the proposed aerial LSA licensee system becomes operational only if $Z(V) > 0$, otherwise, there is no need to activate it.

3.3 Chapter Summary

In this chapter, the many incumbents of the 'LTE Band 40' have been grouped into two broad categories. The first category, the aeronautical telemetry is differentiated from the the class of incumbents by the additional air-to-ground propagation channel that needed to be factored into the design and practical implementation of the LSA sharing scheme under this scenario. Expressions for the possible interference received by the incumbent system from the licensee interferes in both the downlink and uplink transmission was derived. Also in *Proposition 3.2*, it was proven that the interference probability density function of UEs in a Poisson network in [106] is applicable to the peculiar air-to-ground propagation path between the licensee's uplink interferers and the aeronautical telemetry airborne victim receiver. The assumed scenario and the model described in this section is the basis for the proposed methods in **section 4.1**, **section 4.2**, and **section 4.3**. In **section 3.2**, the system model for the second group of incumbents which comprises mainly terrestrial propagation path between the interfering licensee system and the incumbent vicim receivers was presented. Specifically, assuming a hybrid aerial-terrestrial licensee system, the spatial distribution of the UE on the licensee network is modelled by a bivariate marked Poission process. On the basis of this, the total capacity of the hybrid aerial-terrestrial licensee system was formulated as the sum of the installed capacity of the terrestrial eNodeB and the excess traffic demand. The model presented in this section forms the basis of the proposed solution in **section 4.4** and the results analysis in **section 6.4**.

3.4 Conclusion

In this chapter two system models adopted for the research work presented in this thesis were discussed. The justification for the models is the fact that the different incumbents occupying the 2.3 GHz - 2.4 GHz band considered for the LSA in this work can be classified into two distinct groups defined by their peculiar signal transmission as well as operating characteristics. The channel and interference models peculiar to each of the distinct group are adopted to reflect realistic practical implementation and operating conditions as much as possible. This is also factored into the derivation of expressions for the interference received by the incumbent from the licensee's transmission both in the uplink and downlink.

The consideration of a wide circular protection radius in the aeronautical telemetry incumbent system model, made investigation of several scenarios possible. First, a single LSA licensee cell was assumed for both the uplink and downlink propagation direction. This then form a basis for investigating the LSA scheme over a large geographical area with many

eNodeB coverage areas. The peculiarity of the propagation path between the aeronautical transceivers also influence the different scenarios assumed as well as consideration of both the downlink and uplink interference and channel models.

Chapter 4

Spectral - Energy Efficiency and QoS Guarantee in Dynamic Licensed Shared Access

4.1 Energy Efficiency Under the Limited Power Regime

To implement the dynamic LSA specified in [114], the authors of [39] recommended the ‘limited power regime’ amongst the three power regimes considered in their work. Instead of outright shutting down of the licensee transmission when the incumbent expresses its desire to use the spectrum, the limited power regime suggests a reduction in the operating power of the licensee such that the aggregate interfering signal power does not exceed the maximum tolerable interference at the incumbent system. However, while the limited power regime fills the spectrum hole created by the outright revocation of the spectrum, it may nonetheless result in significant degradation of the licensee’s achievable network capacity [41]. The scenario examined in this section is analogous to the eNodeB coverage area A of Fig. 3.1.

Firstly, the required power adjustment necessitated by the revocation of the licensee’s spectrum access right is computed from the potential interference received at the incumbent system and the incumbent interference threshold. Taking into account the peculiar interference propagation paths in both the uplink and the downlink, corresponding expressions for the limited transmit power are derived as a function of the licensee’s maximum transmit power and, the computed power adjustment in both transmission directions. Consequently an optimization problem is formulated to maximize the EE when the licensee is operating under the limited power regime.

Since the ensuing optimization problem has an objective that is a ratio of two functions, it is not convex. The Charnes-Cooper transformation method is then used to convert the fractional objective function into a quasi-convex function. Solving the transformed optimization problem using the classical Karush-Kuhn Tucker method, yields an optimal allocation of the limit power that maximizes the licensee's EE.

4.1.1 The Limited Transmit Power

When the licensee has unrestricted access to the spectrum, the MNO can transmit up to its maximum rated power. However, when the incumbent demands the use of its spectrum, the MNO must reduce its transmit power by an amount that will ensure the aggregate interference at the incumbent receiver (either the aircraft or the ATC tower, depending on the transmission link direction) is at most equal to its maximum tolerable interference. Similar to the approach in [41], this transmit power differential, P_{Δ} , is defined as follow:

$$P_{\Delta} = I_{\Xi} - I_{\text{th}}, \quad (4.1)$$

where I_{Ξ} represents the interference received by the incumbent as a result of the licensee's transmission, which could be from the eNodeB or the UEs', hence $\Xi \in \{\text{UPLINK}, \text{DOWNLINK}\}$ and I_{th} is the incumbent's interference threshold. The limited power can then be written as:

$$P_{\text{LT}} = \begin{cases} P_{\text{max}} - P_{\Delta} & P_{\Delta} > 0, \\ P_{\text{max}} & \text{otherwise,} \end{cases} \quad (4.2)$$

where P_{LT} , is the limited power which the licensee must transmit with, during the revocation of its spectrum access right; while P_{max} , is the transmit power of the licensee when it has full and unrestricted access to the LSA spectrum.

Eq. (4.2) implies that, if the interfering signal power of the licensee is less than or equal to the incumbent's tolerable interference threshold, it will not be necessary for the transmit power of the licensee to be reduced. However, as expected, if the interfering power of the licensee is greater than the incumbent's maximum tolerable interference, the licensee's transmit power must be reduced by an equivalent amount when the incumbent demand the use of its spectrum.

Assuming an incumbent receiver is located at a point y , within the interfering range of the licensee, I_{Ξ} is given as

$$I_{\Xi} = \sum_{k \in K} P_k F_k l(\|y - x_k\|), \quad (4.3)$$

$$l(r) = \|r\|^{-n},$$

where K is the set of all transmitting nodes, F_k represents the power fading coefficient for a node k with transmit power P_k , l denotes distance-related power loss, r is the transmitter-receiver separation distance, while n is the path loss exponent.

In the downlink direction, I_{Ξ} is the interference due to the eNodeB transmission. Assuming a single eNodeB coverage area, (4.3) is, therefore, written as

$$I_{\Xi} = I_{BS} = P_B F_B l(B), \quad (4.4)$$

where I_{BS} is the interference received at the ATC tower due to the eNodeB's transmissions with transmit power P_B , while h_B and $l(B)$ are the power fading and path loss along the transmission path between the MNO eNodeB and the ATC tower.

However, for the uplink direction, I_{Ξ} is the aggregate or cumulated interference of many transmitters (UEs) characterized by the Poisson spatial distribution of the UEs in the eNodeB coverage area. Therefore, the interference to a given incumbent receiver (both the terrestrial ATC tower and the airborne aircraft) located at a point within the vicinity of the UEs transmission range is

$$I_{\Xi} = I_{MS} = \sum_{k \in \varphi} P_k F_k l(k), \quad (4.5)$$

$$\varphi = \{k_1, k_2, \dots, k_K\},$$

where similarly to (4.4), I_{MS} , P_k , h_k and $l(k)$ are the UEs equivalent interference, transmit power, fading and path loss respectively, along the transmission path between the MNO UEs and the flying aircraft. φ is the stochastic point process describing the spatial distribution of the UEs in the eNodeB coverage area of the LSA licensee. For $n > 2$, the probability density function (PDF) of I_{MS} is [105]:

$$f_I(i; \beta) = \frac{1}{\pi i} \sum_{k=1}^{\infty} \frac{\Gamma(\beta k + 1)}{k!} \left(\frac{\lambda_I \pi \Gamma(1 - \beta)}{i^\beta} \right)^k \sin k \pi (1 - \beta), \quad (4.6)$$

where $\beta = \frac{2}{n}$, $\Gamma(\cdot)$ is the gamma function.

By substituting (4.1) and (4.4) into (4.2), the limited power for the downlink is obtained thus:

$$P_{LT} = P_B \left(1 - F_{Bl}(B) \right) + I_{th}, \quad P_{max} = P_B. \quad (4.7)$$

In order to obtain the limited power for the uplink, I_{th} as in [115] is decoupled by introducing a new set of variables $[I_{thk}, \dots]$. Thus the uplink limited transmit power for each UE can be written as:

$$P_{LT} = P_k \left(1 - F_{kl}(k) \right) + I_{thk}, \quad P_{max} = P_k. \quad (4.8)$$

From (4.5), the UEs' to eNodeB channel set are defined as $\mathbf{K} = [k_1, \dots, k_K]$. Similarly, the equivalent downlink (eNodeB to UEs') channel set can be defined as $\mathbf{B} = [b_1, \dots, b_B]$. Hence for $P_{\Delta} > 0$, the limited transmit power in the licensee downlink as well as uplink transmission direction is re-written as:

$$P_{LT} = \begin{cases} \sum_{b=1}^B P_b \left(1 - F_{Bl}(B) \right) + I_{th}, & P_{max} = P_B, \\ P_k \left(1 - F_{kl}(k) \right) + I_{thk}, & P_{max} = P_k, \end{cases} \quad (4.9)$$

where $\sum_{b=1}^B P_b = P_B$.

By substituting the interference propagation path loss models in (3.28) and (3.30), the expression for limit power in (4.9) can be re-written as:

$$P_{LT} = \begin{cases} \sum_{b=1}^B P_b \left(1 - F_B(\text{PL}_{eH})^{-1} \right) + I_{th} & P_{max} = P_B, \\ P_k \left(1 - F_k \text{PL}_{eH}^{-1} \right) + I_{thk} & P_{max} = P_k, \\ P_k \left(1 - F_k \text{PL}_k(v_d, g_d)^{-1} \right) + I_{thk} & P_{max} = P_k, \end{cases} \quad (4.10)$$

where $l(k)$ in (4.9) could be PL_{eH} or $\text{PL}_k(v_d, g_d)$ depending on the victim receiver of the incumbent.

4.1.2 The Licensee Energy Efficiency

EE reflects the communication system energy performance and is defined as the achieved spectrum efficiency (SE) in bit/sec/Hz for a Joule of energy consumed in the system. Therefore, EE, η_{EE} , is:

$$\eta_{EE} = \frac{\eta_{SE}}{P_S}. \quad (4.11)$$

Algorithm 1 Algorithm for Decoupling I_{th}

-
- Step 1.** Initialise the eNodeB radius(R), No. of UEs (K), ATG model parameters, and the incumbent's interference threshold (I_{th});
- Step 2.** Generate the random radial x and y coordinates of the UE's in a circular region of radius R .
- 2.1. Compute the distance of each UE to the aircraft,
 - 2.2. Compute the propagation losses each UE to the aircraft path, $PL_k(v_d, g_d)$;
- Step 3.** for $k = 1$ to K ,
- $$I_{\text{th}k} = I_{\text{th}} \times \frac{PL_k(v_d, g_d)}{\sum_{k=1}^K PL_k(v_d, g_d)}.$$
-

The achieved spectrum efficiency, η_{SE} , is

$$\eta_{\text{SE}} = \sum_{\Xi=1}^{\{K,B\}} \log_2 \left(1 + P_{\Xi} g_{\Xi} \right).$$

where g_{Ξ} is the normalised channel gain over noise [78] for either the uplink or downlink transmission direction. The total consumed power, P_S , is

$$P_S = P_c + \frac{1}{\varepsilon} \sum_{\Xi=1}^{\{K,B\}} P_{\Xi},$$

where P_c is the circuit power and ε is the amplifier efficiency.

During the time when the incumbent system revokes the unrestricted right of access to its spectrum, the EE of the licensee is

$$\eta_{\text{EE}} = \frac{\sum_{\Xi=1}^{\{K,B\}} \log_2 \left(1 + P_{LT} g_{\Xi} \right)}{P_c + \frac{1}{\varepsilon} \sum_{\Xi=1}^{\{K,B\}} P_{LT}}. \quad (4.12)$$

4.1.3 Energy Efficient Limited Power Allocation

Assuming perfect channel state information (CSI) at the transmitter, in this section we formulate optimal power allocation to maximize the EE of the licensee system, during the period its right of spectrum access is constrained by the interference threshold of the incumbent. By substituting (4.9) into (4.12), the EE optimization problem for the uplink is

formulated as follows:

$$\eta_{\text{UL}}^* = \max_{(\mathbf{P})} \frac{\sum_{k=1}^K \log_2 \left(1 + \frac{P_k(1 - F_{kl}(k)) + I_{\text{thk}}}{L_k N} \right)}{P_c + \frac{1}{\varepsilon} \sum_{k=1}^K P_k (1 - F_{kl}(k)) + I_{\text{thk}}}, \quad (4.13)$$

and for the downlink as

$$\eta_{\text{DL}}^* = \max_{(\mathbf{P})} \frac{\sum_{b=1}^B \log_2 \left(1 + \frac{P_b(1 - F_{Bl}(B)) + \frac{I_{\text{th}}}{B}}{L_d N} \right)}{P_c + \frac{1}{\varepsilon} \sum_{b=1}^B P_b (1 - F_{Bl}(B)) + \frac{I_{\text{th}}}{B}}, \quad (4.14)$$

where $g_{\Xi} = \frac{1}{L_{\Xi} N}$ and L_{Ξ} is the transmission channel path loss between the eNodeB and the UEs in both uplink and downlink and N is the noise power. In (4.13), to obtain the fraction of the interference to be factored into each of the downlink channel power allocation, the I_{th} is decoupled by averaging it over the total number of the downlink channels.

As ratio of two functions, (4.13) and (4.14) are fractional optimization problems. The implication of this, as shown in [116], is that in optimization problem involving objective functions of such fractional nature, the classical convex optimization solution might not be directly applicable. This is because there is no guarantee that the problem lends itself to properties and results which holds for convex optimization problems even when it is assumed that both functions (numerator and denominator) are affine functions. For instance, such fractional problems could have stationary points that are not globally optimal. Besides, while the Karush-Kuhn- Tucker (KKT) conditions of such problems might be necessary they might not be not sufficient for optimality [116].

However in [117], it is noted that such problems that are neither convex nor concave can be characterised by an extension to convexity/concavity termed *generalised concave/convex functions*. Such functions include: quasi-concave/convex, pseudo-concave/convex, logarithmic-concave/convex, etc. Since (4.13) and (4.14) are strictly quasi-concave; classical convex optimization solution can thus be applied.

Proposition 4.1: The objective functions in (4.13) and (4.14) are strictly quasi-concave.

Proof: Here it is first shown that the numerator in (4.13) or (4.14) is a concave function of P_k . From (4.14) we have:

$$\sum_{k=1}^K \log_2 \left(1 + \frac{P_k(1 - F_{kl}(k)) + I_{\text{thk}}}{L_k N} \right). \quad (4.15)$$

Therefore,

$$\frac{\delta \eta_{SE}}{\delta P_k} = \frac{\frac{1-F_k l(k)}{L_k N}}{\ln(2) \left(1 + \frac{P_k(1-F_k l(k)) + I_{thk}}{L_k N}\right)}. \quad (4.16)$$

To investigate the concavity of η_{SE} , its Hessian is obtained,

$$\frac{\delta^2 \eta_{SE}}{\delta P_k^2} = -\frac{\left(\frac{1-F_k l(k)}{L_k N}\right)^2}{\ln(2)} \left[\frac{1}{\left(1 + \frac{P_k(1-F_k l(k)) + I_{thk}}{L_k N}\right)^2} \right] < 0. \quad (4.17)$$

As it is seen, $\frac{\delta^2 \eta_{SE}}{\delta P_k^2} < 0$, therefore, (4.13) and (4.14) as a ratio of a concave to an affine function according to [117] is strictly quasi-concave. ■

Therefore, the solutions to the optimization problems in (4.13) and (4.14) can be obtained using fractional programming [117]. Using the Charnes-Cooper transformation[116], a ratio of a concave to an affine function optimization problem of the form: $\max_x \frac{f(x)}{g(x)}$ can be transformed into a convex optimization problem as:

$$\max_{t,x} t \cdot f\left(\frac{\phi}{t}\right), \quad (4.18)$$

$$\text{s.t. } t \cdot g\left(\frac{\phi}{t}\right) = 1, \quad \forall i = 1, \dots, I, \quad (4.19)$$

by substituting $\phi = xt$, i.e., $x = \frac{\phi}{t}$, and $t = \frac{1}{g(x)}$ [116].

Adopting a similar procedure, we introduce $\wp = \mathbf{P}\Psi$, where $\Psi = [P_c + \frac{1}{\varepsilon} \sum_{\varepsilon=1}^{\{K,D\}} P_{LT}]^{-1}$. By substituting the introduced variables, (4.13) for the uplink is transformed to:

$$\eta_{UL}^* = \max_{(\wp, \Psi)} \Psi \cdot \sum_{k=1}^K \log_2 \left(1 + \frac{\wp_k (1 - F_k l(k)) + I_{thk}}{\Psi L_k N}\right), \quad (4.20)$$

$$\text{s.t. } \Psi \cdot \left(P_c + \frac{1}{\varepsilon} \sum_{k=1}^K P_k (1 - F_k l(k)) + I_{thk}\right) = 1 \quad (4.21)$$

Therefore, by the Charnes-Cooper variable transformation method[116], the equivalent concave optimization problems for the uplink then becomes:

$$\max_{\mathbf{P}} \Psi \cdot \eta_{SE}, \quad (4.22)$$

$$\text{s.t. } \Psi \cdot \left(P_c + \frac{1}{\varepsilon} \sum_{k=1}^K P_k (1 - F_k l(k)) + I_{thk}\right) = 1 \quad (4.23)$$

$$\rho_k > 0 \quad k = 1, 2, \dots, K. \quad (4.24)$$

and for the downlink is:

$$\max_{\mathbf{P}} \Psi \cdot \eta_{SE}, \quad (4.25)$$

$$\text{s.t.} \quad \Psi \cdot \left(P_c + \frac{1}{\varepsilon} \sum_{b=1}^B P_b (1 - F_{Bl}(B)) + \frac{I_{th}}{B} \right) = 1 \quad (4.26)$$

$$\rho_b > 0 \quad b = 1, 2, \dots, B. \quad (4.27)$$

The Lagrangian function corresponding to (4.22), (4.23) and (4.24) (for the uplink) is:

$$\mathcal{L}(P_k, \chi, v_k) = \Psi \cdot \eta_{SE} - \chi \left[\Psi \cdot \left(P_c + \frac{1}{\varepsilon} \sum_{k=1}^K P_k (1 - F_{kl}(k)) + I_{thk} \right) - 1 \right] + \sum_{k=1}^K v_k P_k. \quad (4.28)$$

The KKT stationarity conditions corresponding to the Lagrangian in (4.28) are:

$$\frac{\delta \mathcal{L}(P_k, \chi, v_k)}{\delta P_k} = 0, \quad \frac{\delta \mathcal{L}(P_k, \chi, v_k)}{\delta \Psi} = 0,$$

which are respectively written as:

$$\frac{(1 - F_{kl}(k)) \cdot \Psi}{\ln(2)(L_k N + P_k (1 - F_{kl}(k)) + I_{thk})} - \chi \cdot \Psi \left[\frac{1 - F_{kl}(k)}{\varepsilon} \right] + v_k = 0 \quad (4.29)$$

and

$$\eta_{SE} - \chi \left[\left(P_c + \frac{1}{\varepsilon} \sum_{k=1}^K P_k (1 - F_{kl}(k)) + I_{thk} \right) \right] = 0. \quad (4.30)$$

Solving for P in (4.29), the optimal power allocation in the uplink transmission direction is then obtained as

$$P_k^* = \frac{\varepsilon}{\ln(2) \cdot \chi (1 - l(k) F_k)} - \left[\frac{L_k \cdot N + I_{thk}}{1 - l(k) F_k} \right], \quad k = 1, \dots, K. \quad (4.31)$$

Following similar steps, the solution to the optimization problems in (4.25)-(4.27), yields the equivalent optimal power allocation in the downlink transmission direction as

$$P_b^* = \frac{\varepsilon}{\ln(2) \cdot \chi \left(1 - l(B)F_B\right)} - \left[\frac{B(L_b \cdot N) + I_{th}}{B \cdot \left(1 - l(B)F_B\right)} \right], \quad (4.32)$$

$$b = 1, \dots, B.$$

Algorithm 2 describes the procedure for implementing the proposed method in this section.

Algorithm 2 Optimal Power Allocation for Maximizing the Licensee EE Under Limited Power Regime

- Step 1.** Initialise circuit power (P_c^Λ), eNodeB radius (R^C), No. of UEs (K^M), eHata pathloss model parameters: f, r, h_B, h_R , ATG parameters: a, b, f, c , LoS & NLoS, values θ^{opt} , transmit power (P_k^Q & P_B^Q), incumbent's interference threshold (I_{th}), Channel Bandwidth (B_w) Noise Power Density (N_0), Amplifier Efficiency (ε);
- Step 2.** Generate the random radial x and y coordinates of the UE's in a circular region of radius R .
- 2.1. Compute the distance of each UE to the eNodeB, and to the ATC and the airborne victim receiver;
 - 2.2. Compute the propagation losses along the paths,
 - 2.3. Compute interference to the incumbent victim receivers,
- Step 3.** Compute the limited power, P_{LT} , using (4.10)
- Step 4.** for $\Lambda = 1$ to length of P_c^Λ ,
for $C = 1$ to length of R^C ,
for $M = 1$ to length of K^M ,
for $Q = 1$ to length of P_k^Q ,
- 4.1. Compute optimal power for the uplink, P_k^* from (4.31)
 - 4.2. Compute optimal energy efficiency, η_{UL}^*
 - 4.3. Repeat steps 4.1 and 4.2 for the downlink using (4.32)
-

4.2 Spectral Efficiency of Dynamic Licensed Shared Access

Protective measures are applied to protect the normal operation of the incumbent system from being adversely affected by the licensees' communication activity. Such measures are therefore crucial components of the LSA, and thus fundamentally affect the achievable spectrum efficiency. Against this background and in view of the envisaged future capacity

demand, this section focuses on investigating and improving the system throughput of an MNO licensee in a vertical LSA sharing while the incumbent, an ATC system is utilizing the spectrum for telemetry services. The scenario investigated assumed many eNodeB coverage areas (see Fig. 3.1) of the license in a geographical area of about 200 km radius along the flight path of the airport. To ensure protection against harmful interference to the incumbent system, the incumbent interference threshold is imposed as constraint on the optimization of the licensee system's maximum achievable SE.

Furthermore, the utilization efficiency of the LSA spectrum within the considered geographical radius is examined. To do this, the availability or not of the LSA spectrum is characterized as a tandem queue with multiple service layers, and then an expression for the utilization efficiency was derived as a utility function of the achievable SE and the ratio of the busy period of each service layer (eNodeB coverage) to the busy period of all the service layers in the tandem queue. It is pertinent considering the fact that the challenge of spectrum scarcity was as a result of inefficiency in the spectrum utilization. Hence, quantifying the efficiency of the spectrum utilization achieved by the LSA is an important consideration.

4.2.1 Licensee System Spectrum Efficiency

In a similar way to 4.1.3, it is assumed that perfect channel state information (CSI) is available at the transmitter. In cases where the incumbent system is not utilizing its spectrum, the licensee is able to transmit at maximum power to guarantee the desired signal to noise ratio (SNR) for each UEs according to its QoS requirement. In the considered model, the users are assumed to be randomly distributed according to (3.3) within the eNodeB coverage area, thus the total system SE, η_{SE} , is the summation of the achievable bit rate for K UEs,

$$\eta_{SE} = \sum_{k=1}^K \log_2 \left(1 + P_k g_k \right), \quad (4.33)$$

where g_k is the channel gain to noise ratio.

4.2.2 Maximizing the Licensee Spectrum Efficiency

If the LSA spectrum is unavailable, the licensee has to limit its transmit-power to ensure that the total interference power of the licensee (the MNO) at the incumbent receiver does not exceed the interference threshold. In other words, the transmit power should be reduced such that the incumbent's outage probability, $1 - \mathcal{P}_s\{\theta\}$, does not exceed a given performance threshold, θ , where $\mathcal{P}_s\{\theta\} = \Pr\{\text{SINR} > \theta\}$ is the transmission success probability. Thus,

while maximizing the achievable SE, the sum transmit power of the licensee must be such that the total interference caused to the incumbent does not cause outage.

To facilitate performance evaluation, and to differentiate uplink and downlink transmissions in the analysis P_{Uk} is defined for the transmit power of the k^{th} UE in the uplink, and equivalently P_{Bk} for the fraction of the eNodeB downlink transmitted power to the k^{th} UE. Therefore, maximizing SE for the uplink is formulated as the following:

$$\eta_{\text{SE}}^* = \max_{P_U} \sum_{k=1}^K \log_2 \left(1 + P_{Uk} g_k \right), \quad (4.34a)$$

$$\text{s.t.} \quad \sum_{k=1}^K P_{Uk} F_k l(r_k) \leq I_{\text{th}}, \quad (4.34b)$$

and for the downlink as:

$$\eta_{\text{SE}}^* = \max_{P_B} \sum_{k=1}^K \log_2 \left(1 + P_{Bk} g_k \right), \quad (4.35a)$$

$$\text{s.t.} \quad P_B F_B l(r) \leq I_{\text{th}}. \quad (4.35b)$$

In (4.34) and (4.35), (4.34b) and (4.35b), are the constraint on the total interference from the licensee's transmissions in the uplink, and downlink, respectively, and I_{th} represents the incumbent's interference threshold, i.e., the maximum allowed interference for incumbent's safe operation.

Since in the uplink, the interference constraint is imposed by multiple randomly distributed sources, to solve (4.34), the sum constraint on the interference power is decomposed as in [115], such that $I_{\text{th}} = \sum_{k=1}^K I_{\text{th}k}$. Thus (4.34) is rewritten as:

$$\eta_{\text{SE}}^* = \max_{P_U} \sum_{k=1}^K \log_2 \left(1 + P_{Uk} g_k \right), \quad (4.36a)$$

$$\text{s.t.} \quad \sum_{k=1}^K P_U \cdot F_k \cdot \text{PL}(v_{dk}, g_{dk}) - \sum_{k=1}^K I_{\text{th}k} \leq 0, \quad (4.36b)$$

$$P_{Uk} > 0 \quad \{k = 1, 2, \dots, K\}. \quad (4.36c)$$

Using $P_B = \sum_{k=1}^K P_{Bk}$, (4.35) is transformed to

$$\eta_{\text{SE}}^* = \max_{(P_B)} \sum_{k=1}^K \log_2 \left(1 + P_{Bk} g_k \right), \quad (4.37a)$$

$$\text{s.t. } F_B \cdot \text{PL}_{eH}(f, r, h_B, h_R) \cdot \sum_{k=1}^K P_{Bk} - I_{\text{th}} \leq 0, \quad (4.37b)$$

$$P_{Bk} > 0 \quad \{k = 1, 2, \dots, K\}. \quad (4.37c)$$

In (4.36) and (4.37), (4.36c) and (4.37c) are the non-negative allocated power constraints for the uplink and downlink, respectively, and the corresponding optimization decision variables are $P_U = [P_{U1}, \dots, P_{UK}]$ and $P_B = [P_{B1}, \dots, P_{BK}]$. Furthermore, $\text{PL}(v_{dk}, g_{dk})$ is the path loss for the air-to-ground channel as a function of the height difference v_{dk} and horizontal separation g_{dk} between the k^{th} UE and the aircraft while $\text{PL}_{eH}(f, r, h_B, h_R)$ stands for the path loss between the eNodeB and the ATC tower as a function of the carrier frequency f , transmitter-receiver separation r between them, h_B is the eNodeB antenna height and h_R is the ATC tower antenna height.

Using the Lagrangian method, we have:

$$\mathcal{L}(P_{Uk}, \lambda, v_k) = \sum_{k=1}^K \log_2 \left(1 + P_{Uk} g_k \right) - \lambda \left(\sum_{k=1}^K P_{Uk} \cdot F_k \cdot \text{PL}(v_{dk}, g_{dk}) - I_{\text{thk}} \right) + \sum_{k=1}^K v_k P_{Uk}, \quad (4.38)$$

and for the downlink

$$\mathcal{L}(P_{Bk}, \lambda, v_k) = \sum_{k=1}^K \log_2 \left(1 + P_{Bk} g_k \right) - \lambda \left(F_B \cdot \text{PL}_{eH}(f, r, h_B, h_R) \cdot \sum_{k=1}^K P_{Bk} - I_{\text{th}} \right) + \sum_{k=1}^K v_k P_{Bk}, \quad (4.39)$$

where $\lambda \geq 0$ and $v_k \geq 0$ are Lagrangian multipliers for the interference and non negative power constraint. For the sake of brevity we will forthwith proceed with the solution of the uplink alone. Consequently, the Karush Kuhn Tucker (KKT) conditions [118] are:

$$\frac{\delta \mathcal{L}}{\delta P_{Uk}} = \frac{g_k}{\ln(2) \text{PL}_k \cdot N_k (1 + P_{Uk} g_k)} - \lambda \left(F_k \text{PL}(v_{dk}, g_{dk}) \right) + v_k = 0, \quad (4.40a)$$

$$\lambda \left(\sum_{k=1}^K I_{\text{thk}} - P_{Uk} \cdot F_k \cdot \text{PL}(v_{dk}, g_{dk}) \right) = 0, \quad (4.40b)$$

and

$$\sum_{k=1}^K v_k P_{Uk} = 0, \quad (4.40c)$$

for the stationarity condition (4.40a) and the complimentary slackness conditions (4.40b) & (4.40c), respectively. If it is assumed that strict inequality holds in the non-negative power constraints of (4.36c), then by virtue of the complimentary slackness (4.40c), the Lagrange multiplier ν_k becomes zero. Thus in order to find the optimal allocated power P_k^* , possible cases of having a non-positive power allocation in some channels needed to be addressed.

In the first case, i.e., where $P_k \geq 0$ for all $k = 1, 2, \dots, K$: applying the KKT stationarity condition in (4.40a) gives,

$$\frac{g_k}{\ln(2)} \left[\frac{\prod_{j \neq k}^K (1 + P_{Uj} g_j)}{1 + P_{Uk} g_k \prod_{j \neq k}^K (1 + P_{Uj} g_j)} \right] = \lambda F_k \text{PL}(v_{dk}, g_{dk}), \quad \forall k \in K, \quad (4.41)$$

Therefore, the optimal allocated power P_{Uk}^* is

$$P_{Uk}^* = \left[\frac{1}{\lambda \ln(2) (F_k \text{PL}(v_{dk}, g_{dk}))} - \frac{1}{g_k} \right], \quad \forall k \in K. \quad (4.42)$$

Following similar steps, the solution to the optimization problems in (4.34)-(4.36), yields the equivalent optimal power allocation in the downlink transmission direction as

$$P_{Bk}^* = \left[\frac{1}{\lambda \ln(2) (F_B \text{PL}_{eH}(f, r, h_B, h_R))} - \frac{1}{g_k} \right], \quad (4.43)$$

$$\forall k \in K.$$

In order to find the optimal allocated power P_k^* , in a situation where some channels have a non positive allocated power, we need to define and redistribute the available power to a set $K_p \subset K$ that contains strictly non-negative power allocations. In this case the optimal allocated power, $P_{\{U,B\}k}^*$, becomes

$$P_{Uk}^* = \left[\frac{1}{\lambda \ln(2) (F_k \text{PL}(v_{dk}, g_{dk}))} - \frac{1}{g_k} \right], \quad (4.44)$$

$$\forall k \in K_p | P_k > 0,$$

and

$$P_{Bk}^* = \left[\frac{1}{\lambda \ln(2) \left(F_{BPL_{eH}}(f, r, h_B, h_R) \right)} - \frac{1}{g_k} \right], \quad (4.45)$$

$$\forall k \in K_p | P_k > 0.$$

Using (4.42) and (4.44) one can numerically determine the optimal λ^* that gives P_{Uk}^* for the optimization problem in (4.34). Similarly, the optimal λ^* that gives P_{Bk}^* for the optimization problem in (4.35) is obtained using (4.43) and (4.45). Algorithm 3 describes the procedure for implementing the proposed method in this section.

Algorithm 3 Optimal Power Allocation for Maximizing the SE
Under Incumbent Interference Threshold Constraint

- Step 1.** Initialise eNodeB radius (R^C), No. of UEs (K^M),
Noise Power Density (N_0), eHata pathloss model parameters:
 f, r, h_B, h_R , ATG parameters: a, b, f, c , LoS & NLoS,
values θ^{opt} , transmit power (P_k^Q & P_B^Q), incumbent's
interference threshold (I_{th}), Channel Bandwidth (B_w),
Aircraft take off speed (V_i), acceleration (A_a),
and protection zone radius (zR);
- Step 2.** Generate the random radial x and y coordinates
of the UE's in a circular region of radius R .
- 2.1. Compute the distance of each UE to the eNodeB,
and to the ATC and the airborne victim receiver;
 - 2.2. Compute the propagation losses along the paths,
 - 2.3. Compute interference to the incumbent victim receivers,
 - 2.4. Compute elements of busy period ratio array, $\text{BP}^{\left(\frac{zR}{R}\right)}$
using Algorithm 6
- Step 3.** for $C = 1$ to length of R^C ,
for $M = 1$ to length of K^M ,
for $Q = 1$ to length of P_k^Q ,
- 3.1. Compute optimal power for the uplink, P_{Uk}^* from (4.44)
 - 3.2. Compute optimal spectrum efficiency, η_{SE}^* in (4.34),
 - 3.3. Repeat steps 3.1 and 3.2 for η_{SE}^* in the downlink.
-

4.2.2.1 Optimal Power Allocation: Rated Transmit Power Constraint

In 4.2.2, the formulated SE optimization problem only considers non-negative power allocation. In reality however, there is an upper bound imposed by the engineering specification on the allocated transmit power, which is the maximum transmit power rating of either

the individual UE or the eNodeB. The rated transmit power is the manufacturer specified maximum power for each transmitting device. It is usually specified as effective isotropic radiated power (EIRP). Factoring this engineering design consideration into the SE maximisation, the corresponding optimization problem in (4.34) and (4.35) can then be re-formulated accordingly. For the uplink transmission, the optimal power allocation for the k^{th} user is upper bounded by the maximum transmit power rating. Thus, (4.34) simplifies to

$$\eta_{\text{SE}}^* = \max_{(P_U)} \sum_{k=1}^K \log_2 \left(1 + P_{Uk} g_k \right), \quad (4.46a)$$

$$\text{s.t.} \quad \sum_{k=1}^K P_{Uk} \cdot F_k \cdot \text{PL}(v_{dk}, g_{dk}) - \sum_{k=1}^K I_{thk} \leq 0, \quad (4.46b)$$

$$P_{Uk} > 0 \quad \{k = 1, 2, \dots, K\}, \quad (4.46c)$$

$$P_{Uk} \leq P_{Rk} \quad \{k = 1, 2, \dots, K\}, \quad (4.46d)$$

where P_{Rk} is the rated power of each individual UE. In the uplink, the rated power constraint is for each individual transmitting node.

However, for the downlink case, the rated power constraint is a sum power constraint across all the receiving UEs. Thus (4.35) is re-formulated as

$$\eta_{\text{SE}}^* = \max_{(P_B)} \sum_{k=1}^K \log_2 \left(1 + P_{Bk} g_k \right), \quad (4.47a)$$

$$\text{s.t.} \quad F_B \cdot \text{PL}_{eH}(f, r, h_B, h_R) \cdot \sum_{k=1}^K P_{Bk} - I_{th} \leq 0, \quad (4.47b)$$

$$P_{Bk} > 0 \quad \{k = 1, 2, \dots, K\}, \quad (4.47c)$$

$$\sum_{k=1}^K P_{Bk} \leq P_{RB} \quad \{k = 1, 2, \dots, K\}, \quad (4.47d)$$

where P_{RB} is the rated transmit power for the eNodeB. The constraint in (4.47d) is on the optimization decision variable P_B itself and is strictly non binding since it can be directly implied by simply changing P_B to P_{RB} in the objective function.

4.2.3 Efficiency of Spectrum Utilization Under LSA

The LSA spectrum utilization efficiency depends on the availability or unavailability of the spectrum. In this thesis, the availability of the LSA spectrum within the incumbent's

exclusion zone is characterised as a tandem queuing system with Q multiple successive service layers. The Q eNodeBs whose coverage area are located within the exclusion zone represents the Q service layers. The arrival rate of the airplane landing or taking off at the airport is assumed to follow an exponential distribution. Therefore the LSA spectrum availability across all the Q service layers is given as,

$$\mathbf{X} = \{\mathbf{X}_1(j), \mathbf{X}_2(j), \dots, \mathbf{X}_q(j)\}, \quad (4.48)$$

where $\mathbf{X}_q(j)$ denotes the state space of q th service layer and j th service request (ATC communication with an aircraft).

Furthermore $\mathbf{X}_q(\cdot)$ is described as a two state Markov chain analogous to a birth – death process. The first state (birth–to–death) describes the cases where the spectrum is being used by the ATC, while the second state (death–to–birth) characterizes the cases where the spectrum is available. For the sake of clarity the following parameters of the LSA spectrum availability tandem queueing system are defined:

- γ^{-1} : The time interval between successive flight take-off or landing(s), i.e., a cycle of the birth-death process,
- μ^{-1} : The duration of the ATC communication with an aircraft, i.e., duration of the spectrum occupancy(s) also referred to as busy period (BP),
- τ^{-1} : The duration of the spectrum vacancy(s), i.e., idle period (IP),
- s : The LSA spectrum status given as $s \in \{s_1, s_2, \dots, s_Q\}$,
 $s_q \in \{0, 1\}$, “0” where the spectrum is not available, and “1” where it is available,
- $j = \{0, 1, \dots, J\}$: The number of aircraft landings or take–offs in the airport (service request) at different times with an exponential arriving rate, $\gamma \in \{\gamma_1, \gamma_2 \dots \gamma_Q\}$, and service rate, $\mu \in \{\mu_1, \mu_2, \dots, \mu_Q\}$.

Based on the above, LSA spectrum utilization for each service layer (eNodeB coverage area) is described by the state space equation,

$$\mathbf{X}_q = \{(j, s), \in \{0, 1, \dots, J\} \times \{0, 1\}\}. \quad (4.49)$$

Similarly, $\tau^{-1} \in \{\tau_1^{-1}, \tau_2^{-1}, \dots, \tau_q^{-1}\}$, and $\Pr\{\text{ATC}\} \in \{\Pr\{\text{ATC1}\}, \Pr\{\text{ATC2}\}, \dots, \Pr\{\text{ATCq}\}\}$, where $\Pr\{\text{ATC}\}$ is the probability of ATC transmission occurring during the time interval between successive flight take-offs or landings, i.e., the probability of the LSA spectrum

being busy, the distribution of which is given by Laplace–Stieltjes transform [119]:

$$\mathcal{L}_{P_{\text{ATC}}}(s) = \frac{1}{2\gamma} \left(\gamma + \mu + s - \sqrt{(\gamma + \mu + s)^2 - 4\gamma\mu} \right). \quad (4.50)$$

Thus three following scenarios can be deduced from the process described above:

- An aircraft landing/taking–off service request is being handled and there is telemetry communication with an aircraft within and around the coverage area of a particular eNodeB. Thus the spectrum is *busy* or *unavailable*,
- There is still an ongoing ATC communication with an aircraft, but the aircraft is not within the coverage area of the particular eNodeB, hence the spectrum is *free* or *available* for unrestricted licensee communication,
- There is no ATC transmission hence the spectrum is *free* or *available* across all q service layers.

Spectrum utilization efficiency is usually measured in time and space dimension. However, here the LSA spectrum utilization efficiency, $\eta_{UT} \in \{\eta_{UT1}, \eta_{UT2}, \dots, \eta_{UTQ}\}$ is defined as a utility function of the v_q , the effective server's (in this case the LSA spectrum) busy period ratio of each layer to all the service layers, and the achievable SE η_{SEq} for each q successive service layer (eNodeB coverage area) where the spectrum is not available or occupied by the incumbent.

$$U_{v_q}(\eta_{SEq}) = \begin{cases} (1 - v_q)SE_{q\max} + v_q \cdot \eta_{SEq}, & 0 < v_q < 1, \\ SE_{q\max}, & v_q = 0, \\ \eta_{SEq}, & v_q = 1, \end{cases} \quad (4.51)$$

where v_q is given by $\frac{\mu}{\mu_q}$ for $q = \{1, 2, \dots, Q\}$. $SE_{q\max}$ is the maximum achievable system SE when the licensee transmission is not constrained by the incumbent's operational activities, i.e., where the spectrum is free.

The first part of (4.51) occurs when the incumbent and the licensee transmission shadow radius intersects. In the uplink direction, when this occurs, the spectrum utilization efficiency becomes a utility measure of the ratio of each eNodeB BP to the total duration of the service time. For this to occur, the distance between the aircraft and the UEs must not be greater than the summation of the transmission shadow of the aircraft and the UEs. Since the eNodeB and the ATC tower are stationary, this scenario does not apply in the downlink direction.

However the second and third equation in the utility function, in (4.51), defines the utilization efficiency for distant and close eNodeB coverage areas respectively. In the former case, at a certain distance, the interference generated by the eNodeB is significantly less than the the interference threshold of the ATC system, hence the MNO licensee can operate at its rated transmit power. In the latter, for eNodeB coverage areas close to the ATC tower, the MNO must adjust its transmission power to prevent harmful interference to the incumbent's system, hence the maximum achievable rate for the total duration of the ATC communication is the constrained busy spectrum SE, η_{SEq} , for those eNodeB coverage areas. Furthermore, the second equation of (4.51) also applies to the uplink SE in those distant eNodeB coverage areas where the aircraft has attained considerable height such that the distance separation between it and UEs on the ground is more than their shadow radius combined.

4.3 The Energy and Spectrum Efficiency of the Dynamic LSA

This examines the optimum system efficiency (EE and SE) of the licensee in a vertical LSA sharing scheme while the incumbent's interference threshold is not exceeded during the period the LSA spectrum is not available. Specifically, the goal is to maximize the licensee system's EE and SE while both the incumbent, the airport telemetry system, and the licensee, a cellular MNO, (two different systems) are transmitting simultaneously. This is of vital importance considering the fact that simultaneously increasing the system SE and EE is not always achievable as both metrics often conflict one another. In fact, in wireless communication resource allocation problems, obtaining a trade-off between the SE and EE seems to be the achievable practical solution [120]. In a LSA spectrum sharing, the management of the incumbent's tolerable interference added a new dimension to the already challenging task of maximizing the licensee's EE and SE.

However, in this section, the more severe air to ground interference path between the omni- directional transmissions of the UEs and the incumbent's airborne victim receiver is considered in this section, see eNodeB coverage area C of Fig. 3.1 . The reasoning behind this is two fold: (i) the licensee's eNodeB antenna height within the vicinity of the airport incumbent could be designed to be lower than the ATC antenna height and directed downwards thereby preventing its transmissions from causing interference to the ATC receiver. (ii) For sufficient separation distance between the licensee's eNodeB coverage area and the ATC tower, the possibility of interference from the UE transmissions to the ATC receiver becomes a lot easier to control.

Considering a LSA system with an exclusion zone as in [39], the distribution of the licensee's interference is obtained and from this the received maximum interference probability of the incumbent is derived. Formulating the system operation as a multi-objective optimization problem (MOP), the maximum interference probability is then imposed as a constraint on the operating transmission power of the MNO during the period of communication between the ATC and aircrafts landing or taking off. The weighted sum method is then adopted to convert the MOP into a single objective optimization, which is then solved by fractional programming.

4.3.1 Interference Threshold

When the incumbent is transmitting on its spectrum, the licensee has to adjust its transmission appropriately to prevent outage or disruption in the ATC communication. At these time instants, the licensee must adjust its transmit power to ensure that the maximum incumbent's tolerable interference (the interference threshold) is not exceeded. This requirement is expressed by the interference probability equation [121]:

$$\Pr\{I > I_{th}\} \leq \zeta, \quad (4.52)$$

where $\zeta \ll 1$ denotes the maximum probability that the interference is larger than the threshold that can be tolerated by the incumbent system. Furthermore, (4.52) can be construed of as the complementary cumulative distribution function (CCDF) of the interference distribution $f_I(i)$ (see (3.23)) at the Interference threshold, I_{th} . Thus (4.52) can be expressed as:

$$\Pr\{1 - I \leq I_{th}\} \leq \zeta, \quad (4.53)$$

Therefore, to derive the expression for the constraint placed on the licensee operation as stated in (4.52), we proceed by taking the integral of the distribution function in (3.23) with I_{th} as the limit of the integration interval:

$$\Pr\{I \leq I_{th}\} = \int_0^{I_{th}} P_k \frac{1}{\pi i} \sum_{k=1}^{\infty} \frac{\Gamma(\theta k + 1)}{k!} \left(\frac{\rho}{i^\theta}\right)^k \sin k\pi(1 - \theta) di. \quad (4.54)$$

Equation (4.54) is the cumulative distribution of (3.23) at $i = I_{\text{th}}$ scaled by P_k . Following the same line of argument as in [106], this can be approximated as an infinite series

$$\Pr\{I \leq I_{\text{th}}\} = \frac{1}{\pi} \sum_{k=1}^{\infty} \frac{P_k \Gamma(\theta k)}{k!} \left(\frac{\rho}{I_{\text{th}}^\theta}\right)^k \sin k\pi(1-\theta). \quad (4.55)$$

Thus, the probability of exceeding the incumbent's interference threshold can then be written as:

$$\Pr\{I > I_{\text{th}}\} = 1 - \frac{1}{\pi} \sum_{k=1}^{\infty} \frac{P_k \Gamma(\theta k)}{k!} \left(\frac{\rho}{I_{\text{th}}^\theta}\right)^k \sin k\pi(1-\theta). \quad (4.56)$$

4.3.2 Energy and Spectrum Efficiency

Following the convention adopted in [78], the UE to eNodeB channel set is defined as $\mathbf{K} = [1, \dots, k]$, the normalised channel gain over noise from UE to eNodeB as g and the transmit power as P_k and thus the total SE is

$$\eta_{\text{SE}} = \sum_{k=1}^K \log_2(1 + P_k g_k). \quad (4.57)$$

The total consumed power, P_S is

$$P_S = P_c + \frac{1}{\varepsilon} \sum_{k=1}^K P_k,$$

where P_c is the circuit power and ε is the amplifier efficiency. The circuit power is the consumed power in the electronics of the transmitter. Transmission power is the actual transmitted signal power. In many cases, the circuit power is constant and the transmission power is adjusted based on the resource allocation strategy. Therefore, EE, η_{EE} is:

$$\eta_{\text{EE}} = \frac{\eta_{\text{SE}}}{P_S}. \quad (4.58)$$

4.3.3 SE-EE Trade-off Optimal Power Allocation

The EE and SE are two conflicting objectives hence, to investigate the trade-off between them, the system operation is formulated as the following multi-objective optimization problem:

$$\begin{aligned}
& \max_{\mathbf{P}} \{ \eta_{SE}, \eta_{EE} \}, \\
& \text{s.t. } \Pr\{I > I_{th}\} \leq \zeta, \\
& P_k > 0, k = 1, 2, \dots, K.
\end{aligned} \tag{4.59}$$

To obtain the solution to the above problem, the weighted sum method is adopted to convert the multi objective optimization problem in (4.59) to a single objective optimization problem by assigning weights to the objectives [122] as the following:

$$\begin{aligned}
& \max_{\mathbf{P}} w \left(\frac{\eta_{SE}}{\eta_{SE}^{\max}} \right) + (1-w) \frac{\eta_{EE}}{\eta_{EE}^{\max}}, \\
& \text{s.t. } 1 - \frac{1}{\pi} \sum_{k=1}^{\infty} \frac{P_k \Gamma(\theta k)}{k!} \left(\frac{\rho}{I_{th}^{\theta}} \right)^k \sin k\pi(1-\theta) \leq \zeta, \\
& P_k > 0, k = 1, 2, \dots, K.
\end{aligned} \tag{4.60}$$

The main challenge in using the weighted sum method for solving a MOP is to establish a consistent comparison between the different objective functions. Hence the two conflicting objectives (SE and EE) are normalized with η_{SE}^{\max} , and η_{EE}^{\max} , correspondingly. In this formulation, η_{SE}^{\max} , and η_{EE}^{\max} are defined as the maximum achievable η_{SE} and η_{EE} when the spectrum is idle such that the licensee transmit power is not constrained by the interference threshold. The optimization problem in (4.60) is then converted to a minimization as the following:

$$\begin{aligned}
& \min_{\mathbf{P}} w \left[\frac{\eta_{SE}^{\max}}{\eta_{SE}} \right] + (1-w) \left[\frac{\eta_{EE}^{\max} P_s}{\eta_{SE}} \right], \\
& \text{s.t. } 1 - \frac{1}{\pi} \sum_{k=1}^{\infty} \frac{P_k \Gamma(\theta k)}{k!} \left(\frac{\rho}{I_{th}^{\theta}} \right)^k \sin k\pi(1-\theta) \leq \zeta, \\
& P_k > 0, k = 1, 2, \dots, K,
\end{aligned} \tag{4.61}$$

and equivalently (4.61) is

$$\begin{aligned} \max_{\mathbf{P}} \quad & \left[\frac{\eta_{\text{SE}}}{w\eta_{\text{SE}}^{\max} + (1-w)\eta_{\text{EE}}^{\max} P_s} \right], \\ \text{s.t.} \quad & 1 - \frac{1}{\pi} \sum_{k=1}^{\infty} \frac{P_k \Gamma(\theta k)}{k!} \left(\frac{\rho}{I_{\text{th}}^{\theta}} \right)^k \sin k\pi(1-\theta) \leq \zeta, \\ & P_k > 0, k = 1, 2, \dots, K, \end{aligned} \quad (4.62)$$

Proposition 4.2: The objective function in (4.62) is strictly quasi-convex.

Proof: We show that η_{SE} in (4.62) is a convex function of P_k . By substituting (4.57) into (4.62), we have:

$$\eta_{\text{SE}} = \max_{P_k} \sum_{k=1}^K \log_2 \left(1 + P_k g_k \right). \quad (4.63)$$

Therefore,

$$\frac{\partial \eta_{\text{SE}}}{\partial P_k} = \frac{g_k}{2 \ln(2) (1 + P_k g_k)}. \quad (4.64)$$

To investigate the convexity of η_{SE} , here we obtain its Hessian,

$$\frac{\partial^2 \eta_{\text{SE}}}{\partial P_k^2} = - \frac{(g_k)^2}{2 \ln(2)} \left[\frac{1}{(1 + P_k g_k)^2} \right] < 0, \quad (4.65)$$

As it is seen, $\frac{\partial^2 \eta_{\text{SE}}}{\partial P_k^2} \leq 0$, therefore, η_{SE} is concave. Thus, (4.62) is a ratio of a concave to an affine function, and according to [123] the objective function is strictly quasi-convex. ■

Since the objective function in (4.62) is strictly quasi-convex, the solutions of this problem can be obtained using fractional programming [117]. Using the Charnes-Cooper transformation [116], a ratio of a concave to an affine function optimization problem of the form: $\max_x \frac{f(x)}{g(x)}$ can be transformed into a convex optimization problem as:

$$\begin{aligned} \max_{t, x} \quad & t \cdot f\left(\frac{\phi}{t}\right) \\ \text{s.t.} \quad & t \cdot g\left(\frac{\phi}{t}\right) = 1, \quad \forall i = 1, \dots, I \end{aligned} \quad (4.66)$$

by using the transformation variable: $\phi = \frac{x}{g(x)}, t = \frac{1}{g(x)}$, where $t > 0$.

Adopting similar techniques we introduce $\Psi = [w\eta_{SE}^{\max} + (1-w)\eta_{EE}^{\max}P_s]^{-1}$, and $\wp = \mathbf{P}\Psi$. By substituting the introduced variables, the objective function of (4.62) is transformed to:

$$\begin{aligned} \max_{(\wp, \Psi)} \quad & \Psi \cdot \sum_{k=1}^K \log_2 \left(1 + \frac{\wp_k}{\Psi} g_k \right), \\ \text{s.t.} \quad & \Psi \cdot (w\eta_{SE}^{\max} + (1-w)\eta_{EE}^{\max}P_s) = 1, \end{aligned} \quad (4.67)$$

and thus the equivalent concave optimization problem is as the following.

$$\begin{aligned} \max_{\wp, \Psi} \quad & \Psi \cdot \eta_{SE}, \quad 0 < w < 1, \\ \text{s.t.} \quad & \Psi \cdot (w\eta_{SE}^{\max} + (1-w)\eta_{EE}^{\max}P_s) = 1, \\ & 1 - \frac{1}{\pi} \sum_{k=1}^{\infty} \frac{P_k \Gamma(\theta k)}{k!} \left(\frac{\rho}{I_{th}^{\theta}} \right)^k \sin k\pi(1-\theta) \leq \zeta, \\ & \wp_k > 0 \quad k = 1, 2, \dots, K. \end{aligned} \quad (4.68)$$

The Lagrangian function corresponding to (4.68) is:

$$\begin{aligned} \mathcal{L}(P_k, u, \chi, v_k) = & \Psi \eta_{SE} + u \left[\Psi (w\eta_{SE}^{\max} + (1-w)\eta_{EE}^{\max}P_s) - 1 \right] \\ & - \chi \left(1 - \frac{1}{\pi} \sum_{k=1}^{\infty} \frac{P_k \Gamma(\theta k)}{k!} \left(\frac{\rho}{I_{th}^{\theta}} \right)^k \sin k\pi(1-\theta) - \zeta \right) + \sum_{k=1}^K v_k P_k. \end{aligned} \quad (4.69)$$

The stationarity conditions corresponding to the Lagrangian in (4.69) are:

$$\frac{\partial \mathcal{L}(P_k, u, \chi, v_k)}{\partial P_k} = 0, \quad \frac{\partial \mathcal{L}(P_k, u, \chi, v_k)}{\partial \Psi} = 0,$$

which are respectively written as:

$$\frac{g_k \cdot \Psi}{2 \ln(2)(1 + P_k g_k)} + u \cdot \Psi \left[\frac{(1-w)\eta_{EE}^{\max}}{\varepsilon} \right] - \chi \Phi_k + v_k = 0 \quad (4.70)$$

and

$$\eta_{SE} + u [w\eta_{SE}^{\max} + (1-w)\eta_{EE}^{\max}P_s] = 0. \quad (4.71)$$

The optimal power allocation is then obtained as

$$P_k^* = \frac{\Psi \cdot \varepsilon}{2 \ln(2) [\chi \varepsilon \Phi_k - u \Psi (1-w) \eta_{EE}^{\max}]} - \frac{1}{g_k}, \quad k = 1, \dots, K. \quad (4.72)$$

where $\Phi_k = \frac{1}{\pi} \sum_{k=1}^{\infty} \frac{\Gamma(\theta k)}{k!} \left(\frac{\rho}{I_{th}^\theta} \right)^k \sin k\pi(1-\theta)$. Algorithm 4 describes the procedure for implementing the proposed method in this section.

Algorithm 4 Algorithm for EE-SE Trade-Off Optimization

- Step 1.** Initialise circuit power (P_c^Λ), eNodeB radius (R^C),
 No. of UEs (K^M), trade-off importance weight (\mathbf{w}^i)
 transmit power (P_k^Q), incumbent's interference
 threshold (I_{th}), Channel Bandwidth (B_w),
 Noise Power Density (N_0), Amplifier Efficiency (ε);
- Step 2.** Generate the random radial x and y coordinates
 of the UE's in a circular region of radius R .
- 2.1. Compute the distance of each UE to the eNodeB,
 to the airborne victim receiver;
- 2.2. Compute the propagation losses along the paths;
- Step 3.** Compute the maximum interference probability
 in equation(4.56);
- Step 4.** for $\Lambda = 1$ to length of P_c^Λ ,
 for $C = 1$ to length of R^C ,
 for $M = 1$ to length of K^M ,
 for $Q = 1$ to length of P_k^Q ,
 for $i = 1$ to length of \mathbf{w}^i ,
- 4.1. Compute optimal power for the EE-SE, P_k^* from (4.72),
 4.2. Compute the normalization functions, η_{EE}^{\max} & η_{SE}^{\max} ,
 4.3. Compute the optimal EE-SE trade-off function in (4.68).
-

4.4 Quality of Service Guarantee in Drone Assisted LSA

A major feature of the LSA is predictable guaranteed QoS not only for the incumbent system but also for users on the licensee network. However, the adoption of the limited transmission power when and where the LSA spectrum is being used by the incumbent system, and the resulting reduction of achievable data rate poses a serious challenge to the actualization of this feature. This section, proposes to leverage the agility/mobility of the Drone-BS to

compensate for the UEs QoS/ data rate degrading effect of the licensee operating under the limited power regime. Without loss of generality, this work is a demonstration of the robustness of dynamic three- dimensional D-BS positioning towards actualizing predictable guaranteed QoS requirement of the licensee network in a LSA sharing. As a proof of concept, this work only presents a single D-BS in a hybrid aerial-terrestrial system based on LSA. The consideration of aerial-terrestrial based LSA with multiple D-BS in multiple terrestrial eNodeB coverage area is left for future work.

4.4.1 Dynamic D-BS Positioning

We define a two-mode dynamic D-BS placement scheme referred to as *idle* and *active incumbent* modes. The general idea is to ensure efficiency of our system by jointly optimizing the achievable capacity and D-BS positioning subject to surplus traffic requirement while enforcing the incumbent's interference threshold during the active incumbent mode.

We begin with mathematical formulations of D-BS LSA configuration when the incumbent's system is not operational within the interfering range of the licensee. If we define UEs' to D-BS channel set $S_{\text{UE}} = [k_1, \dots, k_S]$, the D-BS 3-D positioning is given by:

$$\max_{h_D, x_D, y_D} \sum_{k=1}^{S_{\text{UE}}} R_k^\xi \cdot k_\xi, \quad (4.73)$$

$$\text{s.t.} \quad \sum_{k=1}^{S_{\text{UE}}} R_k^\xi \geq \mathbf{R}_{\text{TG}}, \quad (4.74)$$

$$\sum_{k=1}^{S_{\text{UE}}} R_k^\xi \leq C_D, \quad k = 1, 2, \dots, K, \quad (4.75)$$

$$\xi \in \{\mathbf{V}, \mathbf{eB}\},$$

where h_D, x_D, y_D are the D-BS height and horizontal co-ordinates respectively. Unlike placement of D-BS in a non LSA setting, which aims for maximum coverage, the objective function in (4.73) is set to optimize our LSA D-BS positioning to achieve the targeted data rate, the surplus traffic requirement of the network. Hence the key decision variable in (4.73) is not the number of UEs i.e., k_ξ , covered but the summation of the UEs achieved data rate R_k^ξ . The second constraint in (4.75) ensures that the total capacity of the D-BS is not exceeded while the constraint in (4.74), ensures that the achieved capacity is not less than the required surplus traffic. However, in order to optimize the system configuration and ensure that the achieved capacity is not over allocated, we introduce a surplus variable to control or upper bound it in relation to the required capacity. The optimization problem therefore is

transformed into the following:

$$\max_{h_D, x_D, y_D} \sum_{k=1}^{S_{UE}} R_k^\xi \cdot k_\xi, \quad (4.76)$$

$$\text{s.t.} \quad \sum_{k=1}^{S_{UE}} R_k^\xi - \delta_j = \mathbf{R}_{TG}, \quad j = 1, 2, \dots, J, \quad (4.77)$$

$$\sum_{k=1}^{S_{UE}} R_k^\xi \leq C_D, \quad k = 1, 2, \dots, K, \quad (4.78)$$

$$\xi \in \{\mathbf{V}, \mathbf{eB}\}, \quad (4.79)$$

$$\delta_j = \min\{\delta_1, \delta_2, \dots, \delta_J\}, \quad (4.80)$$

where $\delta_j = \sum_{k=1}^S R_k^\xi - \mathbf{R}_{TG}$, is difference between the achieved and the required surplus capacity. From (4.80) we can see that there is a set of J possible δ_j , the minimum of which gives the capacity closest to the desired capacity or the required surplus traffic of the network. Thus (4.80) ensures that the constraint in (4.77) provides a tight bound to the magnitude difference between the target surplus traffic and the achieved capacity.

In cases where the incumbent becomes active in its spectrum, the challenge of D-BS positioning is no longer only to ensure excess capacity demand is met but more importantly to avoid causing harmful interference to the incumbent's system. This constraint is expressed mathematically as:

$$\sum_{k=1}^{S_{UE} \subset K} P_k \text{PL}(h, r)^{-1} F_D \leq I_{th}. \quad (4.81)$$

The constraint on interference in (4.81) applies when the D-BS is transmitting at its maximum rated power. For the limited power regime, (4.81) becomes:

$$\sum_{k=1}^{S_{UE} \subset K} P_k \leq P_{LT}. \quad (4.82)$$

where P_{LT} is the limited power and is given as:

$$P_{LT} = \sum_{k=1}^{S_{UE}} P_k \left(1 - F_D \cdot \text{PL}(h, r)^{-1}\right) + I_{th}. \quad (4.83)$$

In (4.83), $\sum_{k=1}^{S_{UE}} P_k = P_{\max}$, is the summation of the allocated power to the UEs associated to the licensee D-BS while F_D and $\text{PL}(h, r)$ are the power fading coefficient and path loss along

the transmission path between the D-BS and the incumbent receiver. We can then formulate the D-BS positioning for the *active incumbent* mode by inserting (4.82) into the following optimization problem:

$$\max_{h_D, x_D, y_D} \sum_{k=1}^{S_{UE}} R_k^\xi \cdot k_\xi, \quad (4.84)$$

$$\text{s.t.} \quad \sum_{k=1}^{S_{UE}} R_k^\xi - \delta_j = \mathbf{R}_{TG}, \quad j = 1, 2, \dots, J, \quad (4.85)$$

$$\sum_{k=1}^{S_{UE}} R_k^\xi \leq C_D, \quad k = 1, 2, \dots, K, \quad (4.86)$$

$$\xi \in \{\mathbf{V}, \mathbf{eB}\}, \quad (4.87)$$

$$\delta_j = \min\{\delta_1, \delta_2, \dots, \delta_J\}, \quad (4.88)$$

$$\sum_{k=1}^{S_{UE} \subset K} P_k \leq P_{LT}. \quad (4.89)$$

As it is seen, the D-BS positioning optimization problem is a mixed integer non-linear problem (MINLP) and it is complex and difficult to obtain its exact closed form solution. Therefore, Algorithm 5 was formulated to solve the D-BS placement in the *active incumbent* mode.

4.5 Chapter Summary

In this chapter, methods are proposed to improve the several efficiency metrics of the licensee system which are adversely affected when the incumbent becomes active on the spectrum in the dynamic LSA spectrum sharing scheme. In particular, mathematical models for the proposed methods are presented in this chapter. Starting with **section 4.1**, mathematical formulations are presented for optimization of the licensee's energy efficiency when its operations is constrained by the incumbent's activity on the LSA spectrum. Taking into account the different propagation characteristics existing between the licensee downlink and uplink transmitters, the power adjustment required to guarantee that the incumbent victim receivers do not suffer from excessive harmful interference is determined. Thus an expression for this is derived as a function of the incumbent's interference threshold and the respective received interference from the licensee's downlink and uplink transmitters. On the basis of the determined power differential, the limited transmit power equation is formulated for each

Algorithm 5 Optimal LSA D-BS positioning in the *active incumbent* mode

-
- Step 1.** Initialise the eNodeB radius(R), ATG parameters:
 a, b, f, c , LoS & NLoS values, θ^{opt} , limited power(P_{LT}), incumbent's interference threshold, I_{th} the surplus traffic requirement \mathbf{R}_S ;
- Step 2.** Define the 3D search space boundary :
 $\{x_{\min}, y_{\min}\} = 0 - R$, $\{x_{\max}, y_{\max}\} = 0 + R$,
and $h_{\max} \leq R \tan \theta^{\text{opt}}$;
- Step 3.** Divide the search space into “ Q ” partitions such that $Q = G_q \times V_q \times \alpha_q$ where G_q is the ground or horizontal partitions, V_q is the vertical partition and α_q is the azimuth angle partitions;
- Step 4.** Trim search space dimension by:
4.1. Compute interference from all points in Q to incumbent at point $\{x_{\text{icb}}, y_{\text{icb}}\}$
4.2. If interference $\leq I_{\text{th}}$ keep point, otherwise discard.
4.3. Create vector \mathbf{J} to store candidate points for D-BS positioning.
- Step 5.** Sort \mathbf{J} in ascending order of interference power
- Step 6.** While $j \leq N_{\text{itm}}$, do :
6.1 for $\mathbf{J}(1)$, Compute and compare individual UE achieved rate R_k^{ach} with individual QoS rate requirement R_k
6.2 for every $R_k^{\text{ach}} \geq R_k$,
Compute $\delta_{j(1)} = \sum_{k=1}^{S'} R_k^{\text{ach}} - \mathbf{R}_{\text{TG}}$.
6.3 Next repeat step 6.1 and 6.2 for $\mathbf{J}(\text{end})$
6.4 if $\delta_{j(1)} > \delta_{j(\text{end})}$,
set $\delta_{j(1)} = \lfloor (\delta_{j(\text{end})} - \frac{\delta_{j(\text{end})}}{\delta_{j(1)}}) \times \text{length of } \mathbf{J} \rfloor$
6.5 else if $\delta_{j(1)} < \delta_{j(\text{end})}$,
set $\delta_{j(\text{end})} = \lceil (\delta_{j(1)} + \frac{\delta_{j(\text{end})}}{\delta_{j(1)}}) \times \text{length of } \mathbf{J} \rceil$
- Step 7.** if $R_k^{\text{ach}} < R_k$,
then $\min\{\delta_j\} = \sum_{k=1}^{S'} \max\{R_k^{\text{ach}}\} - \mathbf{R}_{\text{TG}}$
- Step 8.** Return : $\{x, y, h\}$ for $\min\{\delta_j\}$
-

group of licensee's transmitter in both the uplink and downlink transmission directions when the spectrum access right is revoked by the incumbent. Finally, by adopting the Charnes-Cooper transformation technique to the non-convex fractional optimization problem, an optimal power allocation technique for optimization of the licensee EE when it is operating with the limited transmit power is proposed.

Section 4.2.2, presents the mathematical formulations for the optimization of the licensee's system spectrum efficiency. Firstly, an expression was derived for the interference received by the incumbent from the licensee's transmission both in the uplink and downlink. Then unlike in the case of the EE model, an SE optimization model was formulated using the maximum transmit power of the licensee while imposing the incumbent interference threshold as a constraint on the optimization problem. Furthermore, by characterizing the availability or not of the LSA spectrum as a tandem queue a novel metric for accurately determining the utilization efficiency of the LSA spectrum was proposed in **section 4.2.3**. The proposed metric was derived as a utility function of the the achievable SE and busy period ratio of each layer within the tandem queue. Unlike the traditional duty cycle measured in percentage that was hitherto used to quantify spectrum utilization efficiency, the proposed utility function in this thesis can help to accurately forecast the achievable capacity that the spectrum can provide and match this to the capacity demand of the data hungry applications of the 5G and beyond technology space.

In **section 4.3**, we obtain the distribution of the licensee's interference and from there derive the received maximum interference probability of the incumbent. This is then imposed as a constraint on the operating transmission power of the MNO during the period of communication between the ATC and aircrafts landing or taking off. Furthermore, an SE and EE optimization of the licensee's system ia formulated as a multi-objective problem (MOP). Using the weighted sum approach and the fractional programming method, subject to the transmission power and the incumbent's interference threshold constraint, an optimal power allocation to maximize the two conflicting metrics of SE and EE is derived. Finally, in **section 4.4**, an hybrid aerial-terrestrial dynamic LSA framework is presented to address the challenge of the QoS degrading effect of the limit transmit power adopted by the licensee when the incumbent is active on the LSA spectrum. We begin by formulating the 3-dimensional D-BS placement problem when the spectrum is free of incumbent's activity and hence licensee D-BS can operate at maximum rated transmission power. We then extend the formulation of the D-BS placement optimization problem to the cases where limited transmission power is employed by the licensee, i.e., when the incumbent is active in its spectrum within/around the licensee network coverage radius.

4.6 Conclusion

In this chapter, the proposed solutions to the performance degrading effect of the uncertainty in the availability of the LSA spectrum were presented. For the dynamic LSA, which is investigated in this research work, the revocation of the spectrum access right by the incumbent implies the licensee can only operate under the limited transmit power policy [39]. Fittingly, the first section of the chapter starts with derivation of the licensee's limited power as a function of the maximum rated transmit power and required power differential needed to ensure the interference threshold of the incumbent is not exceeded. Using the formulated limited power expressions, the achievable EE of the licensee when its spectrum access right is revoked is then derived for both interference paths in the licensee's uplink and the downlink. The section concludes with the formulation of an EE maximizing limited power allocation scheme. A single licensee eNodeB coverage area is considered in this section.

The second section of this chapter discussed the proposed method for the improvement of the licensee's SE when the LSA spectrum is deemed not available as a result of the incumbent demanding the use of its spectrum. The objective function in the optimization problem here is a function of the maximum transmit power and not the formulated limited transmit power of the previous section. The incumbent's interference threshold was then set as the constraint to ensure the protection of the incumbent. The proposed method here also considered multiple eNodeB coverage area unlike the single cell coverage of the first section. This section of the chapter also proposed a novel method for characterising the spectrum utilization efficiency of the LSA scheme.

The findings from the previous two sections revealed that the air to ground interference propagation path between the licensee UE and the incumbent airborne victim receiver is more critical than the other two propagation paths. Consequently the optimization of the EE and SE trade-off presented in the third section of the chapter assumed a scenario where the eNodeB coverage area is so far away from the airport such that both the UE and eNodeB signal power is not strong enough to adversely affect the ATC receiver. Inspired by the interference temperature concept, an expression for the maximum interference probability is derived and set as the optimization constraint. Formulating the system operation as a multi-objective optimization problem (MOP), the weighted sum method is then adopted to convert the MOP into a single objective optimization, which is then solved by fractional programming.

Finally, the chapter discussed the proposed solution to the challenge of predictable QoS resulting from the reduction in achievable data rate when the licensee is constrained to transmit under the limited power regime. Adopting a scenario involving a PPDR or PMSE incumbent, the proposed solution presents a hybrid aerial terrestrial cellular network

configuration based on LSA. The D-BS 3-D placement optimization problem formulated focused on maximizing the achievable data of the UE on the licensee network in order to attain the desired excess capacity requirement of the network.

Chapter 5

Implementation Set-up.

In this chapter, the simulated implementation of the system models discussed in **chapter 3** and the mathematical formulations of the proposed methods discussed in **chapter 4** are presented. The simulation tool used is MATLAB. In addition to the coding and procedure descriptions, also discussed in this chapter are justifications and regulatory standard values adopted in the thesis. The next section discusses the implementation and code set-up for the licensee system.

5.1 The Licensee Network

As mentioned in the preceding chapters, the licensee adopted in this thesis is the cellular system of a mobile network operator. The following describes the steps for simulating the licensee network for the purpose of this research work.

5.1.1 UE Distributions in a Circular eNodeB Coverage Area

In this section, snippets of simulation of the spatial distribution of the UEs in the licensee eNodeB coverage area is provided.

```
# Firstly we define the eNodeB parameters that determines the size and the circular coverage
```

```
R = eNodeB radius (m)
```

```
 $\Delta_a$  = angle increment
```

```
aV = angle vector (radians)
```

```
# Next generate the points for the circumference of coverage area
```

```
ctr = 0
```

```

for :
  aV = 0 :  $\pi/\Delta_a$  :  $2 \cdot \pi$ 
  ctr = 0 + 1
  xr(ctr) = R * cos(aV)
  yr(ctr) = R * sin(aV)
end

# plot the generated points
figure
plot(xr,yr)
hold on

# Generate poisson distributed UE within the circle
nUE = Number of User Equipment in eNodeB coverage area
UEppp = random('Poisson', R, nUE, 1)
xUE = R * cos(UEppp)
yUE = R * sin(UEppp)

# Now display the UE in the circular coverage area as shown in Fig. 5.1.
plot(xUE,yUE,'*m','MarkerSize',8)
axis off

```

5.1.2 The Propagation Paths

The length of the propagation paths (i.e., the spatial separation between a transmitter - receiver link), is computed from the equation for the euclidean distance. For the signal propagation path between the eNodeB and the UEs in the licensee network we use:

$$r_{UE} = \sqrt{(x_{UE} - 0)^2 + (y_{UE} - 0)^2}, \quad (5.1)$$

This is on the basis of the assumption that the eNodeB positioned in the centre (0) of the circular coverage area as depicted in Fig. 5.1. However, for the hybrid-aerial LSA licensee system, the propagation path length is computed with:

$$r_{ATG} = \sqrt{r_{UE}^2 + h^2}, \quad (5.2)$$

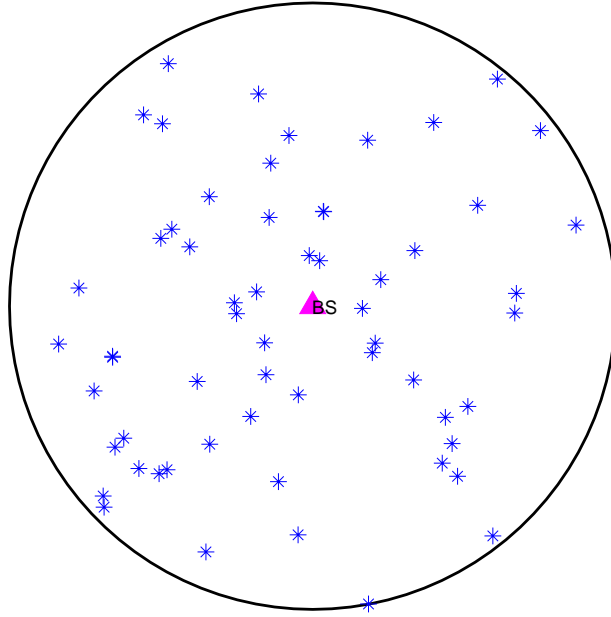


Fig. 5.1 UE in the eNodeB coverage area.

given that $r_{UE} = \sqrt{(x_{UE} - x)^2 + (y_{UE} - y)^2}$, where, x, y, h are the co-ordinates of the D-BS obtained from algorithm 5. The length of the interference propagation path between the licensee transmitter and the incumbent victim receiver is given as,

$$r_{icb} = \sqrt{(x_{UE} - x_{icb})^2 + (y_{UE} - y_{icb})^2}, \quad (5.3)$$

where x_{icb} and y_{icb} are the x and y coordinates for incumbent's position which for the moving airborne victim receiver, is obtained from algorithm 6, while a specific position such as described in Fig. 6.44 is used. The signal attenuation along each path is then computed by slotting the appropriate values from (5.1) - (5.3) into the channel model equations given in chapter 3.

5.1.3 Evaluation of the Proposed Methods for Licensee Optimal Efficiency

For the EE, the next step is to first write the code for computing the limited power for the three propagation paths according to (4.10). Next is the optimal limited power P_k^* , as given

in (4.31) and (4.32). However to obtain the optimal limited power allocation, the Lagrange multiplier, χ , in (4.31) and (4.32) must be chosen such that:

$$\sum \left(\frac{\varepsilon}{\ln(2) \cdot \chi \left(1 - l(k) F_k \right)} - \left[\frac{L_k \cdot N + I_{\text{thk}}}{1 - l(k) F_k} \right] \right) \leq P_{\text{LT}}, \quad k = 1, \dots, K. \quad (5.4)$$

This is done by the simple bisection algorithm. For the SE maximization and EE-SE trade off in **section 4.2** and **section 4.3** respectively P_{LT} becomes the rated maximum transmission P_{max} .

Then the optimal EE, the EE with maximum power and limited power with EPA are computed in the snippets of code as follows:

```

for j = 1 : length(totalPower)
    optPowerj = (epsilon/(2 * log(2) * langrange(j) * (1 - IL))) - ((nChannel(r) * PL. *
    ChannelNoise + I_th) ./ (nChannel(r) * (1 - IL)));
    optPowerPOSj = optPowerj(find(optPowerj > 0));
    optSumRate(j) = 1/2 * sum(log2(1 + optPowerPOSj ./ ChannelNoise(find(optPowerj > 0))));
    optEE(j) = optSumRate(j) / (P_c * r(m) + ((1/epsilon) * ((limitPower(j) * (1 - IL)) + sum(I_th))));
    NormSumRate(j) = 1/2 * sum(log2(1 + ((limitPower(j) * (1 - IL)) ./ nChannel(r)) ./ ChannelNoise));
    NormEE(j) = NormSumRate(j) / (P_c * r(m) + ((1/epsilon) * ((limitPower(j) * (1 - IL)) + sum(I_th))));
    TotalPowerSumRate(j) = 1/2 * sum(log2(1 + (totalPower(j) ./ nChannel(r)) ./ ChannelNoise));
    TotalPowerEE(j) = TotalPowerSumRate(j) / T(j);
end

```

Similar steps were repeated for the SE maximization method as well as the EE-SE trade off.

5.1.4 Drone BS Simulation, Assumptions and Justifications

For the D-BS simulation, the important consideration is the signal characteristics in the ATG channel between the D-BS and a terrestrial receiver. For this, the position of the D-BS in the eNodeB coverage area is the parameter of interest. While it is acknowledged that environmental factors like the weather conditions, size, aerodynamics, time of the day (day/night), and the speed are factors that affect the drone mechanical flight and physical limitations, they are however not considered in this work. Instead, like several previous works [87, 85, 83, 96], the focus in this thesis is the communication capabilities, i.e., the characterization of the signal attenuation in the transmission link between the D-BS and terrestrial receivers. The ATG channel model has been widely adopted for this characterization. It is also assumed

that the D-BS is not constantly moving, especially when it is sending transmission packets to users on the ground [84].

For the D-BS positioning, the considerations are the 3-D coordinates of the drone height and horizontal (x, y) position. This is given from algorithm 5 as

$$\begin{cases} -R \leq \{x, y\} \leq +R \\ h_{\max} \leq R \tan \theta^{\text{opt}} \end{cases} \quad (5.5)$$

where θ^{opt} is the optimal elevation angle between the D-BS and terrestrial users. It is also noteworthy, that due to the influence of the physical and environmental factors mentioned in the previous paragraph, the implementation of the D-BS in practical systems might not yield the exact result as obtained in this thesis.

5.1.5 QoS Provisioning in Aerial-LSA

In addition to the steps in **section 5.1.1**, a second Poisson process was used to simulate the group of UEs making up the excess capacity demand above the installed network capacity of the licensee. Then the 3-D search space for the D-BS placement is defined and partitioned. The following snippets describe this

```

 $\varphi$  = Partition increment
RVec = ( $\varphi$  :  $\varphi$  : R);
aV = 0 : pi/ $\Delta_a$  : 2 * pi;
yRVec = RVec' .* sin(aV);
xRVec = RVec' .* cos(aV);
h = (hmin :  $\varphi$  : R * tand( $\theta^{\text{opt}}$ ));
xC = [x; xm]; # Combined ground and Aerial network UE x coordinates
yC = [y; ym]; # Combined ground and Aerial network UE y coordinates
for j = 1 : length(yC)
tempRCbusy = sqrt((xRVec(:) - xC(j)).2 + (yRVec(:) - yC(j)).2);
RCbusy = [RCbusy, tempRCbusy]; # Combined UE distance from horizontal partitions
end

```

After partitioning, the interference to the incumbent from all points in partition is then computed and the candidate D-BS position is trimmed by applying the interference threshold constraint. The following snippet shows this:

```

for u = 1 : length(h)
Intf2ICBT{u} = LimitPowerdB(m) - PLICBT{u};
ThCidx{u} = find(Intf2ICBT{u} <= Ith);

```

$Th_{Cand}\{u\} = Int f2ICBT\{u\}(Th_{Cidx}\{u\});$
end

From the candidate D-BS positions Th_{Cand} , the achievable data rate is then computed and compared with the required or target rate for each of the UE (both initial ground and aerial network) and the steps in algorithm 5 is further implemented to find the closest achievable rate to the target rate.

5.2 Incumbent's Interference Threshold Measurement

The method for the incumbent's interference threshold computation adopted in this thesis is similar to the procedure recommended in the compatibility studies presented in the Electronic Communications Committee (ECC) report 172 [38] for spectrum sharing in the 2.3 GHz - 2.4 GHz. The method is presented in table 5.1.

Table 5.1 Computation of Incumbent's I_{th} .

Parameter	Symbol	Unit
T_x antenna height	h_t	m
T_x Bandwidth	B_t	MHz
R_x antenna height	h_r	m
R_x Bandwidth	B_r	MHz
R_x Noise Figure	F	dB
Thermal Noise, $N = -174 + 10 \log_{10}(B/Hz) + F$	N	dBm
I/N Requirement	I/N	dB
Max. Transmitted Power	P_{max}	dBm
Effective Interfering Transmitted Power	P_t	dBm
T_x antenna Gain (max)	G_t (dB)	dBi
Feeder loss	G_{fe}	dB
R_x antenna Gain (max)	G_r	dBi
R_x antenna sidelobe attenuation	G_{rd}	dB
T_x antenna discriminator	G_{td}	dB
Maximum Allowable Interference= I/N +N + F	IC	dBm
Minimum Coupling loss= IC+ P_t + G_t + G_r - G_{fe} - G_{td} - G_{rd}	MCL_{50}	dB

Chapter 6

Results Analysis and Discussions

This chapter discusses the results of the simulated implementation of the system models presented in **Chapter 3** and the proposed solutions (in **Chapter 4**) to the identified objectives at the onset of this thesis. Section 6.1 present obtained results and findings on the LSA licensee's EE optimization in **Algorithm 2**, section 6.2, discusses that of the SE and spectrum utilization efficiency in **Algorithm 3**, section 6.3, the SE-EE maximization and trade-off described in **Algorithm 4**, while section 6.4 captures the QoS improvement provided by the proposed D-BS assisted LSA system in **Algorithm 5**.

The first three sections considered the aeronautical telemetry incumbent described in **section 3.1** while for the fourth section, the assumed system model is the PMSE and PPDR incumbent described in **section 3.2**. Typical values of practical system parameters for a commercial MNO are adopted in the simulation and investigation of the licensee's LSA system operation. The proposed method's performance is evaluated and then analysed vis -a-vis critical operational parameters of a conventional MNO system. Moreover, quantitative insight for practical design considerations of a LSA network deployment is provided. At the end of each section, a summary of the discussion on the obtained results and findings from the simulated implementation of the work done on each research objective is presented.

6.1 Energy Efficiency of the Dynamic LSA Under Limited Power

This section presents the numerical analysis of the effect of the incumbent's revocation of spectrum access right on the licensee's system EE. It is noteworthy that while other works have investigated different performance characteristics of the LSA, attention has not been given to the EE, especially as a result of the incumbent's demanding the use of its

Table 6.1 Simulation Parameters for the LSA EE.

Parameter	Value
Cell Radius	100, 250, 500, & 1000(metres)
No. of Users	5, 10, 25, & 100
Downlink Transmit Power	12-60 w (40.8-48 dBm)
Uplink Transmit Power	0.2-2.52 w (23-34 dBm)
Noise Density	-174 dBm
Circuit Power	-5, 0, +5 (dB)
Amplifier Efficiency	38%
ATC Type-B Receiver Noise Figure(NF)	3 (dB)
Noise Power	$10\log(kTB) + NF$ (dB)
Boltzmann's constant(k)	1.38×10^{-23} (J/K)
Bandwidth (B)	10 MHz
Temperature (T)	290 K
Protection Ratio (I/N)	-10 (dB)

borrowed spectrum. In the light of this, this section investigates the effect of incumbent's revocation of the licensee's spectrum access right on the EE of an LSA system. Several previous works have investigated the harmful effect of the licensee's transmission in the uplink and thus analysed the effect on the licensee's various performance metrics. In this section, consideration has been given to both the uplink and downlink transmissions and the effect of this is factored into the analysis of the licensee's system EE during the time the incumbent is utilizing its spectrum.

A single eNodeB coverage area within the vicinity of the incumbent is considered. To capture the effect of large scale fading, the fading component is modeled as a log normal random variable. The ATG propagation parameters used are for the urban environment. Furthermore, a co-channel interference between both systems is assumed, the eNodeB antenna gain is set to 17 dB, the feeder loss is 3 dB, the telemetry receiver main lobe antenna gain is equal to 45 dBi, and 1 dB is its feeder loss as specified in [38] The system parameters are shown in Table 6.1.

In the succeeding paragraphs, the impact of the LSA spectrum access revocation on the allowable transmit power of the licensee is first quantified, while also comparing the effect of different interference propagation path between the UEs and the eNodeB on the incumbent. Next, is an analysis of the performance of the proposed method by comparing it with a

benchmark, the EPA method as in [124]. Then the interplay between some system design parameters with the proposed method is investigated.

6.1.1 Effect of Spectrum Access Revocation on Transmit Power

Fig. 6.1 shows the limit power (blue bar), interference (yellow bar) and power differential (orange bar) for selected maximum transmit power of the licensee in the uplink direction (Fig. 6.1b is the interference propagation path between the UEs and the ATC tower, while Fig. 6.1c is for the interference propagation path to the aircraft) and the downlink direction. It is seen that while the limit power value of the downlink is expectedly higher than the uplink limit power (because of higher rated transmit power in the downlink), the interference to the incumbent in the uplink is significantly higher. The implication of this is that, the adjustment needed for the licensee system to comply with the interference threshold requirement of the incumbent in the uplink is equivalently higher than the downlink as indicated by the power differential values, P_{Δ} , in the graphs.

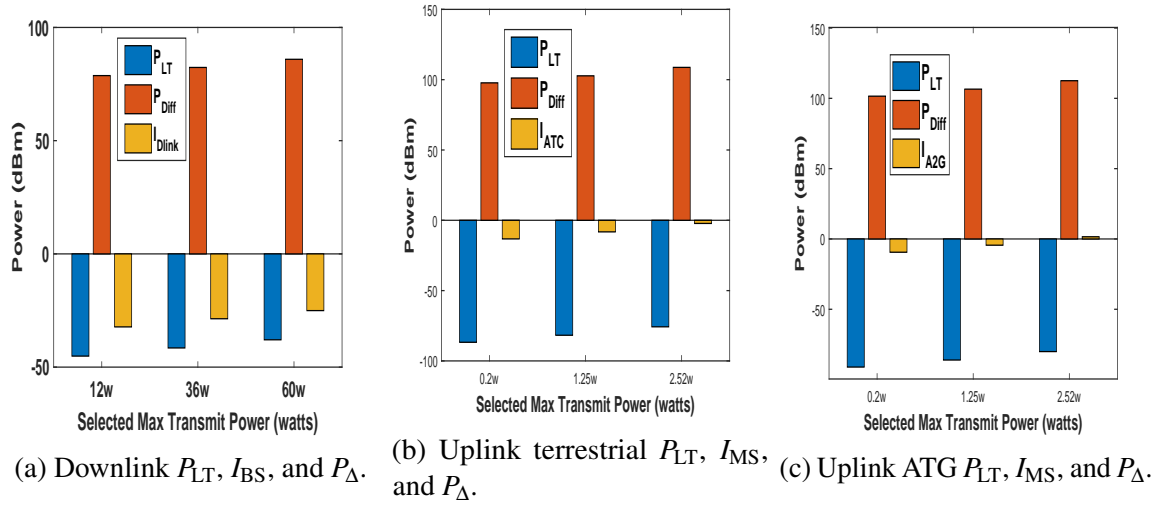


Fig. 6.1 Downlink and uplink limit power, interference power, and power differential for selected values of P_{max} .

The higher interference value in the uplink can be attributed to less attenuation along the UE-incumbent propagation path. For the interference to the aircraft, there exists a strong LoS propagation which means less pathloss. This accounts for the fact that the interference value in Fig. 6.1c is the highest of the three plots. The reason(s) for the higher interference received at the ATC tower from the UEs transmission (compared to the eNodeB interference power) is due to the fact that the ATC tower height is closer to the UE's height than it is to the eNodeB height. This means that for a UE located at the same point as the eNodeB,

the effective separation distance between it and the ATC tower, is smaller than that of the eNodeB to the ATC tower, hence, a lower path loss.

It is worth mentioning that Figs. 6.1b and c represents the mean interference power of all the UEs in the licensee network and not the aggregate interference power. This is because at present, even the simultaneous multiple transmissions made possible by the MIMO systems is still being used primarily in practical deployments for eNodeB simultaneous transmissions to several UEs. It is yet to be implemented in the UEs. We can therefore assume that even though there could be many UEs per eNodeB, there is no more than one UE per eNodeB transmitting at a particular time. The implication of this is that, at any particular point in time the licensee's transmit power adjustment, in the uplink, is dependent on interfering signal from the UE transmitting at the particular time.

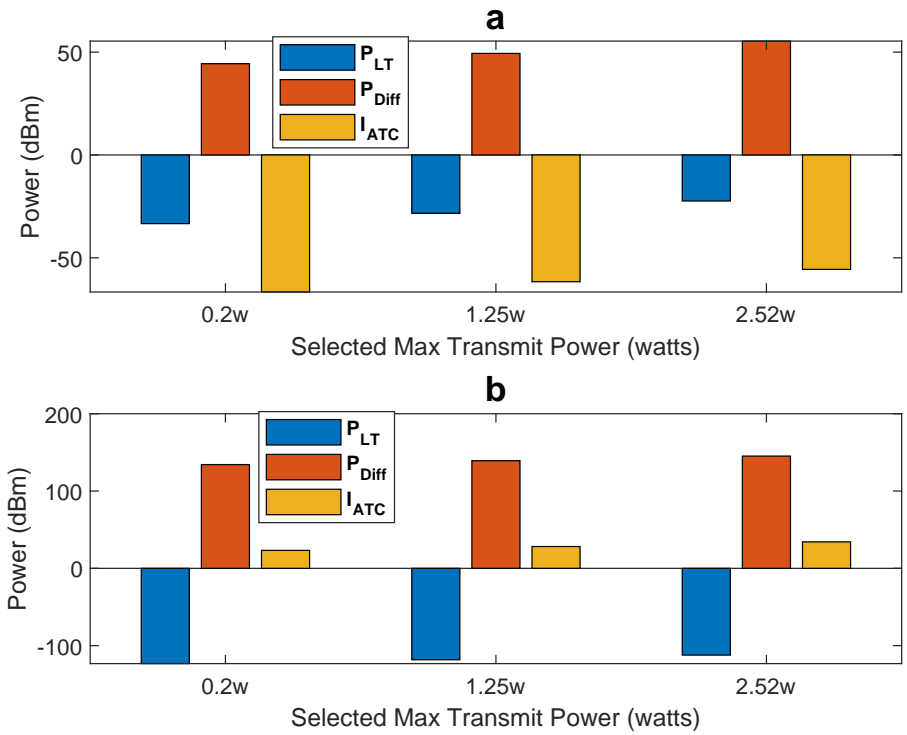
6.1.2 Impact of Different UE Propagation Paths

From the foregoing, it is seen that the required power adjustment differs from one UE's transmission time to the other. Thus for a UE with less attenuation in the propagation path between it and the incumbent's receiver (both the ATC tower and the aircraft), the power adjustment needed will be higher than propagation paths with more attenuation of the signals. The results presented in Fig. 6.2 graphically illustrate this.

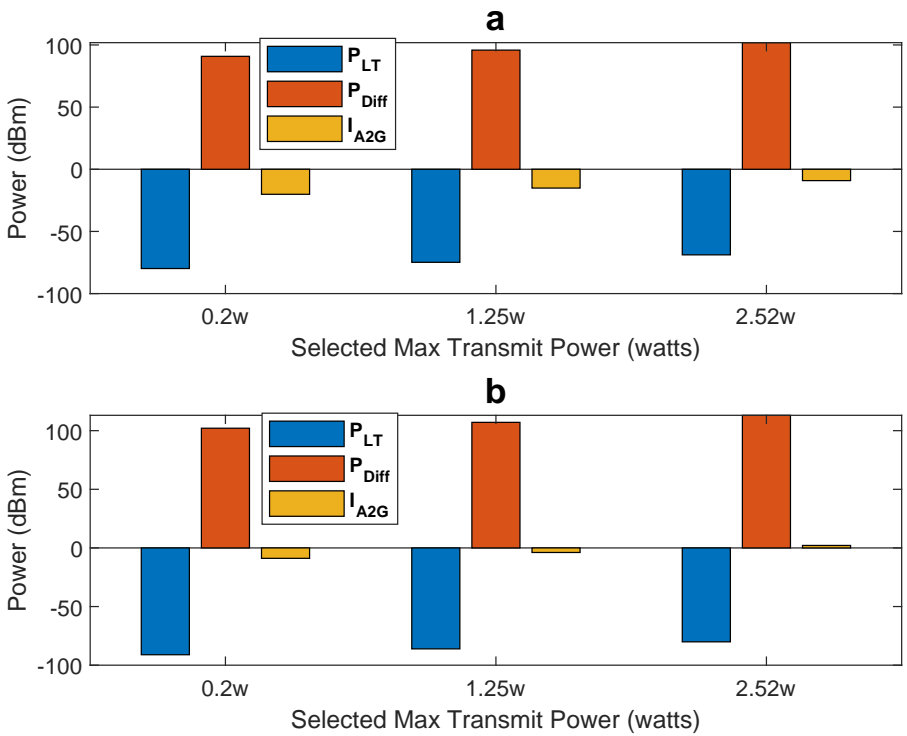
Fig. 6.2(i), shows the UE-ATC tower propagation path with the lowest interference, Fig. 6.2(i)a, and the one with the highest interference Fig. 6.2(i)b, while Fig. 6.2(ii)a and Fig. 6.2(ii)b shows the equivalent UE-aircraft ATG path respectively. The UE-ATC tower path shows significant variation between the lowest and the highest as seen from the positive dB value of interference power in Fig. 6.2(i)b. This leads to almost twice limit transmit power for the UE-ATC path with the lowest interference when compared to the one with highest interference path. When compared to what is obtained in Fig. 6.1b, there is a remarkably improved operating condition for the uplink transmission at this time. The UE- aircraft ATG path shows less variation in the interference values caused by the UEs transmission.

6.1.3 Performance Evaluation of the Proposed Method

In Fig. 6.3, the performance of the proposed method is compared against the EPA benchmark in the licensee downlink. With the proposed method it is seen that there is an improvement of about 120% in the achievable EE over the EPA method. Increasing the number of UE doesn't degrade the improvement achieved by the proposed method, but rather marginally increase its performance. The story is a bit different for the two scenarios in the uplink as shown in Fig. 6.4.



(i) Uplink terrestrial P_{LT} , I_{MS} , and P_{Δ} .



(ii) Uplink ATG P_{LT} , I_{MS} , and P_{Δ} .

Fig. 6.2 Upper and Lower bounds for the Uplink limit power, interference, and power differential.

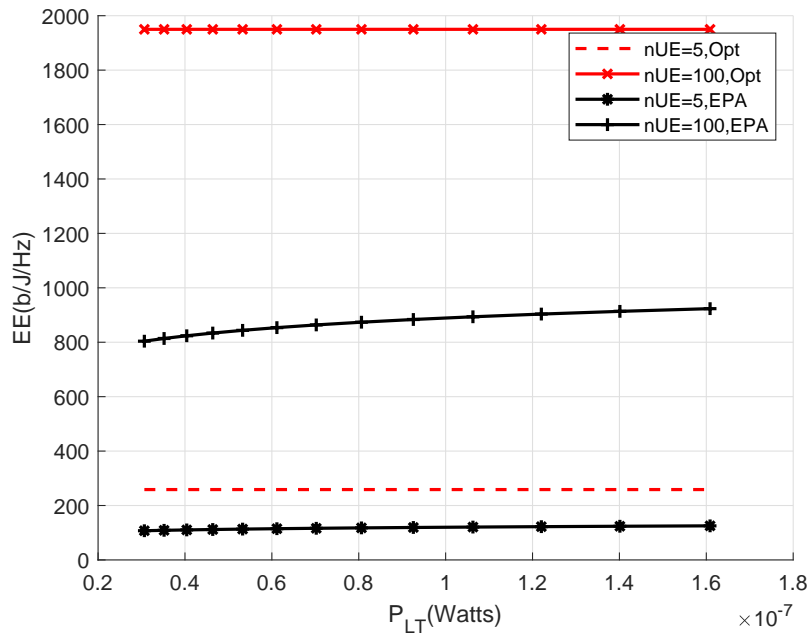


Fig. 6.3 Downlink EE vs. transmit power.

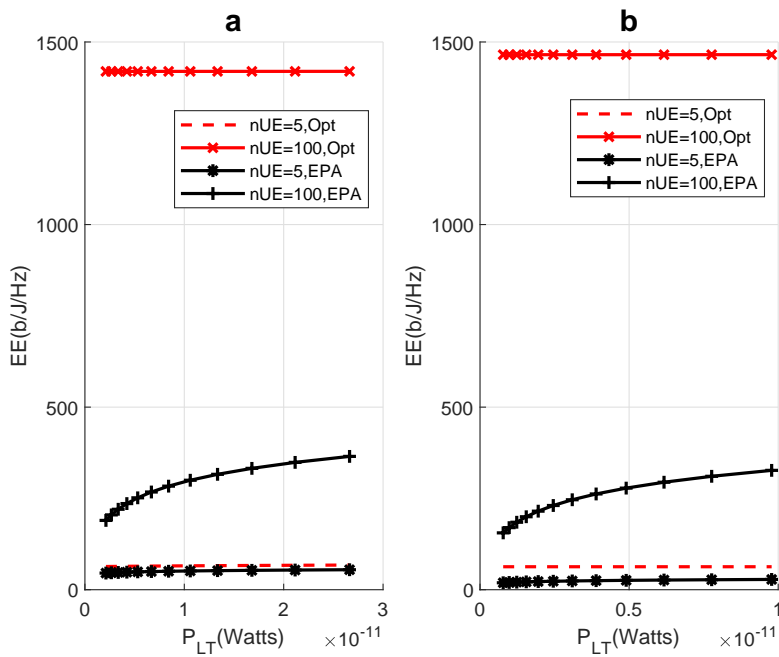


Fig. 6.4 Uplink EE vs. transmit power.

For the terrestrial UE-ATC interference path (Fig. 6.4a), the proposed method doesn't seem to have a significant effect on the achievable EE for small number of UEs. In the ATG UE-aircraft interference path (Fig. 6.4b), the proposed method achieved close to 100%

increase in the EE at low UE number. However, with increase in the number of UEs, the achievable EE with the proposed method improved exponentially to above 300% over the EPA method. It is also observed that for the UE-ATC interference path (Fig. 6.4a), the EE using EPA, is slightly higher than for the ATG UE-aircraft interference path (Fig. 6.4b), while the reverse is the case for the proposed method. This can be attributed to the slightly higher transmit power (P_{LT}), observed in Fig. 6.1 for the UE-ATC interference path. It should be noted that $f_I(i; \theta)$ in (3.23) indicates that $k \rightarrow \infty$, hence it more accurately approximate the interference distribution for very large numbers of UEs in the network. The implication of this is that, by the virtue of the fact the number of UE's considered in the simulations is not infinitely large, the actual gains obtainable in practical systems by the proposed method might deviate from what is obtained here.

To accurately examine the effect of the spectrum access revocation on the licensee system EE, a comparison of the EE under limited transmit power regime should be done with the maximum transmit power EE. Thus, to establish a fair basis of comparison, the limit power is scaled to the maximum transmit power and both EE are compared. In Fig.6.5, the licensee's achieved system EE for the limited transmit power is compared against the obtainable EE for maximum transmit power in the uplink direction. The curve shows that the EE suffers a depreciation similar to the achievable data rate reduction as a result of restriction posed by the revocation of the licensee's spectrum access right by the incumbent. Furthermore, it is seen that the difference in the achieved EE of the two transmit power regime increases with increasing number of transmitting UEs. However, the margin of difference between the two transmit power regimes becomes slightly narrower with increasing operating power.

Fig.6.6, show the comparison of the EE during the time when the licensee has free and unrestricted access to the spectrum and when its access is revoked by the incumbent using both EPA and the proposed optimal power allocation method in the downlink direction. Unlike in the uplink, the EE of the licensee does not suffer significant degradation when the licensee spectrum access is revoked in the downlink. This could be explained by the fact that the interference to the incumbent system in the downlink is from the eNodeB, a static and fixed source and as such, results in a linear relationship between the maximum operating and limited transmit power. As a result, there is a significant improvement in the EE with the optimal power allocation, than even when the licensee has free and restricted access to the spectrum. Furthermore, with increasing number of users in the network, there is no degradation in the EE when the access right of the licensee is restricted.

In Fig. 6.7, we examine how the eNodeB coverage radius affects the improvement in EE achieved using the proposed method. Fig. 6.7(a) is for the downlink, while Fig. 6.7(b) is the ATG interference path in the uplink. Similar result is obtained with the terrestrial interference

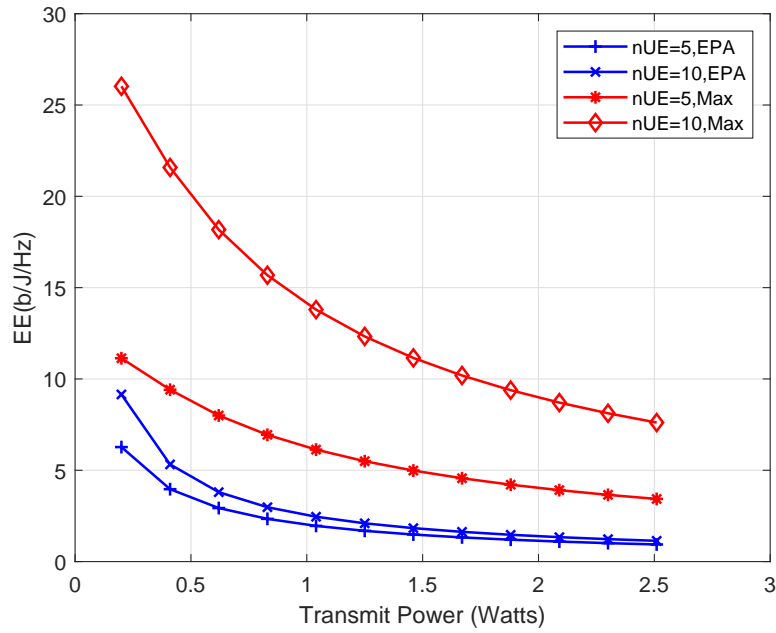


Fig. 6.5 Uplink EE vs.transmit power for limited and maximum power.

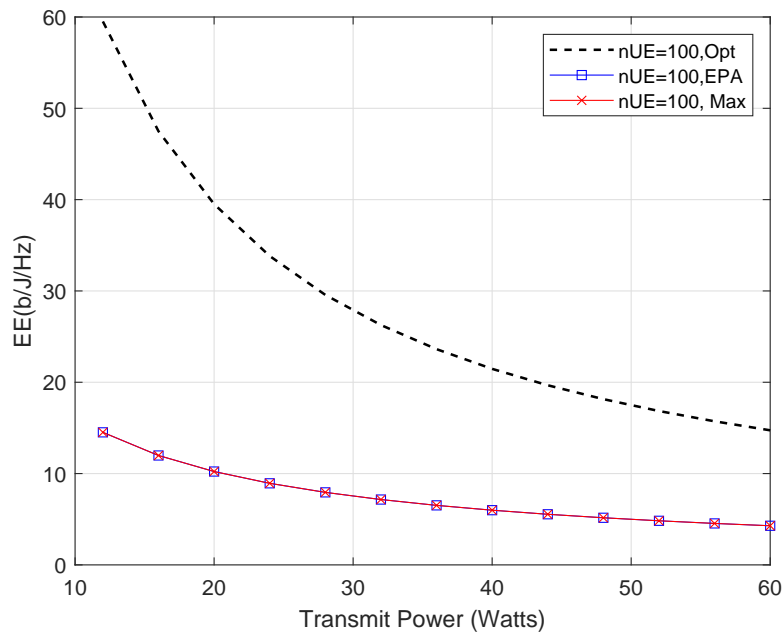
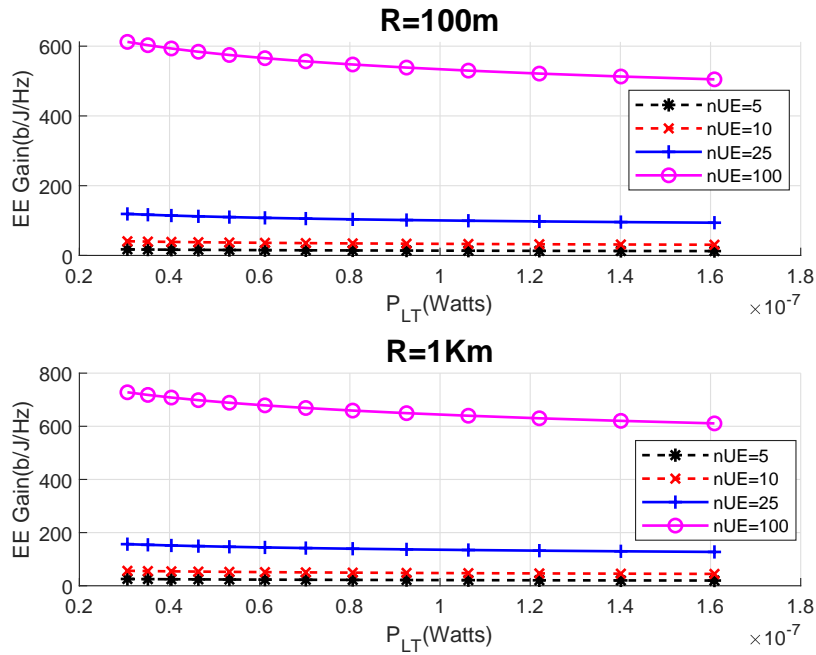
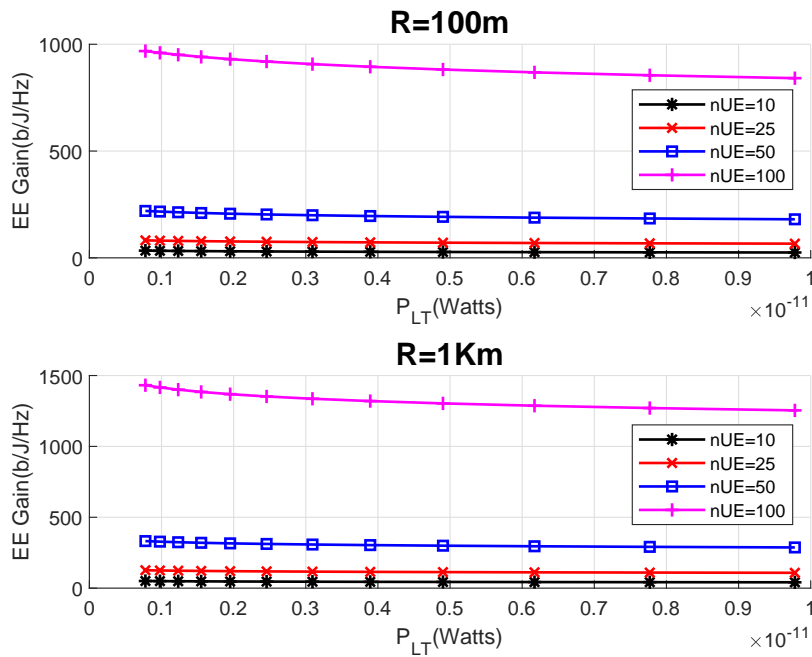


Fig. 6.6 EE vs. maximum transmit power for the optimal limited power, EPA and maximum power spectrum in the downlink.

path between the UEs and the ATC Tower. It is seen that for both the transmission directions, the improvement in the EE achieved by the proposed method increases with increase in



(a) Downlink EE gain for radius 100 m and 1 km.



(b) Uplink EE gain for radius 100 m and 1 km.

Fig. 6.7 Effect of eNodeB coverage radius on the EE gain by the proposed method.

eNodeB radius. Expectedly with increasing number of UEs, the magnitude of the EE gain increases with the uplink outperforming the downlink with an approximate increase of 50% increase between the 100m eNodeB radius and the 1 km coverage radius.

The better EE gain recorded for larger coverage radius is seen from the behaviour of the interference power in relation to the eNodeB coverage area. As seen in Fig. 6.8, the smaller the licensee's eNodeB coverage radius, the larger the interference received by the incumbent system. The larger the interference threat of the licensee to the incumbent, the larger the power adjustment, P_{Δ} , needed to obtain the limit power value that ensures the incumbent's interference threshold is not exceeded. In view of the increasing miniaturization of cellular networks eNodeB coverage area, especially in the 5G technology space of high SE requirement and network densification, this is an interesting network design trade-off challenge worthy of consideration.

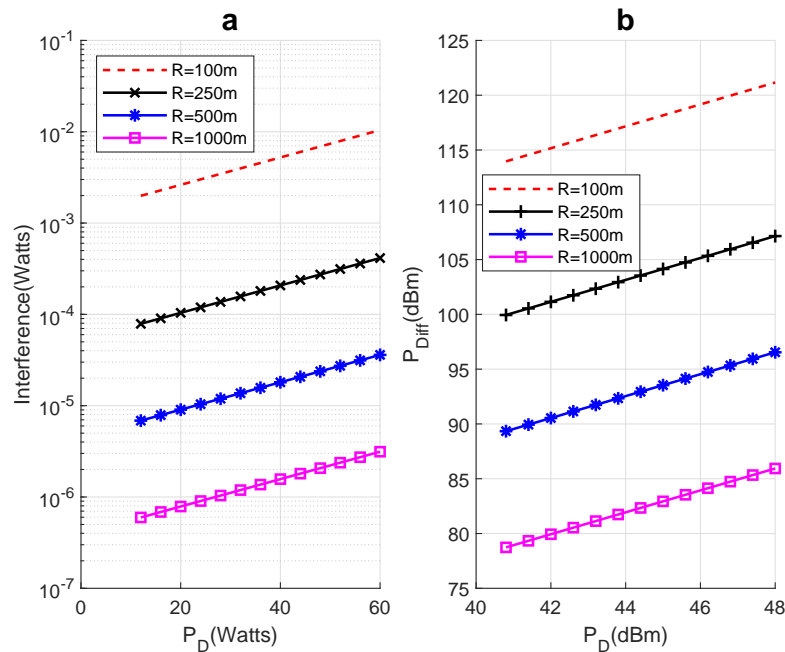
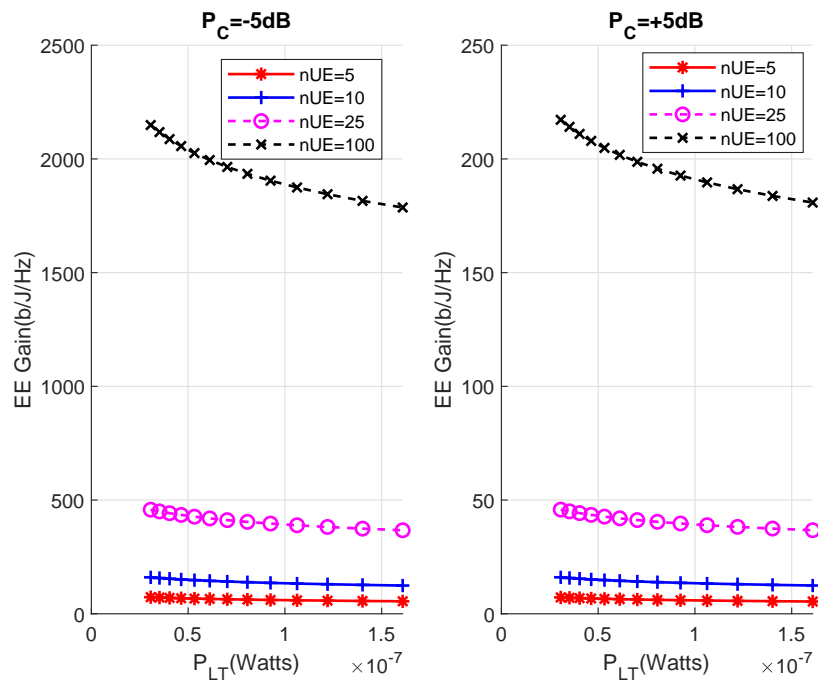
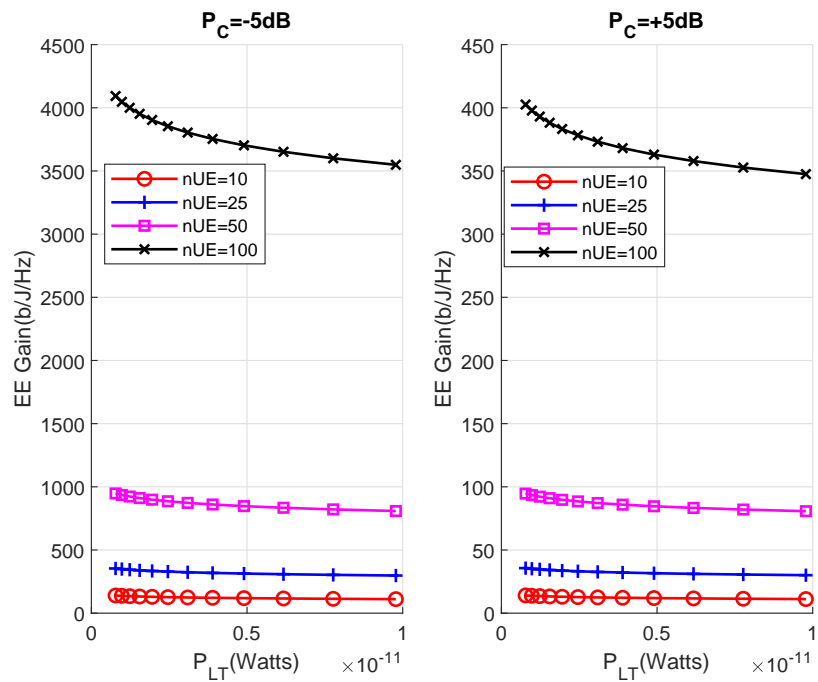


Fig. 6.8 Downlink interference and P_{Δ} for different radius.

Lastly, the effect of the circuit power on the achievable EE of the licensee's network is examined. It is seen in Fig. 6.9 that varying the circuit power leads to variation in the EE gain by a corresponding ratio. This pattern is seen to be consistent in both transmission directions, across different eNodeB coverage radius as well as the number of UEs in the network. The implication of this in practical terms is that, the licensee network design should be geared towards the lowest possible circuit power without compromising system proper



(a) Downlink EE gain for -5dB and $+5\text{dB}$ circuit power.



(b) Uplink EE gain for -5dB and $+5\text{dB}$ circuit power.

Fig. 6.9 Effect of circuit power on the EE gain by the proposed method.

functioning and reliability. This is pertinent considering the global drive for, as well as the 5G requirement for, higher EE in mobile wireless broadband.

6.1.4 Summary of Results

In this section, the effect of the revocation of the licensee's spectrum access right on the energy efficiency (EE) of an LSA sharing between an airport incumbent and a mobile network operator licensee is investigated. On the basis of the expressions for the limited power derived in **Chapter 4**, quantification of the transmit power reduction when the spectrum access right is revoked is done for both the licensee's uplink and downlink transmission directions. Simulation results show that due to the difference in the signal attenuation characteristics of the propagation channel in the uplink and the downlink, the interference to the incumbent in the uplink is significantly higher despite the fact that the downlink rated transmit power is higher. A comparison of the proposed optimal power allocation with the EPA benchmark, indicates an improvement of about 120% in the downlink and a maximum of 300% in the uplink in the achievable EE of the licensee when operating under limit power. However, it should be mentioned that the gains, of the proposed method, recorded here might not be realisable in practical systems because the UEs interference distribution, $f_I(i; \theta)$, in (3.23) assume that $k \rightarrow \infty$, hence it's more accurate for infinitely large numbers of UEs than the limited number of UEs considered in this work. Furthermore, results also show the proposed method is robust to increase in number of UEs on the network. Finally, it is seen that, the improvement in EE provided with the proposed method increases with increase in eNodeB coverage radius. This poses an interesting trade-off challenge in practical network design considering increasing miniaturization of cellular networks eNodeB coverage area, and the 5G technology space of high SE requirement and network densification.

6.2 Spectra Efficiency Results and Analysis

The simulation parameters are summarised in Table 6.2. A circular geographical area with a radius of 200 km centred at the airport consisting of several eNodeBs is considered. The closest eNodeB to the ATC tower is further than 1 km. The UEs are assumed to be distributed in the cell area according to (3.3). The ascent or glide angle (take-off angle) is assumed to change at the rate of 1 degrees per second while the cruising speed is taken as 244.44 m/s (475.16 knots). The ATG propagation parameters used are for the urban environment. Furthermore, we assume a co-channel interference between both systems, the eNodeB

antenna gain set to 17 dB, the feeder loss is 3 dB, the telemetry receiver main lobe antenna gain is equal to 45 dBi, and 1 dB is its feeder loss as specified in [38].

Table 6.2 SE Simulation Parameters.

Parameter	Value
eNodeB Radius	100, 250, 500, 1000 (metres)
No. of UE	5, 10, 25, 100
Downlink Transmit Power	0.2 – 15.85 w (23–42 dBm)
Uplink Transmit Power	0.2 – 2.52 w (23–34 dBm)
Noise Spectral Density	-60 dBm/Hz
eNodeB Antenna Height	30 metres
UE Antenna Height	1.5 metres
ATC Type-B Receiver Noise Figure(NF)	3 dB
Boltzmann's constant(k)	1.38×10^{-23}
Temperature (T)	290 Kelvin
Noise Power	$10\log(kTB) + NF$
Protection Ratio (I/N)	-10 dB
Bandwidth (B)	10 MHz
LSA Frequency Band	2300 - 2400 MHz
Career Frequency	2350 MHz
Height of ATC Tower	8 metres
Airplane take-off angle	7 - 25 degrees
Airplane take-off speed	65 m/s
Airplane Acceleration	0.29 m/s ²

The results discussion starts with the investigation of the performance of the licensee system SE optimization using the optimal power allocation in the downlink, followed by a comparative analysis with the uplink. In Fig. 6.10 the SE is given versus the transmit power for 10 and 5 UEs in the downlink transmission for both the system with our proposed optimal power allocation and without. As it is seen, there is a significant improvement in the system SE with the optimal power allocation proposed. Judging by the graph for 10 UEs, around seven fold (700%) improvement is obtained over the system without the optimal power allocation.

Fig. 6.11 shows the SE gain for different number of UEs versus transmit power. It is seen that the achieved SE gain is directly proportional to the number of UEs similar to Fig. 6.10, where the plot for the larger number of UEs is expectedly higher than the one for smaller number of UEs. This means that the SE gain increases proportionately with increasing number of UEs. Furthermore, to show the actual increase in the SE, a comparative metric, a

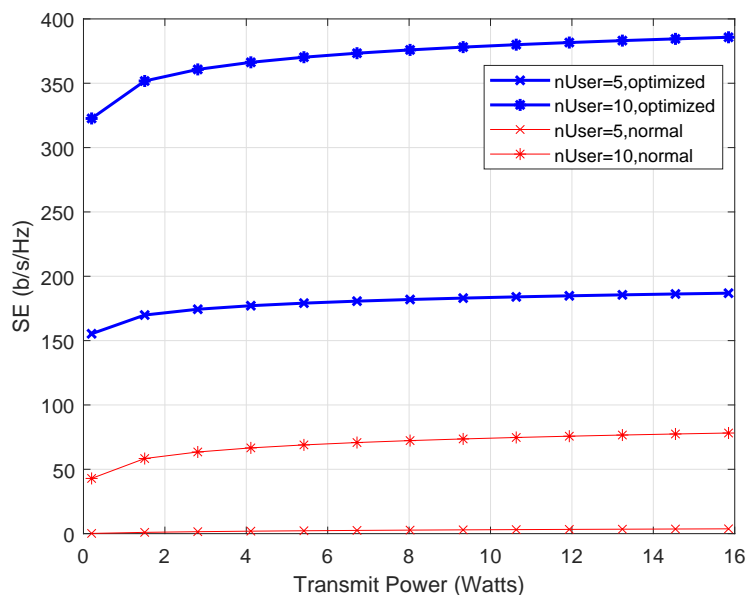


Fig. 6.10 Comparison of the SE in optimized and the non-optimized systems vs. total transmit power.

decibel SE gain is introduced. Interestingly, this revealed further facts not only about the SE gain pattern in relation to the number of UEs, but also with increasing the operating transmit power.

In Fig. 6.11 the decibel SE gain also indicates that a larger SE improvement is obtained at lower transmit power. Moreover, in comparison to the linear SE gain in b/s/Hz, the decibel SE gain shows an approximately equal value at low transmit power for users 10, 25 and 100 at low transmit power while the graph becomes more distinct with increasing operating power. In contrast to the linear SE gain, the decibel SE gain has an inverse proportion to the number of UEs in the system. In the plot for the SE gain in b/s/Hz, higher number of UEs has a higher actual SE gain value than normal, however the decibel SE gain showed that lower number of UEs recorded a better gain ratio than higher number of UEs. This can be explained by the fact that at lower number of UEs, the interference to the incumbent system is low, thus the transmit power reduction required is relatively small and there is a higher degree of freedom to take advantage of the optimal power allocation. Furthermore, this could also be explained by the fact the UEs interference distribution, $f_I(i; \theta)$, in (3.23) is more accurate for infinitely large numbers of UEs than the small number of UEs. Thus the recorded gain for the smaller number of UEs could be slightly exaggerated as a result of this feature of $f_I(i; \theta)$.

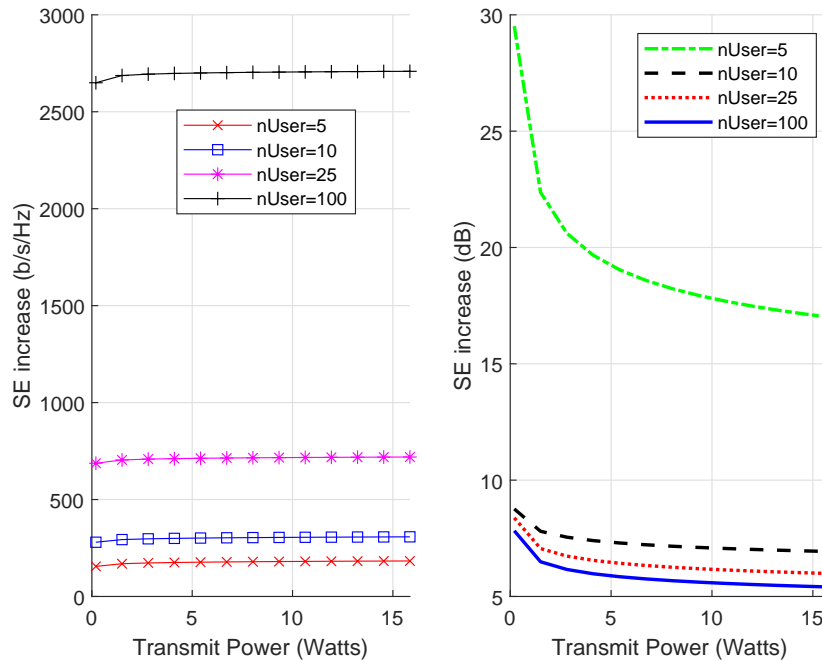


Fig. 6.11 Downlink SE gain vs. transmit power.

In Fig. 6.12, the effect of different cell sizes on the decibel SE gain is investigated. A similar trend is seen for various sizes of eNodeB radius as in the second graph of Fig. 6.11. It is further noticed that the SE gain, increases with increasing eNodeB coverage radius. Similar trend is also seen in the plot for the 5 UEs and 10 UEs, where the gap shows a slight increase with increasing eNodeB coverage radius. The pattern did not change for the uplink.

Fig. 6.13 shows the plot of the decibel SE gain vs. transmit power in the uplink transmission direction. Similar to the downlink decibel SE gain, the uplink SE gain is inversely proportional to the number of UEs. However, there is a difference in the shape of the curve. While for the downlink, the decibel SE gain is a monotonically decreasing curve, in the uplink the decibel SE gain curve initially increases to a peak value after which it gradually decreases. The implication of this is that at very low transmit power the advantage provided by the optimal power allocation is small. By increasing the transmit power, the effect of the optimal power allocation becomes more significant, after which it starts to decrease.

6.2.1 Efficiency of the LSA Spectrum Utilization

For ease of analysis, the focus in this section is on the eNodeB radius of 1000 m, hence for a distance of 200 km from the airport, we have a total of hundred (100) q service layers in the

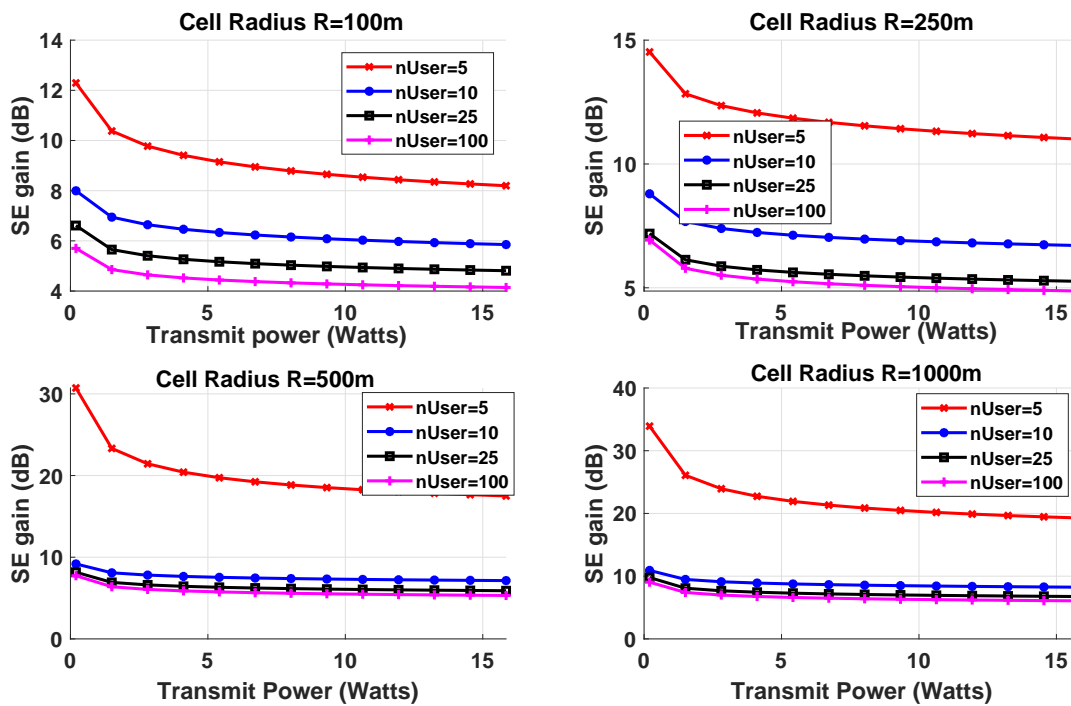


Fig. 6.12 Downlink SE gain vs. transmit power for various eNodeB radius and number of users.

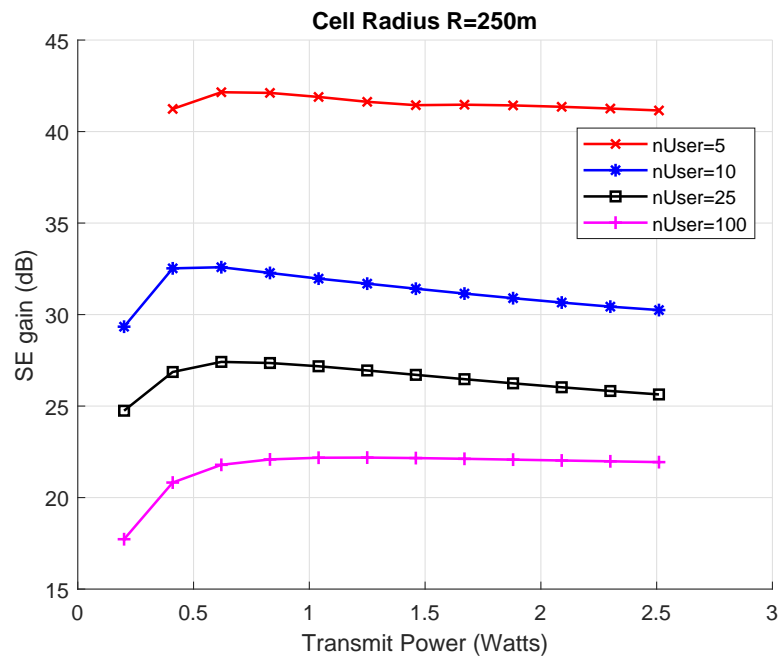


Fig. 6.13 Uplink SE gain vs. transmit power for various number of users, where $R = 250$ m.

utilization efficiency analysis. The busy period ratio v_q for each service layer to all service layers is obtained using the procedure in algorithm 6.

Algorithm 6 Computation of the Busy period ratio v_q .

- Step 1.** Initialise the airplane take off speed(V_i), acceleration(A_a) initial(α_i) and final ascent angle(α_f), glide angle change rate (δ_α) and eNodeB radius(R);
- Step 2.** While $\alpha_i < \alpha_f$ and for each increment (t_s) of δ_α , compute the equivalent horizontal distance by solving $g_d = \sum_{t_s=0}^{\alpha_f-\alpha_i} V_{t_s} \cos(\alpha_i + t_s \cdot \delta_\alpha)$;
- Step 3.** Create a vector (\mathbf{D}) of the spacing of adjacent, service layers $\mathbf{D} = \{R : 2R : 2qR\}$;
- Step 4.** Compute the aerial length(r) of service layer 1 by solving $r_1 = \frac{g_d}{\cos(\frac{\alpha_i+\alpha_f}{2})} + \frac{(D_1-g_d)+R}{\cos(\alpha_f)}$
Compute the aerial length of the remaining layers from $r_1 + \frac{D_q+R}{\cos(\alpha_f)}$ {for $q = 1 \dots q - 1$ } requirement \mathbf{R}_S ;
- Step 5.** Create a vector (\mathbf{V}) of the airplane final velocity , at the edge of each service layers
 $\mathbf{V} = \{V_1, V_2, \dots V_q\}$;
- Step 6.** Solve for the busy period in each q service layer from $\mu_q^{-1} = \frac{V_q - V_{q-1}}{A_a}$ and obtain BP ratio v_q as $\frac{\mu_q^{-1}}{\sum \mu_q^{-1}} \equiv \frac{\mu}{\mu_q}$ where $\mu = \{\mu_1, \mu_2 \dots \mu_q\}$
-

Fig. 6.14 shows the interference power from the eNodeB to the ATC tower for different eNodeB coverage areas within the considered geographical radius. To better visualize, the y-axis is plotted as a log scale in the second graph of Fig. 6.14. In the first graph because of the margin of difference between the interference generated by the first eNodeB and the second one, it was practically impossible to make any comparison even for just the first two eNodeB coverage areas. In the second graph, it was possible to plot the interference of all the eNodeB coverage areas and compare them. It is seen that for a high eNodeB transmit power, the interference power generated by the licensee is still higher than the incumbent threshold even at the 100th eNodeB which is about 200 km away from the ATC tower. This is in agreement with the report of the compatibility studies done by the electronic communications committee in [38] which gives separation distance between an MNO and ATC to be in order of hundreds of kilometres. However, at a low transmit power, starting from the 50th eNodeB (about 100 km distance from the ATC tower), the received interference by the ATC tower is below the prescribed threshold.

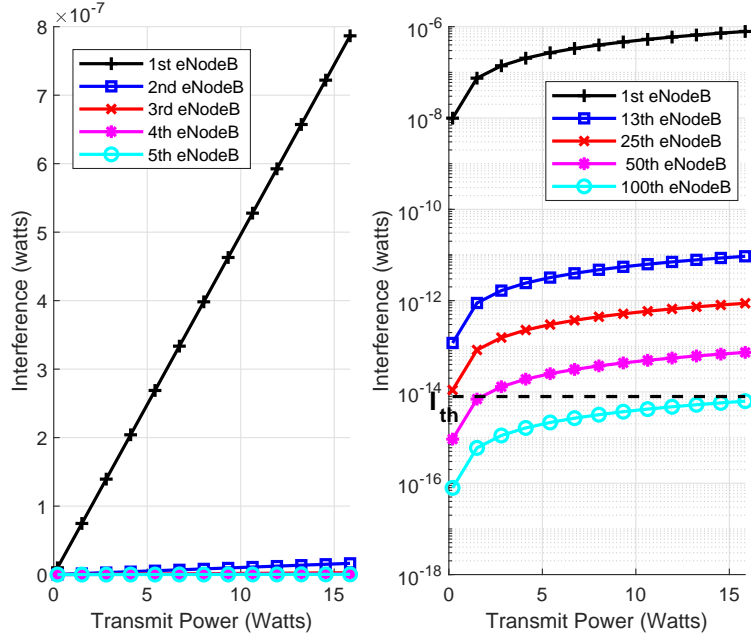


Fig. 6.14 Downlink Interference power for different eNodeB.

The implication of the above observations of Fig. 6.14 from the utility function of (4.51) is that the spectrum utilization efficiency at higher transmit powers and coverage areas close to the airport reduces to η_{SE} since the eNodeBs have to maintain their power reduction policy for the total duration of the ATC tower communication with an airplane while it is still within its airspace. However, for further eNodeBs, as well as low transmit power below a certain threshold even from about 100 km distance from the ATC tower, the licensee can operate at its rated transmit power hence the spectrum utilization efficiency is given by the second part of (4.51).

The bar chart in Fig. 6.15 shows the BP ratio v_q across different eNodeBs. As it is seen, v_q decreases with increasing separation distance between the eNodeB coverage area and the airport. This is because of the increase in the airplane speed as it accelerates across the area. The import of this on the spectrum utilization efficiency is that as a certain eNodeB coverage becomes further removed from the vicinity of the airport, the time for operating under the power reduction policy becomes reduced. To put this in a better context we analyse the first equation in the utility function of (4.51) presented here for ease of discussion

$$(1 - v_q)SEq_{\max} + v_q \cdot \eta_{SEq}, \quad 0 < v_q < 1 \tag{6.1}$$

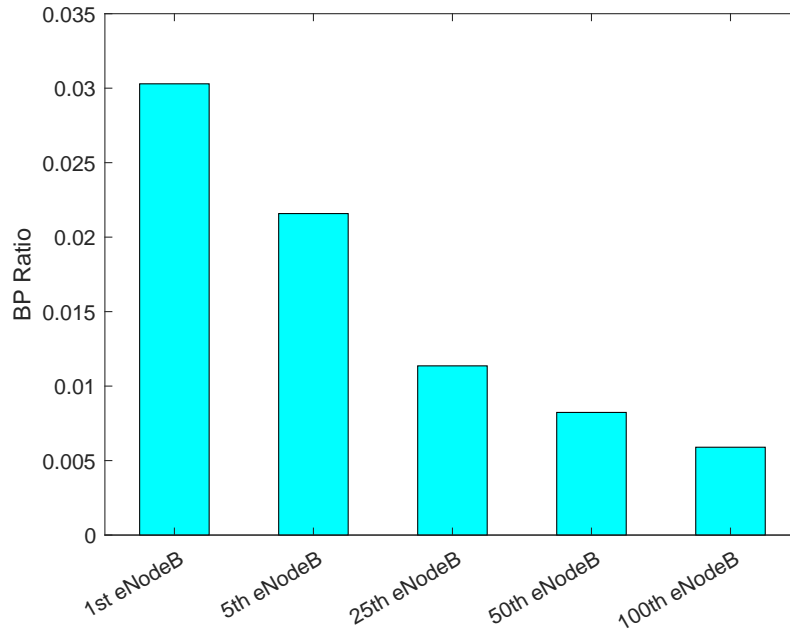
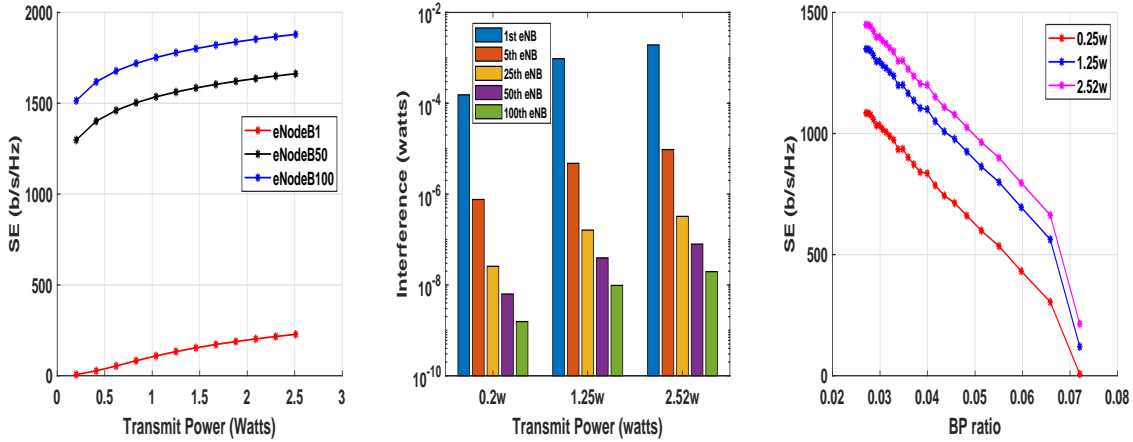


Fig. 6.15 BP ratio, ν_q , for different eNodeB.

From (6.1), it is seen that better spectrum utilization is obtained when the first part of the equation is high, i.e., when the licensee can operate at its maximum transmit power. A high value of ν_q reduces the time the licensee can operate at full power and increases the length of the period it operates under reduced power policy, thus effectively reducing the utilization efficiency.

The above is further confirmed by the graphs in Fig. 6.16. It is seen from the first graph, (Fig. 6.16a), that the achievable SE in the uplink for eNodeB coverage areas farther from the airport is higher than those closer. Thus, for those distant coverage areas, the spectrum utilization efficiency is improved not only because of the smaller ν_q which minimizes the period for limited power regime but also by higher achievable η_{SE} . The monotonically decreasing graphs in Fig. 6.16c, suggests that the achievable SE has an inverse relationship with the busy period ratio of each service layer to all service layers.

Fig. 6.16b shows the uplink interference power at the airplane for selected transmit power levels across the coverage areas in the considered radius around the airport. Similar to the downlink, the interference reduces for eNodeB coverage area farther away from the airport. This is however not due to the distance to the airport but rather due to the increasing height between the airplane and the licensee UEs. Unlike the downlink case, the airplane could receive interference significantly higher than the prescribed threshold at the farthest eNodeB coverage area even at the lowest transmitting power. This can be attributed to the better



(a) Uplink SE gain for different eNodeB. (b) Uplink Interference power for different eNodeB. (c) SE vs. BP ratio ν_q , for different eNodeB.

Fig. 6.16 Uplink SE, interference power and ν_q for eNodeBs across different separation distance.

LoS in the ATG propagation path between the UEs and the airplane. As a result of higher probability of LoS, the signal attenuation is smaller compared to the terrestrial path loss model in the downlink.

This is confirmed by the interference power from the UE to the ATC tower shown in Fig. 6.17 which has a terrestrial propagation similar to the downlink. For the same transmit power and separation distance, it is seen in Fig. 6.17 that the interference power is several orders of magnitude lower than it was in Fig. 6.16b. At low transmit power the obtained results show that the received interference at the ATC tower from the UE is below the prescribed threshold at approximately 23 km distance, i.e., the 12th eNodeB. This suggests that instead of suspending licensee transmission in all the 100 eNodeB and even farther as dictated by the exclusion zone policy [125, 126], the licensee can operate under the full transmit power in the uplink starting from the 13th eNodeB.

6.2.2 Summary of Results

This section presented a LSA sharing arrangement between an ATC incumbent and a MNO licensee, during the period when the incumbent is utilizing its spectrum for telemetry services. A circular protection radius of 200 km is considered, with many eNodeBs located within this geographical radius. In addition, a utility function of achievable SE and busy period ratio of each service layer to all service layers, is proposed as a metric for measuring the additional spectrum utilization efficiency during the period of the incumbents occupation of

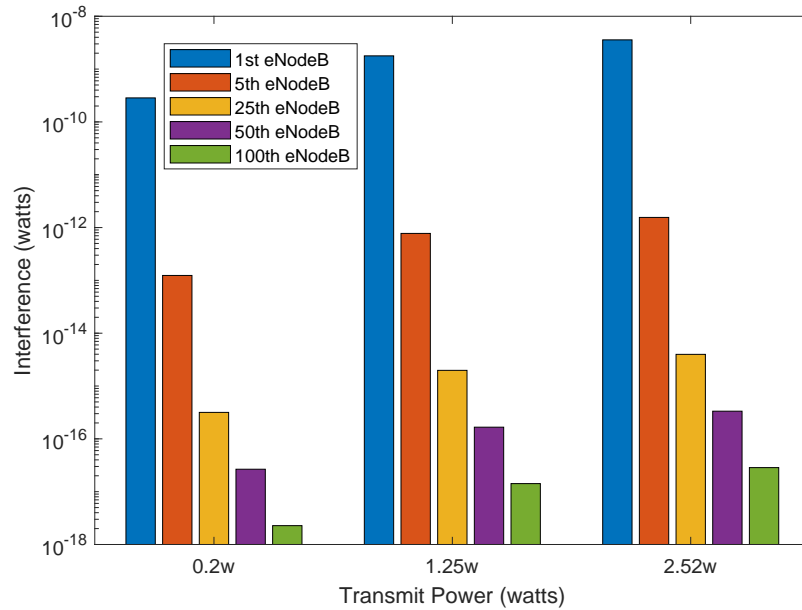


Fig. 6.17 Uplink interference to ATC tower.

its spectrum. Results show that the SE is significantly improved with the proposed optimal power allocation. Furthermore, the introduced decibel SE gain measure reveals that the UE traffic in a eNodeB coverage area is inversely proportional to the achieved SE improvement obtained when using the proposed optimal power allocation.

The implication of this is that for practical LSA deployment scenario, optimal system design must be geared towards achieving the best trade-off between the UE traffic and the desired SE. Moreover, considering the possibility of the LSA system co-existing with the legacy MNO network, this result provides a guide for reliable and optimal traffic distribution between the two systems. It is also seen that the farther the eNodeB coverage area is to the airport, the better is the achievable SE. This is due to reduction in interference power from the licensee to the ATC system. In practical terms, the implication of this is that at farther distance from the airport, the operating parameters of the MNO in an LSA system can be configured with less stringent restrictions. Due to the higher LoS in the ATG path between the licensee interferer and the incumbent airborne receiver, it is seen that the interference suffered by the uplink of the incumbent system persists to far greater distance than received interference in its downlink. In fact, the interfering signal from the licensee UEs to the incumbent downlink receiver (the ATC tower), drops within the tolerated threshold at a considerably shorter distance (when compared to the equivalent uplink scenario).

6.3 EE-SE Optimization- Results Discussion and Analysis

In this section, the results obtained for the EE-SE optimization solution in section 4.3 is presented and discussed. In this analysis, the most severe interference path between the MNO licensee UEs and the incumbent airborne receiver, the worst case scenario, is examined.

The simulated LSA system comprises a single cell licensee. The system parameters are given in Table 6.3. The UE are assumed to be distributed in the eNodeB coverage area according to (3.9). For the simulated system in Fig. 6.18, the weighted trade-off function, SE, and EE are given versus eNodeB transmit power, where we compare how both metrics and their weighted trade-off (at $w = 0.5$) perform in relation to varying number of UE. As it is seen, the magnitude of the SE, EE and their trade-off has a direct relationship with increasing number of users present in the licensee eNodeB coverage area.

Table 6.3 Simulation Parameters for the EE-SE Trade-Off.

Parameter	Value
Cell Radius	100, 250, 500 & 1000 (metres)
No. of UE	5, 10, 15, 20, 25
Transmit Power	0.2 – 15.85 w (23–42 dBm)
Bandwidth (B)	10 MHz
Noise Density	-60 dBm
Circuit Power	-5, 0, 5, 10 (dB)
Amplifier Efficiency	38%
ATC Type-B Receiver Noise Figure(NF)	3 (dB)
Boltzmann's constant(k)	1.38×10^{-23} (J/K)
Temperature (T)	290 K
Noise Power	$10\log(kTB) + NF$ (dB)
Protection Ratio (I/N)	-10 (dB)
UE Total Simulated Movement Time (T)	15 (s)
Simulated Pause Interval	0 – 1 (s)
UE Speed Interval (V)	0.2 – 2.2 (m/s)
Simulated time step	0.1 (s)
Movement Direction Interval (V)	-180 – +180 (degrees)

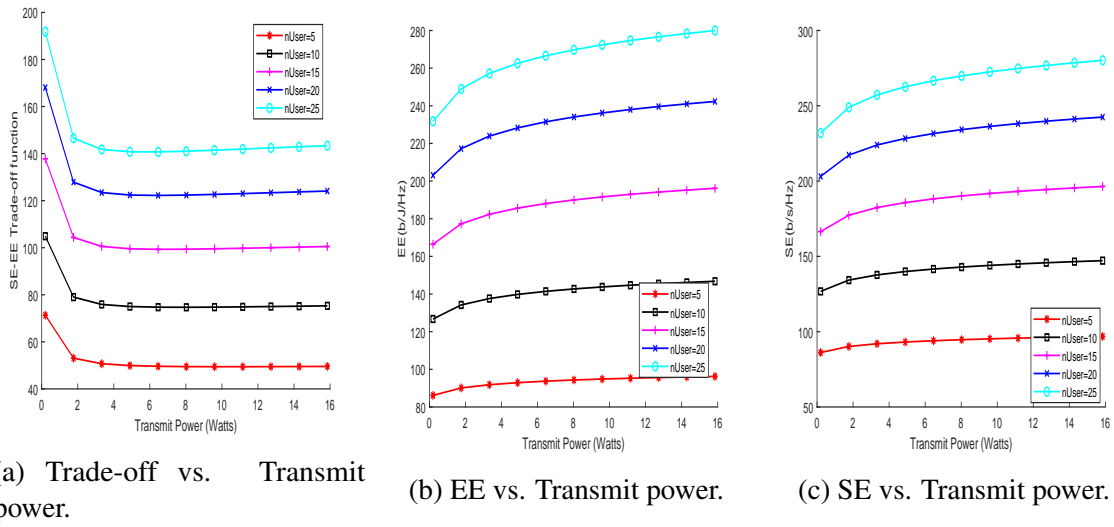


Fig. 6.18 SE, EE, and the Trade-off curves.

Fig. 6.19 examined the impact of the UE movement on the system’s EE and SE and their trade-off. The five different time steps plotted show that there is no significant variation in the investigated performance metrics as a result of the changing location of the UE.

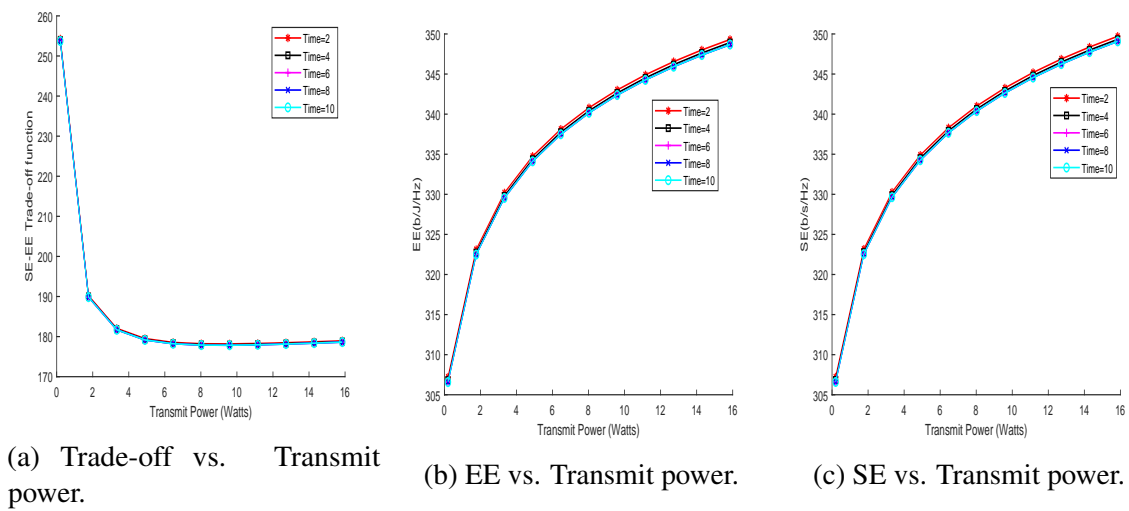


Fig. 6.19 Effect of UE movement on the SE, EE, and the Trade-off curves.

Figs. 6.20 and 6.21, show the effect of the interference threshold constraint on the licensee system’s SE and EE. Both metrics are compared when the spectrum is free, when not constrained by the incumbent’s maximum tolerable interference, and when it is, i.e. when the spectrum is busy. For the EE vs. transmit power, instead of a monotonically decreasing

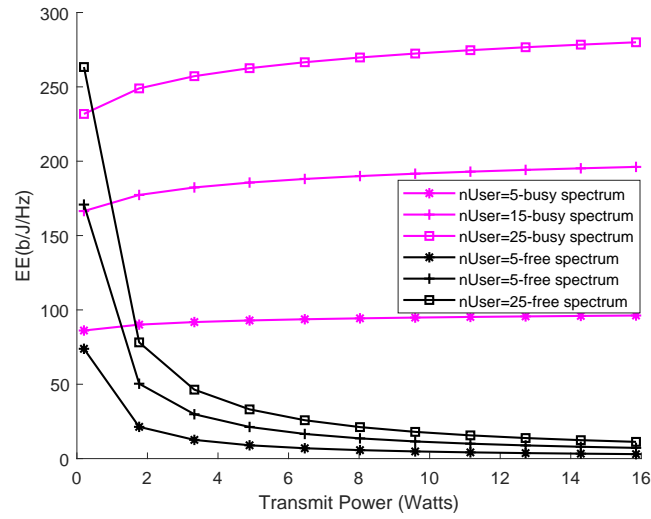


Fig. 6.20 Effect of I_{th} on EE vs. Transmit power for different user number.

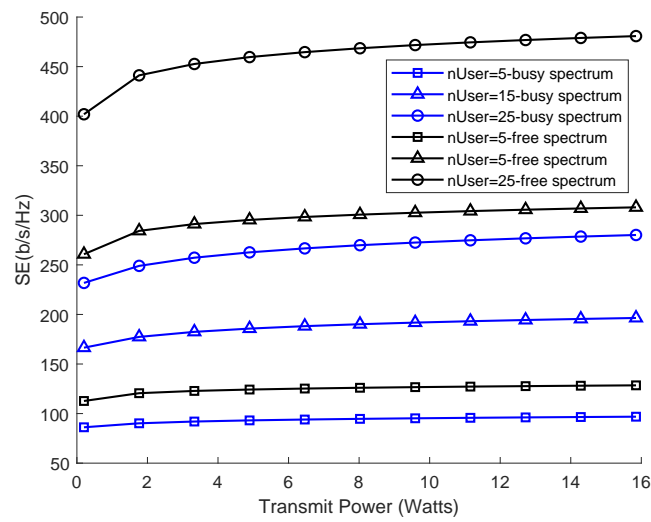


Fig. 6.21 Effect of I_{th} on SE vs. Transmit power for different user number.

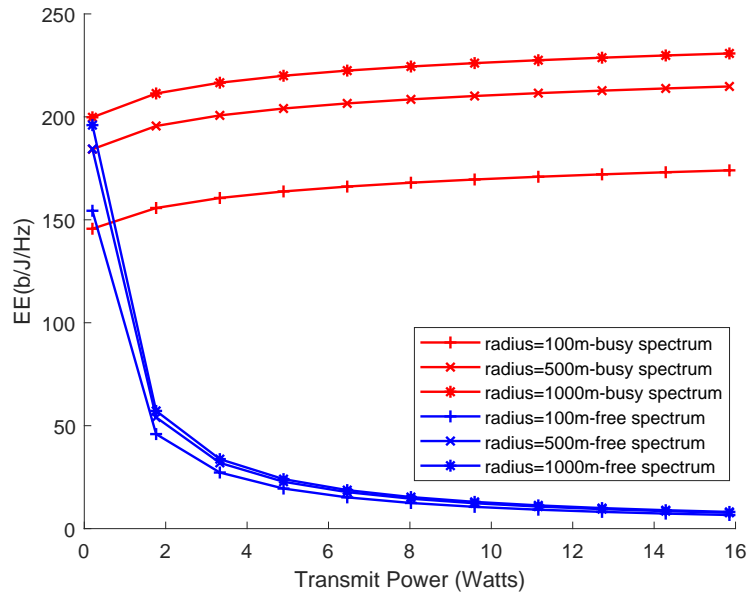


Fig. 6.22 Effect of I_{th} on EE vs. Transmit power for different eNodeB coverage radius.

function observed for the free spectrum curve, the busy spectrum curve gently increases monotonically. This is due to the optimal power allocation adopted to boost the performance of the licensee during the busy spectrum. However, the full impact of reduced transmission power on the SE is reflected in Fig. 6.21, where the SE during the period when the spectrum is free is better than when the spectrum is busy.

Similar to what was established in Fig. 6.18, increase in the number of transmitting UE shows proportionate increase in the EE and SE of the optimized system. Furthermore, while the difference in EE value for different number of users shows a slight increase with increasing transmit power, the reverse is the case in the non-optimized free spectrum system, where the observed marginal difference decreases further with increasing transmit power. Consequently, in Figs. 6.22 and 6.23, the effect of different eNodeB coverage radius on the contrast between the licensee network EE and SE when the LSA spectrum is free and when it is busy is shown. With increasing radius, the EE of the non-optimized system approximately converges to the same value with increasing power, while in the optimized system, the increase with increasing eNodeB coverage radius remains approximately constant for increasing power. The SE for different radius displays the same trend observed for different number of UE.

6.3.1 Effect of Importance Weight on the EE-SE Trade-Off

Next, is the examination of the effect of the trade-off parameter ' w ' (the trade-off importance weight) on the joint SE-EE optimization objective function in (4.62). In Fig. 6.24, it is seen that at $w = 0$, the SE-EE optimization reduces to a EE problem while when $w = 1$, the joint-SE-EE optimization tends to a SE optimization. Also noteworthy is the shape and magnitude of the SE-EE trade-off curve as we move from where the EE is dominant, (i.e., at $w = 0$) to the other extreme where the system's SE is dominant (i.e., at $w = 1$). It is observed that as ' w ' increases, the SE-EE trade-off curve changes from a monotonically decreasing function to an increasing function. Furthermore, the magnitude of the trade-off function shows a five times (5x) increase between the two extremes of w .

A similar trend in terms of the magnitude of the trade-off function is observed in the graph for the effect of w for different eNodeB coverage radius in Fig. 6.25. Analogously, the variation in the shape of the curve is akin to the observation in Fig. 6.24. At $w = 0$, the curve is monotonically decreasing. The same trend is observed at $w = 0.3$, but with a less steep slope. However, at $w = 0.7$, the curve initially decreases, reaches a minimum at approximately the $2w$ mark, and then gradually increases. At $w = 1$, the curve reverts to a monotone but increasing function of transmit power.

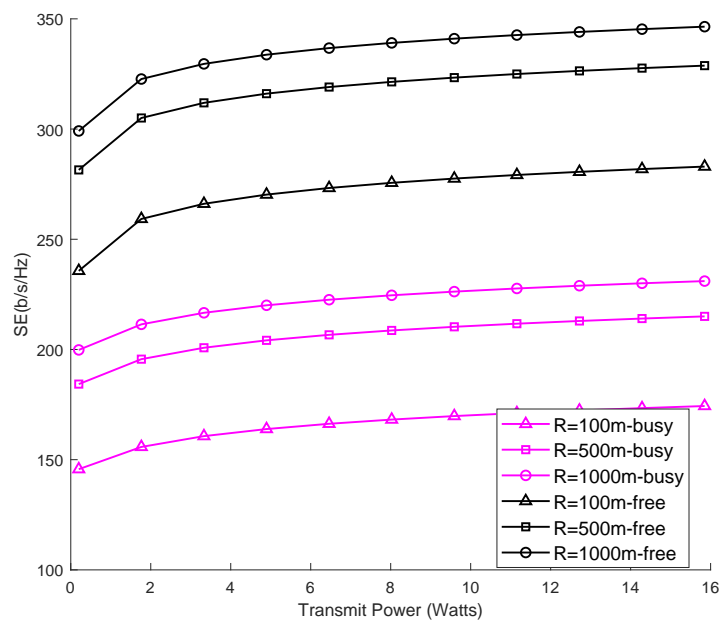
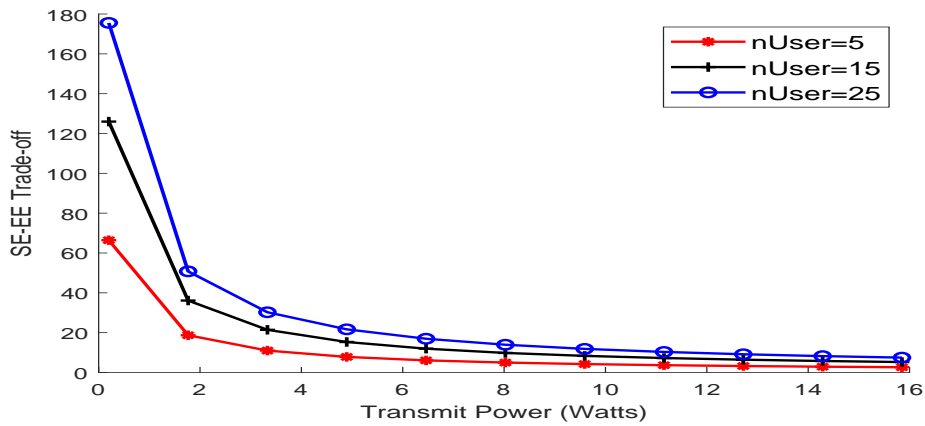
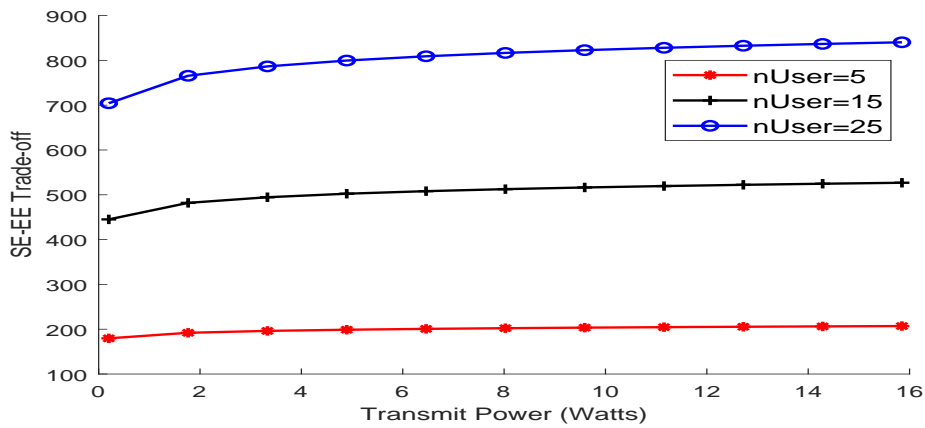


Fig. 6.23 Effect of I_{th} on SE vs. Transmit power for different eNodeB coverage radius.

(a) Trade-off vs. Transmit power at $w = 0$.(b) Trade-off vs. Transmit power at $w = 1$.Fig. 6.24 Effect of w on SE-EE Trade-off vs. Transmit power for different user number.

In Fig. 6.26 the impact of the importance weight parameter, w , on the free and idle spectrum SE of the licensee is shown. As it is seen from the graphs, in the trade-off section between $w = 0.1 - 0.9$ (i.e., Fig. 6.26a, &b), the achievable SE is higher during the period the licensee has the LSA spectrum to itself alone than when the spectrum is occupied by the incumbent. But at $w = 1$, when the SE totally dominates the SE-EE joint optimization function, the relationship is reversed, with the licensee achieving better SE during the period the LSA spectrum is busy than when the spectrum is free. Expectedly, the magnitude increases with increasing number of transmitting UE.

On one hand, this can be attributed to the fact that the system with busy spectrum is, in fact, an optimized system in terms of SE, and not optimized for the case where the spectrum is free. On the other hand, when the difference between the interference from the licensee system and the incumbent's threshold is small, the required reduction in the licensee

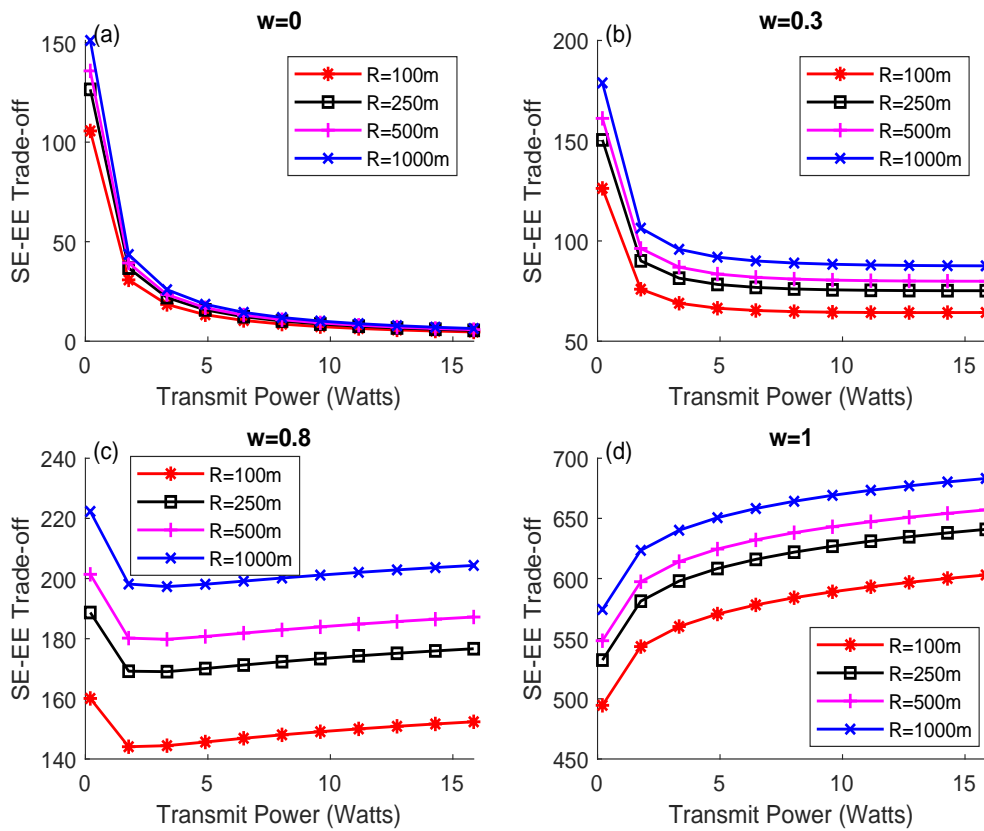
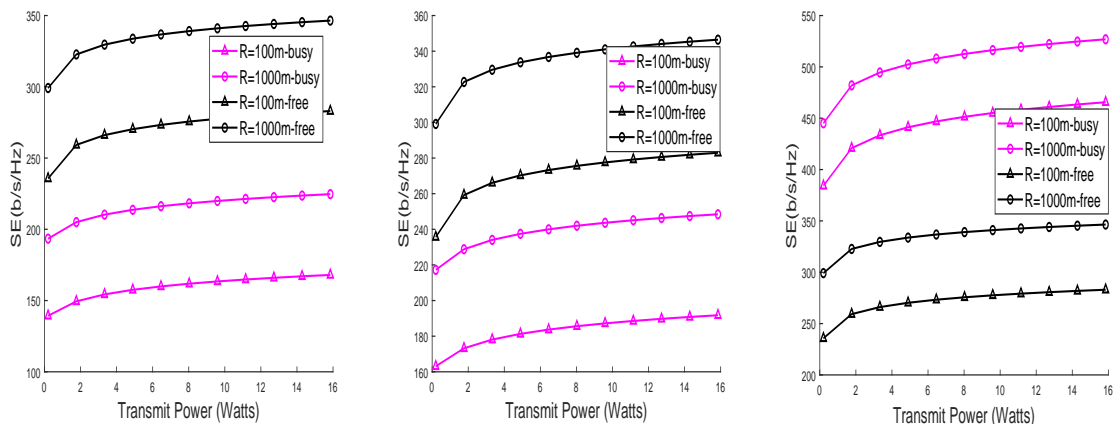


Fig. 6.25 Effect of w on SE-EE Trade-off vs. Transmit power for different eNodeB coverage radius.



(a) Free and idle spectrum SE vs. Transmit power at $w = 0.1$. (b) Free and idle spectrum SE vs. Transmit power at $w = 0.9$. (c) Free and idle spectrum SE vs. Transmit power at $w = 1$.

Fig. 6.26 Comparison of free and idle spectrum SE vs. Transmit power at different values of w .

transmit power could be minimal/marginal. The optimal power allocation adopted for the busy spectrum thus results in a higher SE than the free spectrum SE which is not optimized. Furthermore, we note that at $w = 1$, the joint optimization function is no longer a trade-off between SE-EE, but an outright optimization of the SE only. This is in agreement with what was observed in Fig. 6.24, which indicates a 5x increase in the objective function between $w = 0$ and $w = 1$.

The effect of w on the system's EE was also investigated in Fig. 6.27. It is seen that at $w = 0.1$, the EE of the busy spectrum out performs that of the free spectrum. This is a combination of two effects: the increase in the SE as a result of the optimal power allocation and a reduction in transmit power due to the limited power regime during the time the spectrum is busy. Nominally, the EE is a decreasing function of transmit power as seen in the free spectrum EE vs. transmit power curve. However, the SE-EE joint optimization produces a gently increasing EE vs. transmit power curve. This combined with the reduction in the total power consumed as a result of limited transmit power, further accounts for a better EE during the busy spectrum. The same trend was observed for all values of $w < 1$. Furthermore, the achieved EE for different values of $w < 1$ is approximately the same, while increase in eNodeB coverage radius translates to a larger achieved EE value. However, when w exactly equals 1, the EE curve for the busy spectrum lies on the x-axis. This is expected because, at $w = 1$, the joint SE-EE optimization strictly becomes an SE optimization problem and the EE of the system, no longer comes into play in the optimization objective.

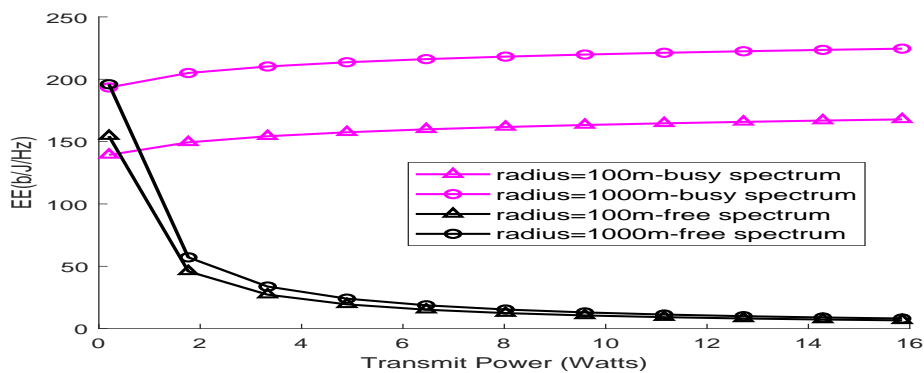
6.3.2 Effect of Circuit Power on the EE-SE Trade-Off

After examining the effect of the trade-off priority, the importance weight w on the licensee network performance, this section proceeds to investigate how the circuit power (P_c) impacts on the optimization objective. In Fig. 6.28, the SE-EE trade-off function is plotted against eNodeB transmit power for different values of P_c at different importance w .

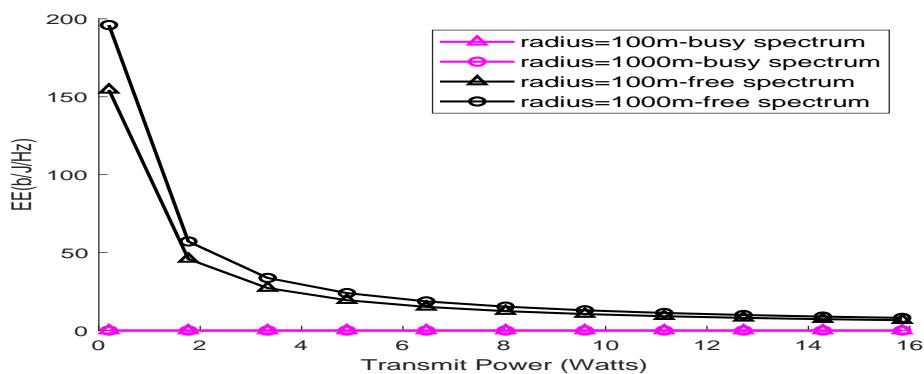
As it is seen, at lower values of transmit power, there is a slight difference in the magnitude of the achieved SE-EE trade-off, but converges to approximately the same value for different values of w . Furthermore, larger value of P_c results to lower value of the trade-off function especially for $w = 0$ and $w = 0.3$ plots. At $w = 0.7$, there is a slight inconsistency, with the largest value of P_c having higher values especially at eNodeB transmit power above the $2w$ mark. At w exactly equals 1, this trend was reserved, with the largest P_c value producing the largest trade-off value. However, across different values of $w < 1$, the values for the case when $P_c = -5\text{dB}$, is approximately the same, while there is an increase with increasing value of w for the other three values of circuit power ($P_c = 0\text{dB}$, $P_c = 5\text{dB}$, $P_c = 10\text{dB}$).

In Figs. 6.29 and 6.30, at a fixed value of the importance weight, $w = 0.5$, we investigate the trade-off function for different user number and different eNodeB coverage radius at different P_c values respectively. For a certain P_c value, we observe that increase in user number and eNodeB coverage radius results into larger values of the SE-EE trade-off function. However, for both cases, we observe a steady decrease in the SE-EE trade-off value with increasing value of P_c . This is consistent with the observation in the first 2 plots (i.e., a, & b) of Fig. 6.28, where lower P_c value yields higher value of the trade-off function.

In Figs. 6.31 and 6.32, we examine the effect of circuit power on the busy and idle spectrum SE and EE comparison respectively. As earlier observed at $w = 1$, the optimal power allocation model ensures a better SE for the busy spectrum than when the spectrum is free while the EE is significantly better especially at $w = 0$. However, while the achievable SE remains constant for different values of P_c , the EE shows a multifold increase with decreasing P_c value. This is expected since the EE is a function of circuit power while the SE is not dependent on circuit power.



(a) Free and idle spectrum EE vs. Transmit power at $w = 0.1$.



(b) Free and idle spectrum EE vs. Transmit power at $w = 1$.

Fig. 6.27 Comparison of free and idle spectrum EE vs. Transmit power at different values of w .

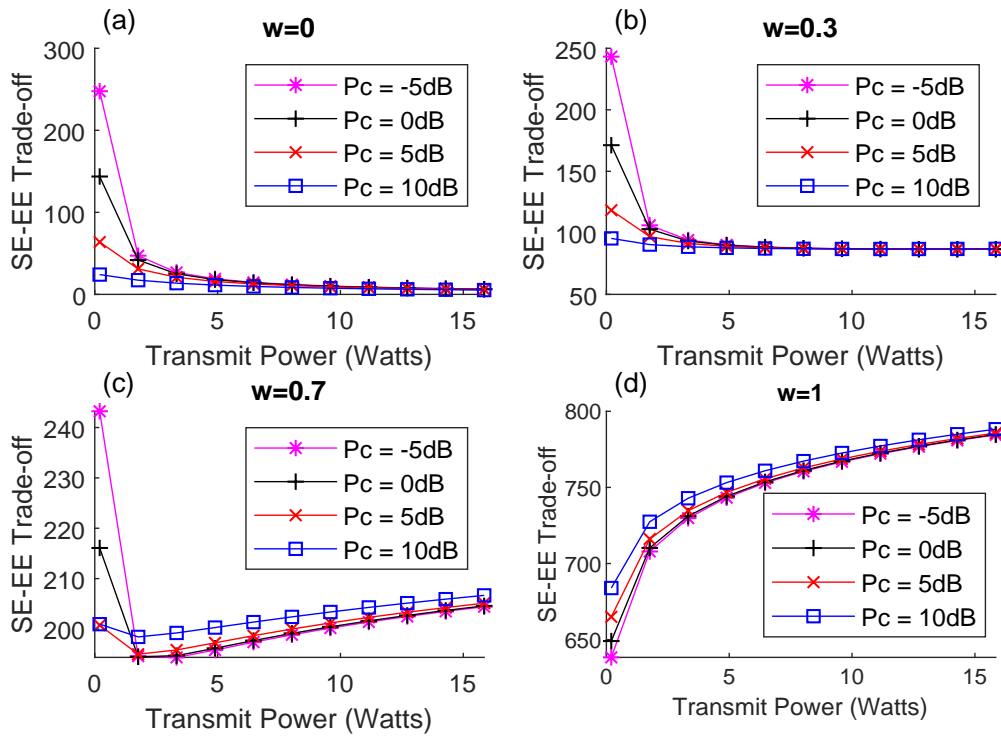


Fig. 6.28 Effect of different values of P_c on the trade-off function at different w .

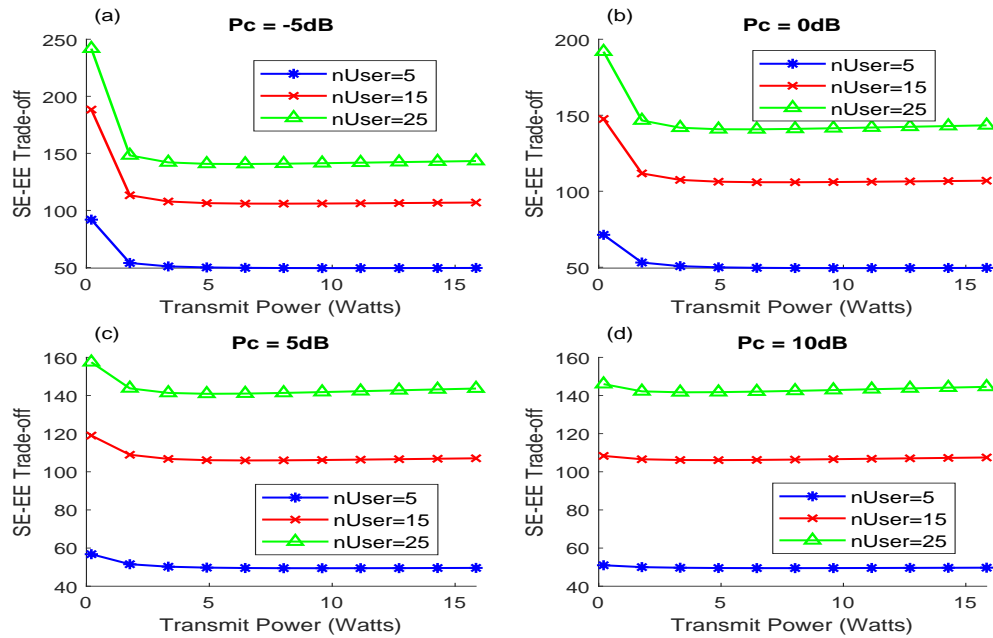


Fig. 6.29 Effect of P_c on the trade-off function for different user number.

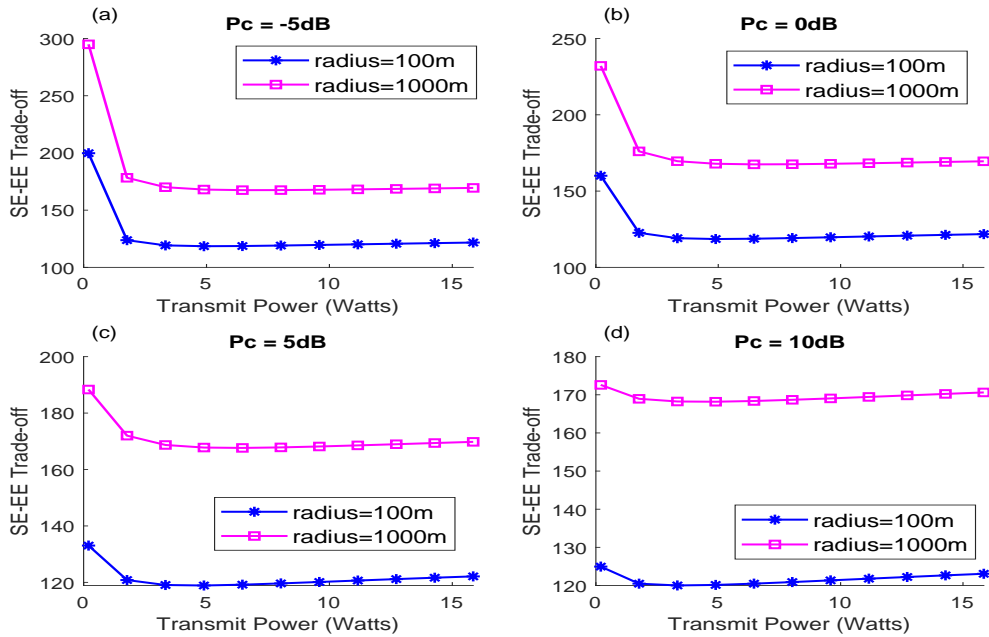


Fig. 6.30 Effect of P_c on the trade-off function for different radius.

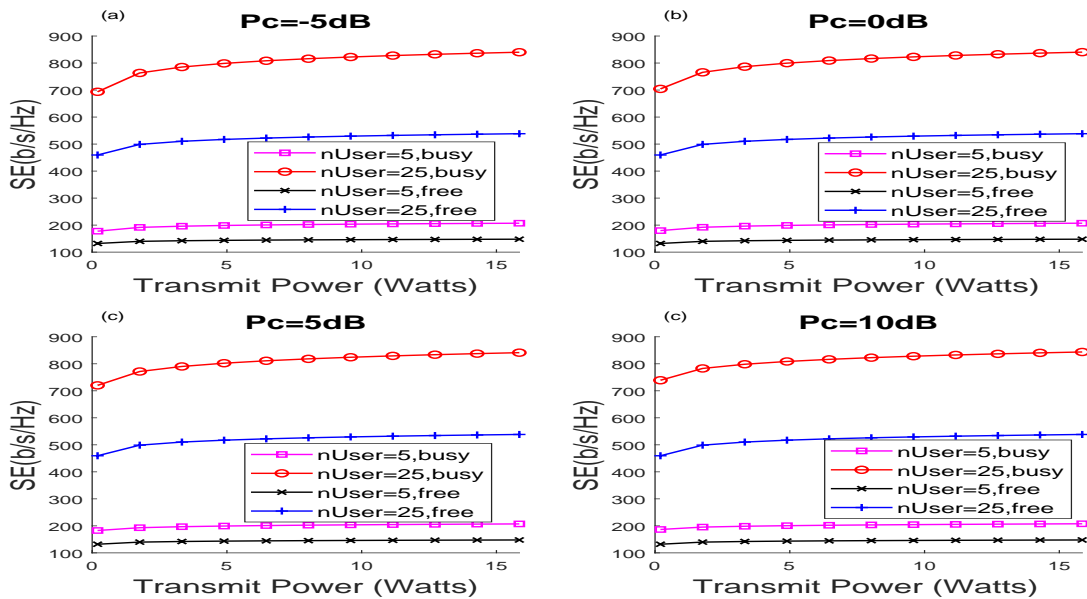


Fig. 6.31 Comparison of free and idle spectrum SE vs. Transmit power at different values of P_c .

Finally in Fig.6.33, EE is given versus SE for different P_c and users number. As it is seen, the curve obtained is a monotone or continuously increasing function even though the increase is approximately linear and the slope is not steep especially at values of $P_c >$

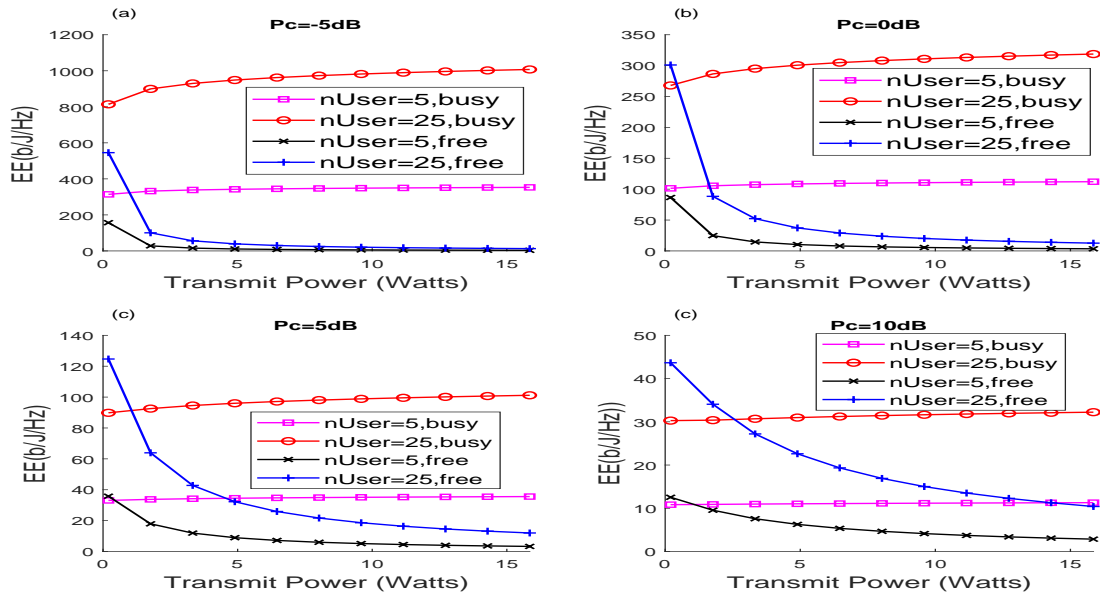


Fig. 6.32 Comparison of free and idle spectrum EE vs. Transmit power at different values of P_c .

0dB. This is a shift from the traditional EE vs. SE curve, that increases exponentially to a peak value and then falls at a similar rate. The implication of this is that with the proposed optimal power allocation model, and especially using low circuit power, the EE-SE trade-off function can achieve simultaneous increase of both performance metrics under the incumbent's interference threshold constraint.

6.3.3 Summary of Results

This section examined the simulation results of the optimization of the EE and SE, two critical performance metrics of wireless networks in a LSA vertical sharing between an airport incumbent, and a MNO licensee. Firstly, the effect of limiting the licensee transmission power as a result of the imposition of the incumbent's maximum interference threshold on the achievable EE and SE of the licensee is compared with when it has the freedom to operate with its maximum transmission power. Furthermore, the impact of various critical operational parameters in conjunction with the two performance metrics and their joint trade-off function is examined.

Results obtained indicate that by adopting the proposed optimal power allocation, the licensee system can even achieve a better EE during the period when the LSA spectrum is not available. The impact of limiting transmit power in order to comply with the incumbent

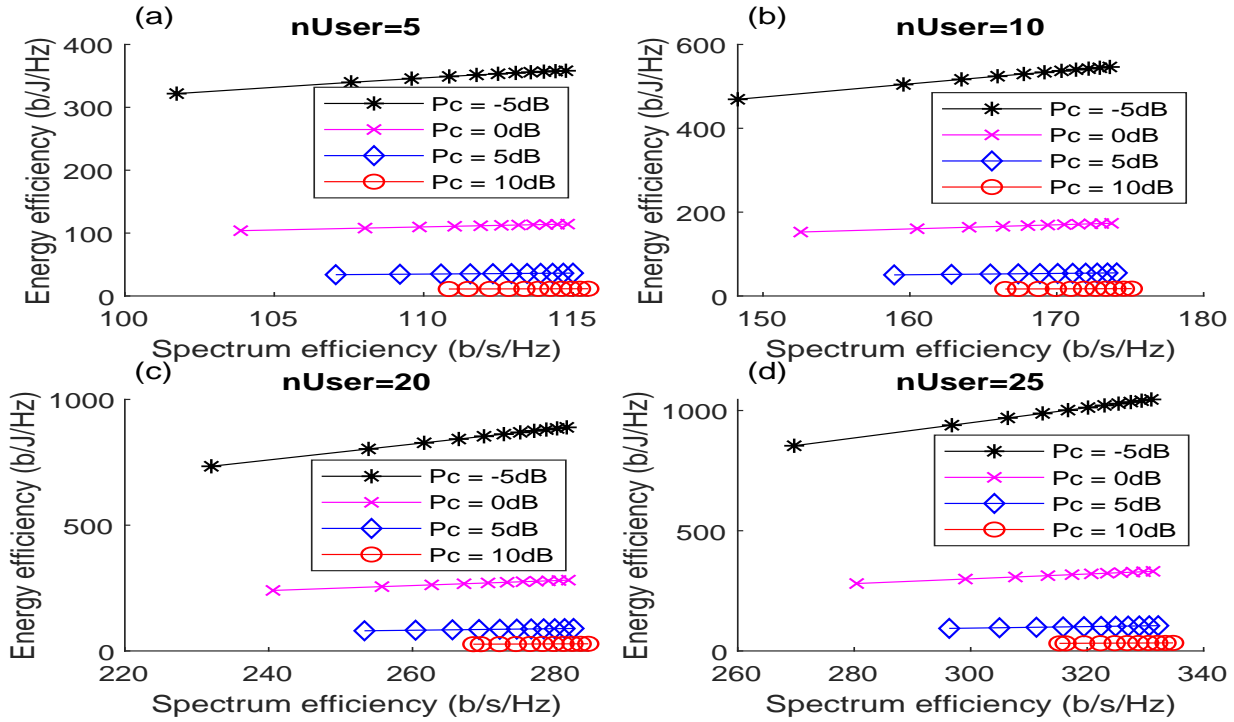


Fig. 6.33 EE vs. SE for different P_c and users number.

interference requirement is seen in the lower achievable SE of the licensee (at least 50%) as compared to when the LSA spectrum is available. However, by increasing the trade-off importance weight parameter w to favour the SE more than the EE, we can equally obtain a better SE during the reduced transmit power regime i.e., when the LSA spectrum is busy. Finally, it is seen that by proper selection of the trade-off priority parameter, the importance weight, and the circuit power, it is possible to achieve simultaneous maximization of both the SE and EE. The results presented in this section provide quantitative insights on the performance of LSA and its feasibility in a rather sensitive application. The presented results can be further utilized in the design of LSA systems as proposed in [47].

For future work, it will be interesting to investigate these performance metrics in a three-tier dynamic sharing scheme like the United States citizens broadband radio service with spectrum assess system (SAS) [46]. Another possible future work of interest is to analyse the performance of the co-existence of a Mobile/Fixed Communication Network operating local high-quality wireless networks under the emerging evolved LSA (eLSA) scheme [47]. Note that it has been shown in [127] that for finite length codewords, in an opportunistic spectrum sharing systems with rate adaptation, the system achievable rate can be severely affected by the length of the codeword. [127] shows that the secondary throughput is significantly

decreased for short codewords (less than 100 channel uses). This negative impact is however decreased by increasing the codeword length. Therefore, as a future work in LSA one can look at the optimal power allocation in both systems so that for a given codeword dropping probability in the incumbent system, the throughput of the licensee is maximized.

6.4 Drone-BS Assisted LSA Simulation Results

A major distinguishing feature and advantage of the LSA over the opportunistic dynamic spectrum access is the predictable QoS guarantee for users on the licensee network. As observed in section 6.2, the adoption of the limited transmission power when and where the LSA spectrum is being used by the incumbent system results in reduced achievable throughput of the licensee system. This poses a serious challenge to the actualization of predictable QoS guarantee for the licensee in a terrestrial network.

The discussion in this section present the findings on exploring the possibility of integrating drone base station (D-BS) with the LSA to tackle this threat to QoS guarantee. An urban environment is assumed for the LSA aerial - terrestrial network model. The ATG propagation parameters a and b values are 9.6 and 0.28 respectively [87]. The remaining simulation parameters are shown in 6.4. Firstly, we look at the proposed method in idle incumbent mode.

Table 6.4 D-BS LSA Simulation Parameters.

Parameter	Value
eNodeB Radius	1000 (metres)
Transmit Power	15–30 dBm (0.2 – 15.85 w)
Noise Spectral Density	-174 dBm/Hz
Thermal Noise Power	-96.99 dBm
Protection Ratio (I/N)	-6 dB
Bandwidth (B)	10 MHz
θ^*	42.44 ⁰
η_{NLoS}	1.0
η_{NNLoS}	20.0
Carrier Frequency	2.35 GHz

In Fig. 6.34 the proposed D-BS placement for LSA aerial-terrestrial network is evaluated. Fig. 6.34a compares the required surplus or excess traffic (Fig. 6.34a(i)) and the achieved

capacity (Fig. 6.34a(ii)). In Fig. 6.34b we show the D-BS position for maximum coverage as in [80] and the 3-D placement for the LSA system, when the spectrum is free of incumbent operational activities, using the proposed method.

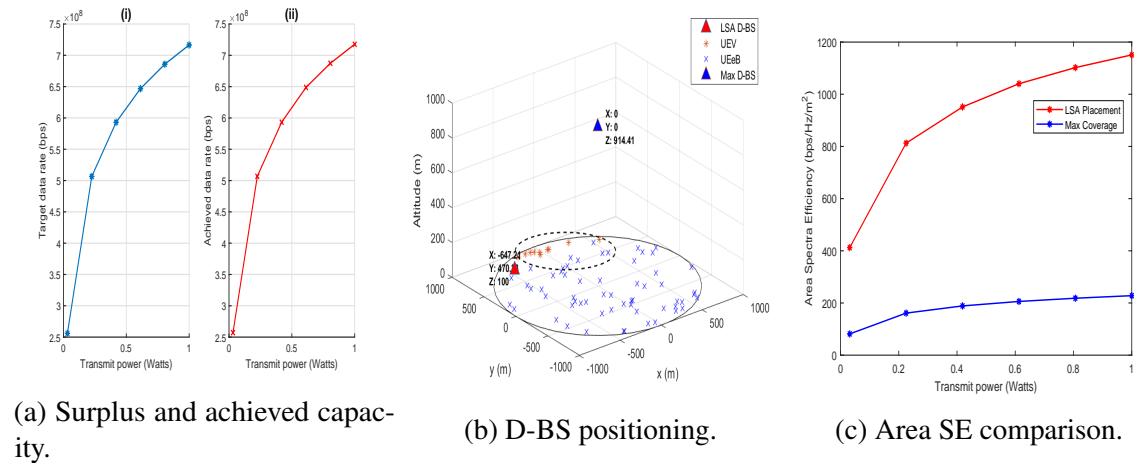


Fig. 6.34 LSA Drone-BS positioning in the idle incumbent mode.

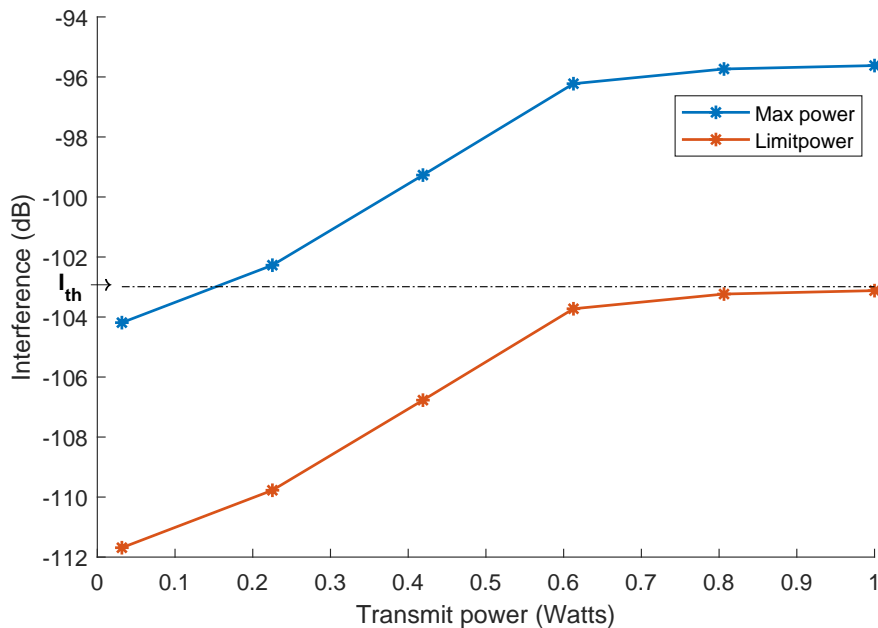


Fig. 6.35 Incumbent received interference vs. transmit power.

From the plot it is seen that the D-BS, using the proposed method, achieved the required data rate over a reduced effective coverage area thereby having a better area spectrum efficiency (ASE) than placement of the D-BS for maximum coverage. A closer look at Fig. 6.34c shows over 400% improvement in the ASE with the proposed method.

In cases where the incumbent becomes active in and around the coverage area of the D-BS, the LSA licensee has to ensure the interference power of its transmission is not above a certain threshold. Fig. 6.35, provides a plot of the interference received at the incumbent vs transmit power. As seen from the plot, when the D-BS operate at the maximum transmit power range adopted for this work, the interference to the incumbent is above the maximum allowed interference, the interference threshold, I_{th} (the blue plot). The red line plot, shows that by reducing the transmit power, it is possible to reduce the incumbent's received interference below the I_{th} .

Fig. 6.36 shows the D-BS position (6.36b) and how the limit power achieved data rate performs in meeting the desired surplus traffic target (6.36a). Except for the highest value in the transmit power range, with the proposed D-BS placement method, it is still possible to satisfy the surplus traffic requirement of the network when the licensee is transmitting under the limited power regime. This is a very interesting observation when compared to the conventional terrestrial licensee eNodeB in which the achievable data rate suffers as a result of reduction in transmit power[41]. This is more so, considering the fact, that a fundamental challenge of the LSA scheme is achieving the desired QoS of each UE in the licensee system, while avoiding harmful interference to the incumbent.

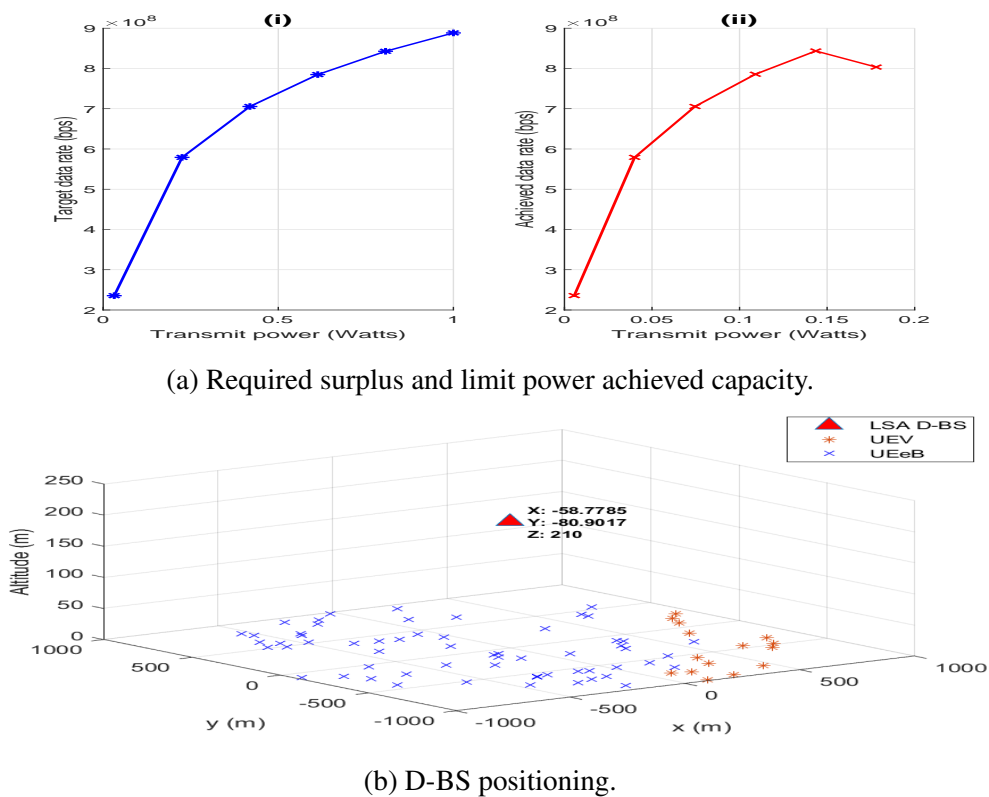


Fig. 6.36 LSA Drone-BS positioning in the active incumbent mode.

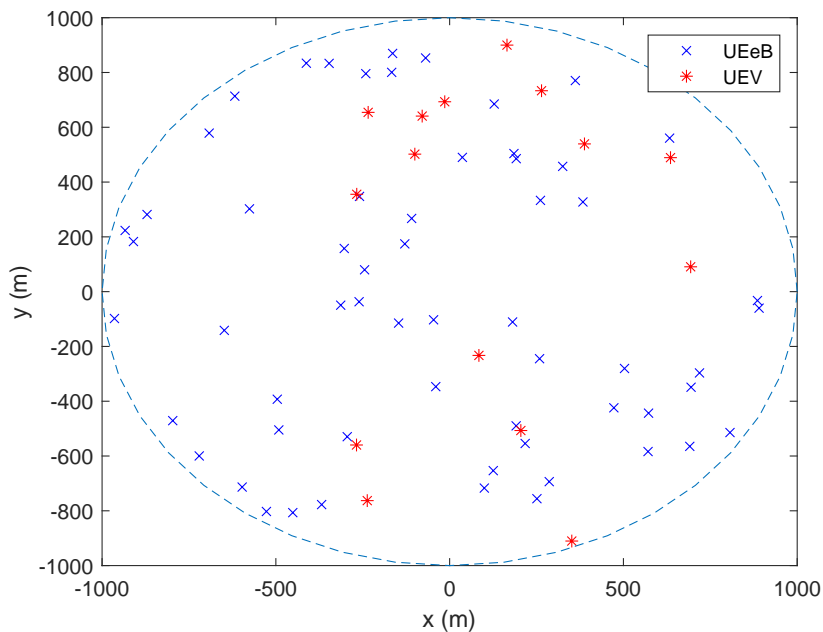
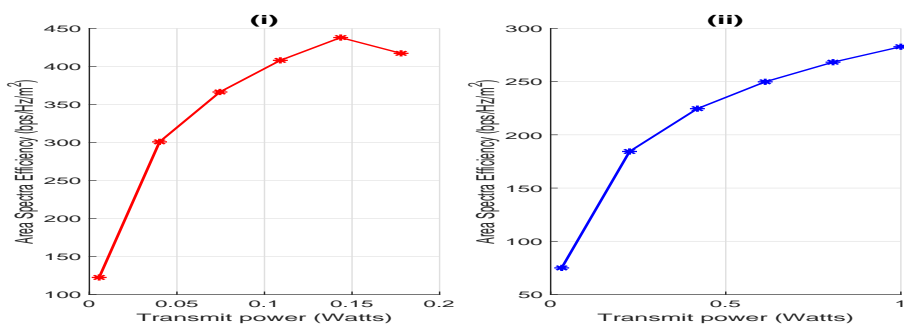
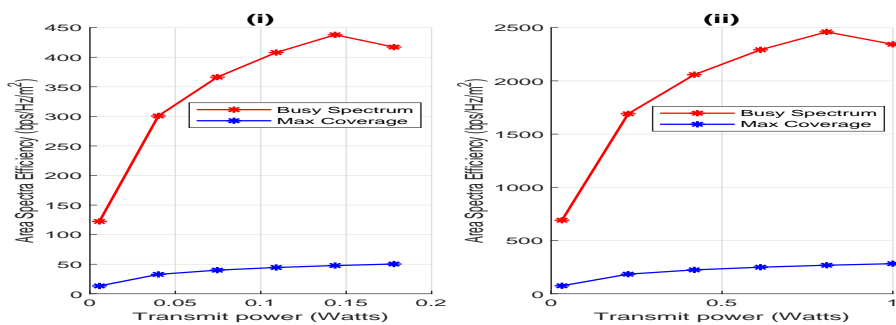


Fig. 6.37 Original UE distribution between the aerial-BS and terrestrial eNodeB.



(a) ASE vs. maximum and limit power.



(b) Scaled ASE vs. transmit power.

Fig. 6.38 Spatial spectral efficiency in the active incumbent mode.

A close examination of Fig. 6.36b indicates that the set of users associated to the D-BS are clustered in a certain part of the coverage area. This is in contrast to Fig. 6.37 which shows that the UEs making up the excess surplus traffic are originally distributed uniformly around the entire coverage region. Hence in-order to meet the target data rate, even while operating with limited transmit power, the proposed method not only took advantage of the agility of the D-BS but also caused a re-ordering of the mark distribution $Z(V)$ for the UEs association with either the terrestrial e-NodeB or the D-BS. Instead of the expected degradation of the network SE, there is rather an improvement in the spatial spectral and energy efficiency of the network. This is indicated in Fig. 6.38.

Fig. 6.38a(i) shows the ASE of the limit transmit power which inspite of its reduced power is still larger than the ASE for D-BS positioning for maximum coverage (6.38a(ii)). The actual improvement in terms of the achieved ASE is aptly indicated in Fig. 6.38b. The first subplot, i.e., Fig. 6.38b(i) is scaled (compressed) with respect to the limit power values while the Fig. 6.38b(ii) is expanded to show the relative ASE of both scenarios with respect to the maximum transmit power. It is seen that the relative improvement obtained with the proposed method is about $9\times$ better.

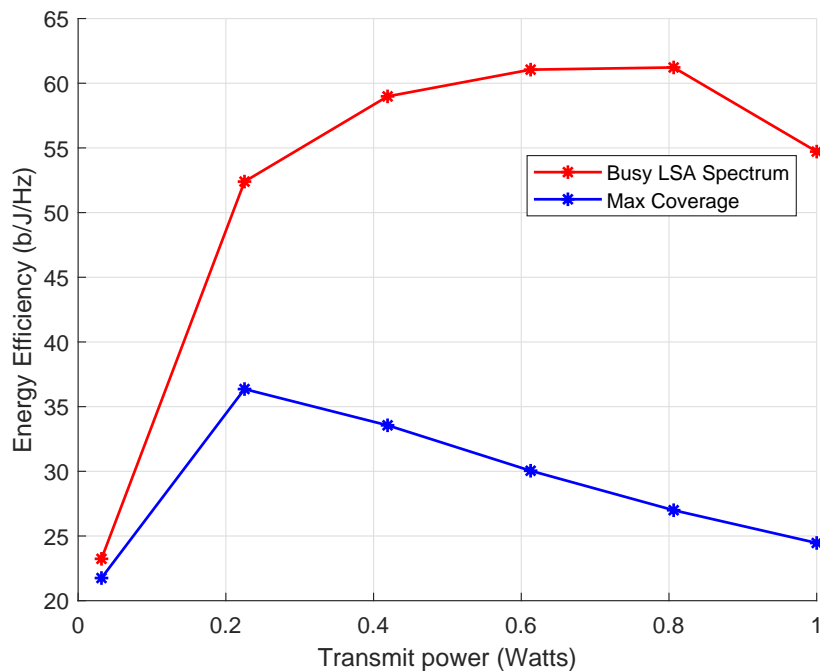
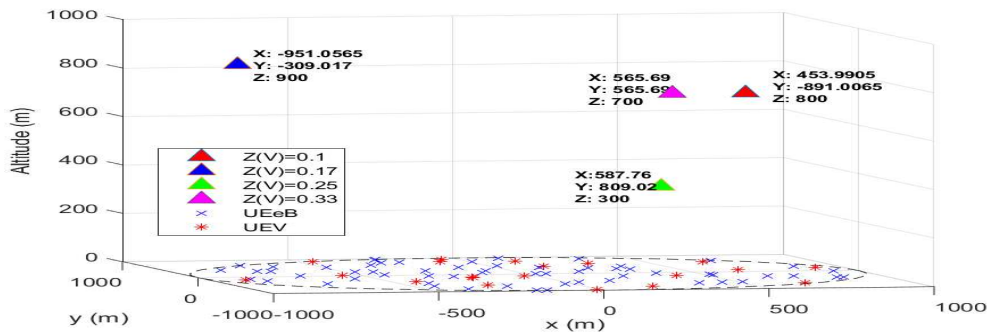


Fig. 6.39 EE vs. transmit power.

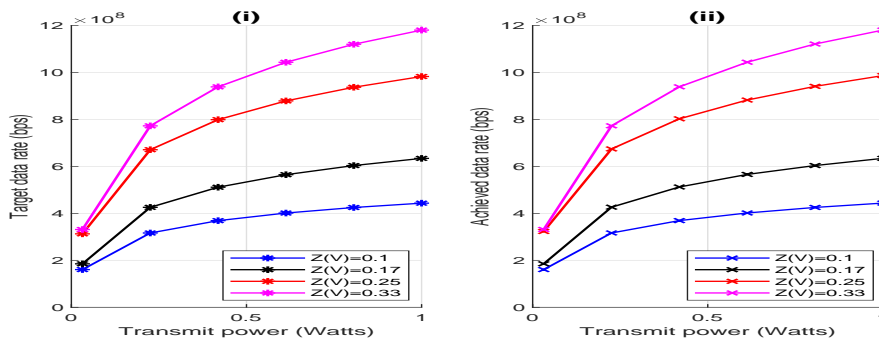
In Fig. 6.39, the energy efficiency of the LSA D-BS positioning in active incumbent mode is shown. It is seen that the energy efficiency of the proposed D-BS positioning technique is at

least 100% better even at the limit power values where the achieved data rate fell short of the target data rate. Contrastingly, in the traditional terrestrial network, it has been shown that the EE of the licensee network suffers degradation when operating under limit power regime [128]. These results are significant in the sense that they show that the aerial-terrestrial configuration of the LSA scheme has the prospect of better utilization of the spectrum than the conventional terrestrial network.

Next, the robustness of the proposed method against variations in the surplus traffic and different locations of the incumbent system within the coverage area is examined. Fig. 6.40 shows four different values of $Z(V)$ and how the system responds to it. From 6.40b it is seen that for various values of $Z(V)$, the system is able to achieve the desired or target data rate effectively. Thus in the idle mode, the licensee system is robust to satisfy different values of traffic requirements.



(a) D-BS position for different $Z(V)$.



(b) Required surplus and achieved capacity.

Fig. 6.40 Variation in mark distribution in the idle incumbent mode.

Similarly in Fig. 6.41, the performance of the system is similar to the case where a single $Z(V)$ is investigated. Except for the highest value of the transmit power, the system is able to meet the target capacity requirement irrespective of the value of surplus traffic requirement of the network. However, it is seen that for the lowest value of $Z(V)$, the target

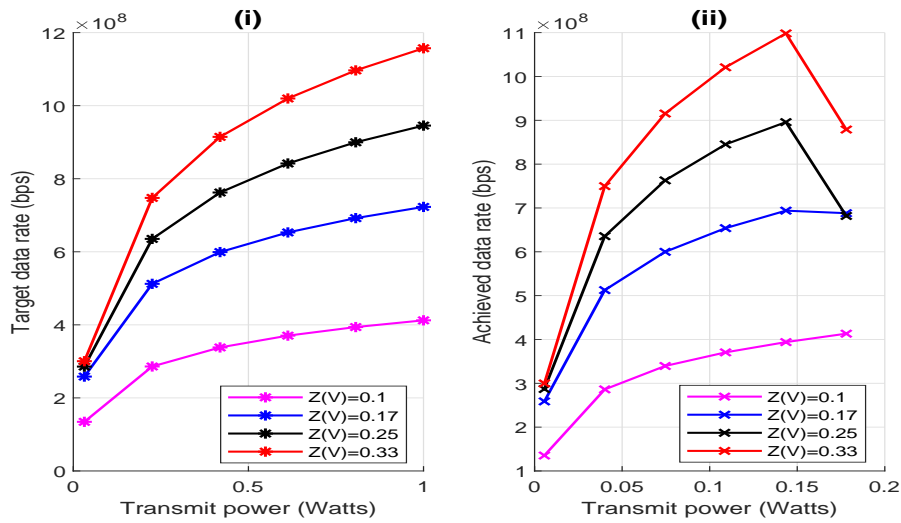


Fig. 6.41 Target and achieved data rate in the active incumbent mode.

capacity requirement was achieved for all transmit power values. The figure also shows that the shortfall in the target capacity at high value slightly increases with increase in $Z(V)$. It can thus be concluded, that the system is relatively robust to variations in the surplus traffic requirement.

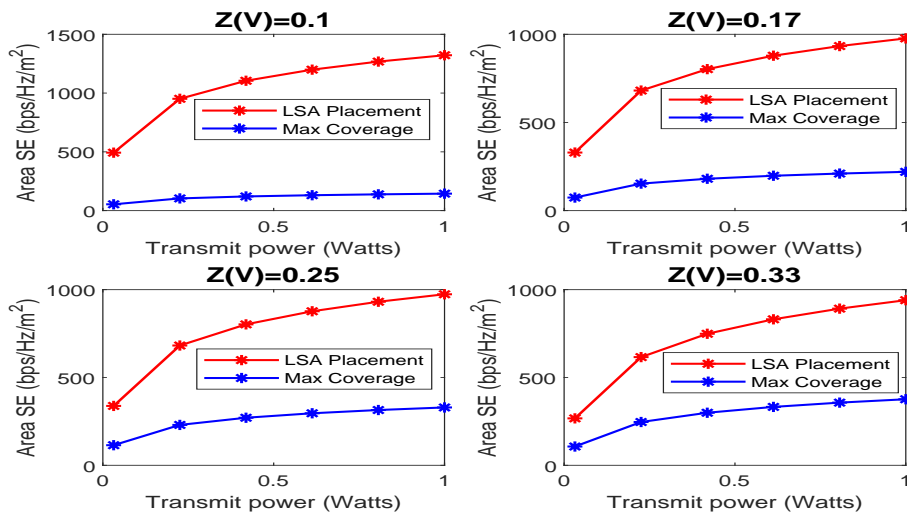
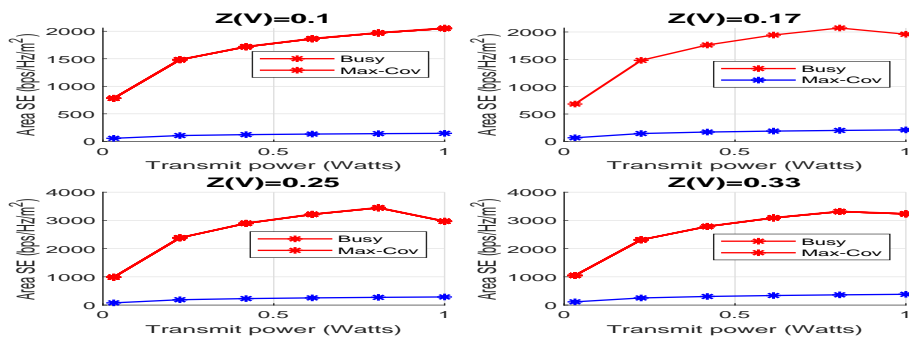


Fig. 6.42 ASE for different $Z(V)$ in idle incumbent mode.

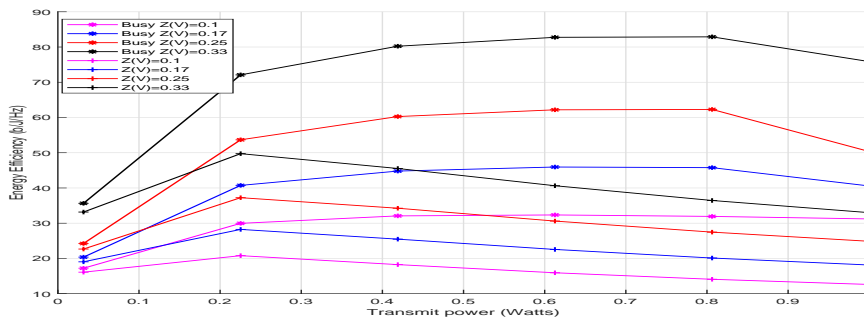
The ASE is plotted against the transmit power for the different values of $Z(V)$ when the LSA spectrum is free for unrestricted use of the licensee in Fig. 6.42. It is seen that the ASE is still better with the proposed method than the placement for maximum coverage. It is however observed that the obtained improvement is reduced when the surplus target requirement is

increased. In cases where $Z(V) = 0.1$, the recorded improvement is about 800% while when $Z(V) = 0.33$, the percentage improvement is around 150% over the maximum coverage D-BS configuration method.

For the period when the incumbent is active in its spectrum, the scaled ASE is plotted against the maximum transmit power to analyse the comparative improvement obtained in Fig. 6.43. It is seen that the comparative improvement in the ASE is the same for the different values of the surplus traffic investigated when the licensee D-BS is operating under the limit power regime. It is worth mentioning that in terms of the actual magnitude of improvement, similar pattern of decreasing value with increasing $Z(V)$ observed in the idle mode was also recorded for the active incumbent mode. Similarly the energy efficiency improvement across the different values of $Z(V)$ is consistently stable. Hence the proposed method performance with regards to the licensee achievable ASE and EE is not adversely affected by variations in surplus traffic requirement.



(a) Scaled ASE for different $Z(V)$.



(b) EE vs. transmit power for different $Z(V)$.

Fig. 6.43 Spatial spectral and energy efficiency for different $Z(V)$ in active incumbent mode.

Finally, in Fig. 6.45 we demonstrate the level of attainment of the surplus traffic requirement for the incumbent’s positions shown in Fig. 6.44 against different limit transmit power levels and different variations of $Z(V)$. Fig. 6.45a compares the target capacity with the

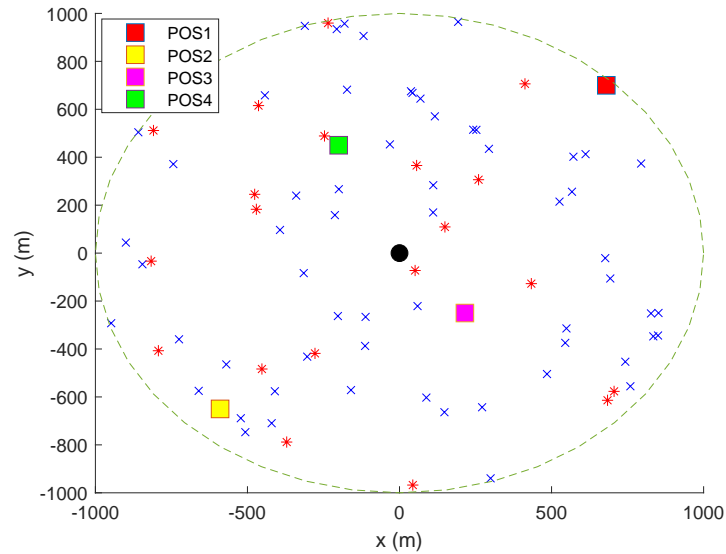
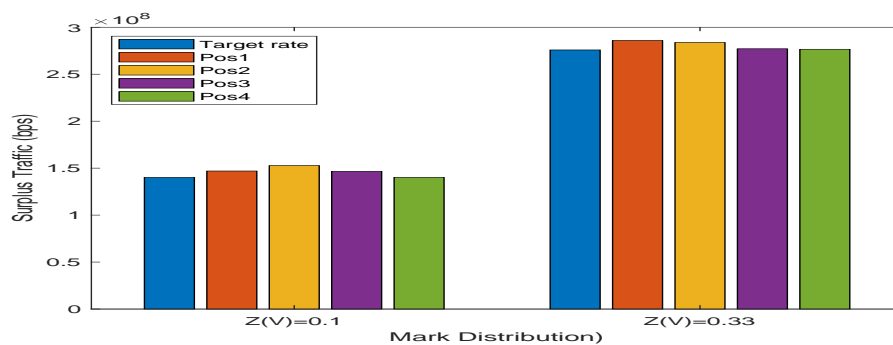


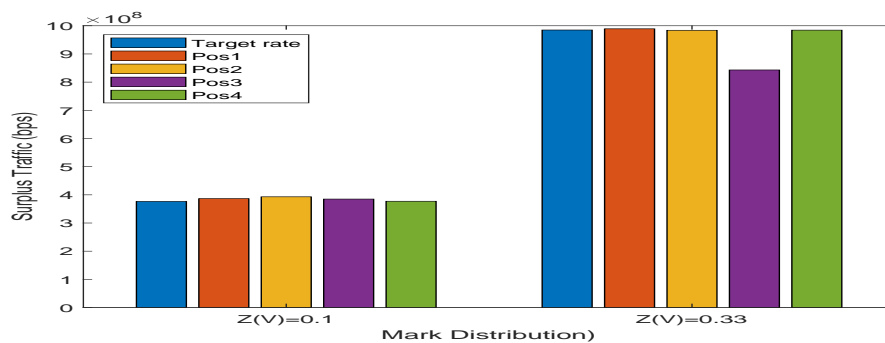
Fig. 6.44 Different incumbent position in the coverage area.

lowest limit transmit power for the two extremes of $Z(V)$ considered in this work while Fig. 6.45b shows for higher values of limit power. It is seen from $Z(V) = 0.1$ at both transmit power levels, the target surplus traffic was attained irrespective of how deep the incumbent position is into the network coverage area. Similarly, at higher value of surplus traffic requirement, the target capacity was easily achieved at all incumbent positions in the case of the low transmit power level. However, for higher transmit power, there is a considerable impact of the location of the incumbent on the attainment of the surplus traffic requirement. In Fig. 6.45b, it is seen that where $Z(V) = 0.33$, while the target data rate demand was achieved in other positions, there was a considerable shortfall for the achievable data rate for incumbent position POS3, which is deeper into the licensee coverage area than the other positions.

These results shows that at lower transmit power, it is still possible to achieve the target data rate even at a relatively high surplus traffic demand of the aerial-terrestrial LSA licensee network when the incumbent is very deep inside the coverage area. However, at high transmit power, the inability of meeting the desired target rate earlier observed, becomes more pronounced with the incumbent transceiver located closer to the centre of the licensee coverage area. This occurs because, the closer the incumbent is to the licensee transmitter, the higher the interference received by the incumbent. Thus, while trying to adjust its position to ensure the interference threshold of the incumbent is not exceeded, it is unable to satisfy the data rate demand by UEs in the network.



(a) Achieved capacity at low transmit power.



(b) Achieved capacity at high transmit power.

Fig. 6.45 Achievement level of surplus capacity requirement at different incumbent's position.

6.4.1 Summary of Results

In this section, a D-BS assisted LSA architecture is proposed to cater for the surplus traffic requirement of a terrestrial eNodeB. In the system model, the D-BS acts as the licensee in a vertical LSA sharing scheme. A two mode dynamic D-BS placement problem corresponding to the cases where the incumbent system is idle or active is defined. To prevent harmful interference when the incumbent is active in its spectrum, we adopt the limited power regime. Results obtained indicate that the D-BS altitude positioning can be configured to ensure that the target excess capacity requirement of the congested network can be met even when the incumbent is active in its spectrum. Interestingly even in cases where the licensee is operating with limited transmit power, the obtained system performance in terms of the EE and ASE is significantly better than a non-LSA system, where the D-BS is configured for maximum coverage. Furthermore, the results show that the system is fairly robust to increasing variations in surplus traffic demand and different incumbent position inside the licensee network. As a future work, it would be interesting to investigate how smart antenna techniques could further improve the dynamic LSA aerial-terrestrial systems performance,

especially with regards to ensuring incumbent interference threshold requirement is met while the licensee transmits at its maximum rated power.

6.5 Chapter Summary

In this chapter, an analytical discussion of the results of the simulated implementation of our proposed methods are presented. The first three sections considered the aeronautical telemetry incumbent described in 3.1 while for the fourth section, the assumed system model is the PMSE and PPDR incumbent described in 3.2. Starting with **section 6.1**, the impact of the LSA spectrum access revocation on the allowable transmit power of the licensee is examined while also analysing the effect of the different interference propagation path between the licensee transmitters and the incumbent victim receivers and, the resulting power differential. Simulation results show that while the limited transmit power value of the downlink is expectedly higher than the uplink limit power (because of higher rated transmit power in the downlink), the interference to the incumbent in the uplink is significantly higher. Furthermore, we analyse the performance of the proposed method by comparing it with a benchmark, the equal power allocation (EPA). A comparison of the performance of the proposed method against the EPA benchmark in the licensee downlink revealed an improvement of about 120% in the achievable EE while the improvement in the uplink is about 300%. Furthermore, it is seen that for both the transmission directions, the improvement in the EE achieved by the proposed method increases with increase in eNodeB radius.

Section 6.2, presents the results of the proposed method for maximizing licensee's system spectrum efficiency. When compared with the non-optimized system, simulation results show a considerable improvement in the licensee achievable SE using the proposed method. Furthermore, the effect of various operational parameters (i.e, the number of UEs, the eNodeB and the transmit power) on the SE is also examined. In addition, we introduce a novel performance measure, "decibel capacity gain" to quantify the improvement obtained by the proposed power allocation technique. Interestingly this performance measure further shed light on the SE gain pattern in relation to the number of UEs and transmit power adjustment. Similarly, the novel measure, the utility function proposed in **Section 6.2.1**, shows that a higher spectrum utilization efficiency is achieved as a result of shorter busy period ratio and higher achievable SE for distant eNodeB coverage. These results provide quantitative insights for practical system design and deployment of LSA system.

In **section 6.3**, we further analysed the results of the proposed licensee's optimal EE-SE trade-off solution presented in **section 4.3**. Simulation results indicate a significantly improved energy efficiency in the licensee network as well as the spectrum efficiency

comparable to even when the LSA spectrum utilization is unrestricted by the incumbent's maximum interference threshold. Furthermore, we show that with careful selection of the licensee eNodeB coverage radius, transmit power, and users number per eNodeB coverage area, one can engineer the best possible trade-off between the spectrum and energy efficiency.

In **section 6.4**, obtained simulation results of the proposed D-BS placement method, show that the target capacity of the network is still attainable even when the licensee is transmitting under the limited power regime. This is a remarkable result, considering the fact that for conventional terrestrial licensee eNodeB, the achievable data rate suffers as a result of reduction in transmit power. The results also shows that the proposed method is reasonably robust to variations in surplus traffic demand and different positions of the incumbent system in the licensee network coverage area. This results in a considerable improvement in the achieved spatial spectrum efficiency (up to 500%) and energy efficiency (up to more than 1000%) of the network. In conclusion, our proposed hybrid aerial - terrestrial LSA system is able to provide solution to the threat posed, to predictable QoS of the licensee, by the incumbent's spectrum access revocation.

6.6 Conclusion

From the discussion and analysis in this chapter, it is seen that the proposed methods provide significant improvement in the key performance metrics of the LSA scheme considered. For the EE, the improvement recorded is up to 300% when compared with the EPA benchmark while up to about 700% improvement is obtained for the system's SE. The proposed spectrum utilization efficiency also provided useful insights for practical deployment of the LSA in a wide geographical area. Similarly, the proposed hybrid aerial- terrestrial configuration provided a very interesting solution to the QoS degradation when the licensee is forced to operate with the limited transmit power. Additionally, the proposed method yielded significantly better EE and ASE than the traditional conventional terrestrial system.

It is interesting to note that the results obtained revealed an increase in the system's EE with increasing number of UEs and eNodeB coverage radius. However in the case of the SE, the introduced decibel SE gain measure reveals that the UE traffic in a eNodeB coverage area is inversely proportional to the achieved SE improvement obtained when using the proposed optimal power allocation. This usually conflicting relationship between the SE and EE is also revealed by the variation of the importance weight parameter in the EE-SE optimization results presented in section 6.3. However, it is also seen that by proper selection of the trade-off priority parameter, the importance weight, and the circuit power, it is possible to achieve simultaneous maximization of both the SE and EE.

Chapter 7

Conclusion and Future Work

7.1 Summary of the Thesis

Chapter 1, introduces this thesis by providing a brief overview and background on the fundamental problem of spectra limitation, that has consistently been a challenge since the invention of wireless communication. It then highlighted the unusual appeal of the wireless communication which is evidenced by the ever increasing high rate of wireless broadband traffic. It further describe how the fragmentation of the spectrum into chunks, to enable simultaneous access by multiple different systems, has addressed this challenge up to date. However, in the past few decades it has become obvious that this static and exclusive utilization is no longer adequate for the expected growth of broadband services going into the 5G technology space. The early candidate for dynamic spectrum access (DSA), the opportunistic cognitive radio (CR) network, has major drawbacks that made turning the promise it holds to cost effective practical implementation a difficult reality. On the basis of these limitations of the CR driven DSA, the licensed shared access (LSA) came to the fore. The remaining portion of the chapter then discusses the motivations and research problems of the LSA, which this thesis aimed to address. After providing a description of the thesis outline, the chapter concludes with the research output of the solutions to the identified research problems.

Chapter 2, a systematic representative review of the existing work on the LSA spectrum sharing scheme was provided. A detailed description of the original LSA framework as a regulatory paradigm shift for a more efficient utilization of the spectrum and its limitation was followed by a description of the dynamic LSA, which in addition to addressing the limitations of the static LSA, also includes further extensions to ensure an improved spectrum utilization efficiency by the LSA. There is also a brief discussion on the evolved LSA (eLSA), which includes modifications in the dynamic LSA to cater for the expected multiple vertical

technologies of the 5G technology space and beyond. Following the discussion of the evolution of the LSA, the chapter highlighted the various flexibility options for spectrum management that the LSA offers as against the traditional static spectrum assignment from both the technical point and the regulatory or administrative perspective.

Furthermore, the several experimental field trials that has been successfully done using commercial grade long term evolution (LTE) test beds was highlighted in the chapter as a compelling proof of concepts for practical commercial deployment of the LSA, with minimal modification to the existing commercial MNO infrastructure. In addition to this, the distribution of the LSA band availability and how it affected key QoS metrics such as the mean data rate, request blocking probability and the number of users suffering service interruption was discussed. Finally, the contributions of this thesis, i.e., the identified gaps in existing research, which is the impact of the licensee's spectrum access revocation on the various efficiency metrics of the dynamic form of LSA scheme concludes the chapter.

In **Chapter 3**, the adopted system models that set the stage for the research work presented in this thesis was discussed. The 2.3 GHz - 2.4 GHz termed the 'LTE band 40' by the 3rd Generation Partnership Project (3GPP) is adopted as the LSA band under consideration in this thesis. The many incumbents of the 'LTE Band 40' was grouped into two broad categories. Furthermore, the chapter also present underlying mathematical models necessary for the investigation of the LSA system under realistic practical conditions. In **section 3.1**, mathematical formulations are presented for the uniquely different interference propagation path and channel models existing between the licensee interfering transmitters and the aeronautical telemetry incumbent victim receivers. In the uplink, two paths were investigated, the air to ground propagation channel between the UEs and the airborne receivers (aircraft) and also the terrestrial interference path to the ATC tower. The second system model presented in **section 3.2** is a hybrid aerial-terrestrial LSA licensee system which consists of the terrestrial eNodeB operating at the cellular bands, and a drone base station of a cellular network operator utilizing the 'LTE Band 40', as a licensee system, while the programme making and special events (PMSE), and the public protection and disaster relief (PPDR) represents the incumbents in this category. Specifically, the spatial distribution of the UE on the licensee network is modelled by a bivariate marked Poission process. On the basis of this, the total capacity of the hybrid aerial-terrestrial licensee system was formulated as the sum of the installed capacity of the terrestrial eNodeB and the excess traffic demand.

In **chapter 4**, methods are proposed to improve the several efficiency metrics of the licensee system which are adversely affected when the incumbent becomes active on the spectrum in the dynamic LSA spectrum sharing scheme. In particular, mathematical models for the proposed methods are presented in this chapter. Starting with **section 4.1**, mathemati-

cal formulations are presented for optimization of the licensee's energy efficiency when its operations is constrained by the incumbent's activity on the LSA spectrum. Taking into account the different propagation characteristics existing between the licensee downlink and uplink transmitters, the power adjustment required to guarantee that the incumbent victim receivers do not suffer from excessive harmful interference is determined. Thus an expression for this is derived as a function of the incumbent's interference threshold and the respective received interference from the licensee's downlink and uplink transmitters. On the basis of the determined power differential, the limited transmit power equation is formulated for each group of licensee's transmitter in both the uplink and downlink transmission directions when the spectrum access right is revoked by the incumbent. Finally, by adopting the Charnes-Cooper transformation technique to the non-convex fractional optimization problem, an optimal power allocation technique for optimization of the licensee EE when it is operating with the limited transmit power is proposed. The contributions from this part of the thesis are presented in part at a workshop in the IEEE GLOBECOM conference 2019 [128].

Section 4.2.2, presents the mathematical formulations for the optimization of the licensee's system spectrum efficiency. Firstly, an expression was derived for the interference received by the incumbent from the licensee's transmission both in the uplink and downlink. Then unlike in the case of the EE model, an SE optimization model was formulated using the maximum transmit power of the licensee while imposing the incumbent interference threshold as a constraint on the optimization problem. Furthermore, by characterizing the availability or not of the LSA spectrum as a tandem queue a novel metric for accurately determining the utilization efficiency of the LSA spectrum was proposed in **section 4.2.3**. The proposed metric was derived as a utility function of the the achievable SE and busy period ratio of each layer within the tandem queue. Unlike the traditional duty cycle measured in percentage that was hitherto used to quantify spectrum utilization efficiency, the proposed utility function in this work can help to accurately forecast the achievable capacity that the spectrum can provide and match this to the capacity demand of the data hungry applications of the 5G and beyond technology space. The contributions from this part of the thesis are published in part in [129].

In **section 4.3**, the distribution of the licensee's interference was obtained and from there an expression for the received maximum interference probability of the incumbent was derived. This is then imposed as a constraint on the operating transmission power of the MNO during the period of communication between the ATC and aircrafts landing or taking off. Furthermore, an SE and EE optimization of the licensee's system ia formulated as a multi-objective problem (MOP). Using the weighted sum approach and the fractional programming method, subject to the transmission power and the incumbent's interference

threshold constraint, an optimal power allocation to maximize the two conflicting metrics of SE and EE is derived. The contributions from this part of the thesis are published in part in [130]. Finally, in **section 4.4**, an hybrid aerial-terrestrial dynamic LSA framework is presented to address the challenge of the QoS degrading effect of the limit transmit power adopted by the licensee when the incumbent is active on the LSA spectrum. We begin by formulating the 3-dimensional D-BS placement problem when the spectrum is free of incumbent's activity and hence licensee D-BS can operate at maximum rated transmission power. We then extend the formulation of the D-BS placement optimization problem to the cases where limited transmission power is employed by the licensee, i.e., when the incumbent is active in its spectrum within/around the licensee network coverage radius.

The proposed methods are validated by simulations and the results are presented in **Chapter 6**. Starting with the achievable EE of the licensee under limit power transmission regime, the performance of the proposed method is analysed by comparing it with a benchmark, the equal power allocation (EPA). Furthermore, the interplay between system design parameters such as the eNodeB coverage radius and circuit power with the proposed method is evaluated. The obtained results show that while the limit power value of the downlink is expectedly higher than the uplink limit power (because of higher rated transmit power in the downlink), the interference to the incumbent in the uplink is significantly higher. This is an interesting insight for practical LSA system design and implementation. Furthermore, to verify the impact of spectrum access right revocation on the licensee's EE, the limit power EE in both directions is scaled to, and compared with the maximum transmit power EE. The comparison shows an interesting result because unlike the achievable data rate that has been reported to be degraded under the limit power regime, the EE however exhibits contrasting performance depending on the transmission direction. Expectedly in the uplink, there is a degradation of the EE under limited power, but in the downlink there is no considerable degradation in the EE. Additionally, a comparison of the proposed method, the EPA benchmark, shows that the proposed method produce a better system performance and is robust to increase in number of UEs on the network. Critically important is the fact that the improvement in EE provided with the proposed method increases with increase in eNodeB coverage radius. This poses an interesting trade-off challenge in practical network design considering increasing miniaturization of cellular networks eNodeB coverage area in the 5G technology space of high SE requirement and network densification.

Similarly, simulation results in **Section 6.2**, show more than a seven fold improvement in the licensee achievable SE with the proposed method. The novel performance measure, the "decibel capacity gain", introduced to quantify the improvement obtained by the proposed method, shed further light on the relation of SE to the number of UEs and transmit power

adjustment. This metric shows that a higher comparative SE gain is achieved with the proposed optimal power allocation in cases where the number of user equipment in the eNodeB coverage area is very small. The implication of this is that optimal system design in practical LSA deployment must be geared towards achieving the best trade-off between the UE traffic and the desired SE. Moreover, considering the possibility of the LSA system co-existing with the legacy MNO network, this metric also provides a guide for reliable and optimal traffic distribution between the two systems. Furthermore, results obtained also show that higher spectrum utilization efficiency is achieved as a result of shorter busy period and higher achievable SE for distant cells. In practical terms, the implication of this is that at farther distance from the airport, the operating parameters of the MNO in an LSA system can be configured with less stringent restrictions. In addition results obtained show that, the UE interference to the aircraft is more critical in system design than the other two possible interference path.

In **section 6.3**, the performance of the proposed optimal EE-SE trade-off is evaluated by comparing the achievable EE and SE of the licensee when operating under the restriction of reduced transmit power with when the spectrum is always available with the ability to transmit at maximum power. Simulation results indicate a significantly improved EE in the licensee network as well as the SE comparable to even when the LSA spectrum utilization is unrestricted by the incumbent's maximum interference threshold. Additionally, an examination of how the network design priorities and circuit power affect the achievable SE and EE trade-off is done. By setting the weight parameter to achieve equitability between both objectives, obtained results from simulations indicate that while the proposed optimal power allocation yields better achievable EE than the EPA benchmark, even when the licensee operates with maximum transmit power, the same can not be said of the SE. The reduction of the transmit power yields a corresponding reduction in the achievable SE of the licensee (at least 50%). However, by increasing the trade-off importance weight parameter w to favour the SE more than the EE, we can equally obtain a better SE during the reduced transmit power regime i.e., when the LSA spectrum is busy. Furthermore, it is seen that with careful selection of the licensee eNodeB coverage radius, transmit power, and users number per eNodeB coverage area, one can engineer the best possible trade-off between the spectrum and energy efficiency. In fact, it is seen that by proper selection of the trade-off priority parameter, the importance weight, and the circuit power, it is possible to achieve simultaneous maximization of both the SE and EE. This is a valuable information for practical LSA network design.

Interestingly, the obtained simulation results of the proposed D-BS assisted LSA architecture, in **section 6.4**, show that the target capacity of the network is still attainable even when the licensee is transmitting under the limited power regime. This is more so, considering the

fact that a fundamental challenge of the LSA scheme is achieving the desired QoS of each UE in the licensee system while avoiding harmful interference to the incumbent. Furthermore, the proposed hybrid aerial-terrestrial LSA system yields a considerable improvement in the achieved spatial spectrum efficiency (up to 800%) and energy efficiency (around 100%) of the network. Finally, the robustness of the proposed method against variations in surplus traffic demand and different positions of the incumbent system in the licensee network coverage area is examined. The results obtained indicate that the system is able to achieve the desired target rate even if the surplus traffic requirement increases. Similarly, the method is fairly robust to the incumbent's positional change. At low transmit power and target surplus traffic, the system is still able to attain the desired throughput even in cases where the incumbent is very close to the centre of the licensee network coverage area.

7.2 Future Work

The 5G technology is expected and designed to host heterogeneous and diverse vertical technologies. Applications such as autonomous self driving vehicles, e-health, augmented realities, industrial automation, connected robots and intelligent sensors, and in fact the wide range of technologies and applications that make up the internet of things and machine-to-machine communication will dominate the 5G landscape [131, 132]. In the light of this, the evolved LSA (eLSA) was extended to include multiple licensees involving such vertical service providers. For future research work, it will be interesting to analyse the performance of the co-existence of a Mobile/Fixed Communication Network operating local high-quality wireless networks (LHQWN) under the emerging eLSA scheme [47]. A main feature of most of these applications is the relatively short length of the codeword when compared to the asymptotically infinite codewords assumed in this thesis. As has been shown in several works, [133–136], for finite block length which is obtainable in the practical communication systems, the assumptions of infinite block length is not entirely accurate especially for applications with short block length. For spectrum sharing schemes, the authors in [127] show that for finite length codewords, in an opportunistic spectrum sharing systems with rate adaptation, the system achievable rate can be severely affected by the length of the codeword. Specifically the work shows that for short codewords (less than 100 channel uses), the secondary system's throughput is significantly decreased. Against this background, a potential future research will be to investigate the performance metrics studied in this thesis for the different systems (the MNO and the LHQWN) in a more complicated sharing arrangement of the eLSA using the finite block length approach. Furthermore, one can look at the optimal power allocation in the several systems so that for a given codeword

dropping probability in the incumbent system or/and maximum interference probability, the throughput of the licensee(s) is maximized. In addition, it will be interesting to investigate these performance metrics in a three-tier dynamic sharing scheme like the United States citizens broadband radio service with spectrum assess system (SAS) [46].

The integration of the unmanned aerial vehicle with the LSA shows very interesting promise in achieving the key performance requirements of the LSA, i.e., protection of the incumbent from harmful interference and actualization of predictable guaranteed QoS for users on the network of the licensee system. In fact, the improvement recorded in the SE and EE is very significant when compared to the traditional terrestrial configuration of the LSA. This is a pointer to the fact that similar emerging technologies potentially holds promise of further enhancements to the efficiency of the LSA. For instance, in the aerial-terrestrial hybrid LSA scheme scenario presented in **section 6.4** it was seen that when the incumbent system is very close to the centre of the eNodeB coverage area, it becomes very difficult to achieve the target surplus traffic of the system and hence the QoS guaranty of some of the users becomes threatened. As a future work, it would be interesting to investigate how smart antenna techniques could address this extreme scenario. For example, a smart antenna could be used by the UAV-BS to adaptively tilt the antenna in the direction to enable it cover enough users of the network to meet the surplus traffic requirement while avoiding its main beam been focused on the incumbent system. It has been noted in [65] that tilting licensee eNodeB antenna downwards in a terrestrial network can ensure a better interference protection for the incumbent system. With the agility of the UAV-BS, it can be assumed that more interference protection for the incumbent system can be engineered with this method while also ensuring better achievable QoS for users on the licensee's network. Similarly, in [102] shows that beam-forming can be used to improve the throughput in a horizontal LSA sharing involving two MNOs. It will be interesting to the integration of such an opportunistic or adaptive beam-forming can as well be engineered in a hybrid aerial-terrestrial LSA system to achieve the two objectives of minimizing interference to the incumbent system to a tolerable level while boosting the achievable throughput of the licensee.

The use of relay to improve the performance of wireless cellular network has been extensively discussed in the literature. In particular, the relay has been used to improve the system throughput, decoding error rate, users' QoS, and fairness as well as better EE-SE trade-off performance [78, 137–140]. Another possible dimension to the hybrid-aerial terrestrial LSA network proposed in **section 4.4** is to use the UAV as a relay. The flexibility in positioning offered by the mobility of the UAV can be leveraged upon in an aerial relay licensee network configuration that integrates the smart antenna techniques mentioned in the previous paragraph (beam-forming and adaptive tilting) for the relay to simultaneously ensure

compliance with the incumbent's interference threshold requirement while also ensuring QoS guarantee of the users on the licensee's network. This has the benefit of ensuring that the limited power policy in the traditional terrestrial LSA system doesn't compromise the target QoS of its network users, while also making use of the UAV technology on a more practical and economically viable as needed basis. Investigating the impact of this configuration on the other key performance metrics of the SE and EE of the LSA will be also be an interesting task.

The considered system in this research work has assumed a time division duplex (TDD) system adopted by the LSA licensee. The results obtained in **sections 6.1** and **6.2** shows that the impact of the air -to- ground interference propagation path as well as the omni-directional nature of the MNO uplink transmitter is significantly higher than the interference caused by the downlink transmitters to an aeronautical telemetry incumbent. In addition to this, is the fact that the ultra dense 5G technology space is expected to feature hierarchical heterogeneous networks in order to support the diverse vertical applications as well as meeting the massive connectivity and throughput requirements. Therefore, it will be worth considering a frequency division duplex (FDD) system that feature an hybrid of the LSA frequency and the traditional cellular frequency for the downlink and uplink licensee transmission respectively. Owing to the very directional nature of the eNodeB antennas and the possibility of reducing the antenna height to a level where the interference to the incumbent victim receiver could be easily managed, the downlink transmission in a FDD system can use the LSA frequency while the omni-directional uplink transmission maintains the traditional cellular frequency. With smart antenna techniques similar idea can be extended to even other types of incumbent systems.

This research work has focused on the evaluation of the performance of the LSA scheme especially that of the licensee's network from the physical layer perspective. However, in the 5G technology space, link layer performance metrics such as the effective capacity are equally important if not more important in network design and configuration considerations. In fact, it has long been established in the literature that the effective capacity provides a means of measuring the effect of the physical layer design consideration on the systems link layer performance [141–144]. From mobile voice over internet protocol, video conferencing, real time online gaming, on-demand video streaming, remote monitoring, device-to-device communication, autonomous self driving cars, online learning, and even national public health safety and emergency services, the 5G networks will be dominated by applications with diverse latency and data rate requirements. In this regard, the effective capacity provides a more appropriate and critical performance measure for these applications. Additionally, considering the statistical variation of the LSA spectrum availability, it becomes pertinent

to understand how the LSA performs especially with applications with very stringent QoS (delay sensitivity) requirements and in some instances deployed for safety and life saving purposes. The outbreak of the COVID - 19 pandemic has further heightened the importance of the reliability of these critical and high latency applications on a global scale, not only for now but also for the future of humanity. Thus it will be worth while to extend the investigation of the LSA as well as the eLSA performance to the link layer in order to be able to understand the limitation and improve on the reliability of the scheme in the 5G technology space and beyond. This might also serve the purpose of providing insight to effective and robust LSA network design and configuration.

Two key features of the LSA spectrum sharing scheme that are essentially important in the design and deployment of the licensee's system are the interference threshold of the incumbent system and variations in the spectrum's availability. These are critical design challenges that may limit the gains provided by the LSA. The power domain non orthogonal multiple access scheme (power domain-NOMA) and radio access network slicing (RAN slicing) are two emerging technologies with the potential of taking centre stage in the 5G and beyond technology space. The power domain-NOMA is based on the principle of transmitting to different users simultaneously on the same channel using differentiated power allocation [145–148]. Applications of the power domain NOMA has been shown to be an enabling technology for the cognitive radio network (one of the predecessor of LSA) [149–151] and the hybrid aerial-terrestrial network [152]. Similarly, network slicing has been proposed to address the diversity in the requirements of the heterogeneous and ultradense 5G system [153]. The authors of [154] shows that RAN slicing can be used not only for customization of network resources to satisfy different communication requirements but also for inter service interference management and significantly improve the bit error rate and SINR performance of the system. It will be an interesting research work to investigate how the differentiated allocated power mechanism of the power domain NOMA can be employed in a network slicing service architecture that involves the licensee using its infrastructure to relay the incumbent transmission in such a way it can simultaneously mitigate harmful interference to the incumbent at the same time providing guaranteed QoS to the users of its network. Similarly, machine learning algorithm and the block chain technology can be integrated to the LSA system to ensure smart resource allocation that takes into account the LSA spectrum availability cycle and historical user's network access behaviour .

References

- [1] Anon, “Ntia.Doc.Gov: The United States Spectrum Allocation Chart (2016),” https://www.ntia.doc.gov/files/ntia/publications/january_2016_spectrum_wall_chart.pdf, January 2016, accessed 5 May 2021.
- [2] “ECC Report 205: Licensed Shared Access (LSA), CEPT Working Group Frequency Management,” February 2014.
- [3] A. Morgado, A. Gomes, V. Frascolla, K. Ntougias, C. Papadias, D. Slock, E. Avdic, N. Marchetti, N. Haziza, H. Anouar, Y. Yang, M. Pesavento, F. Khan, and T. Ratnarajah, “Dynamic LSA for 5G Networks the ADEL Perspective,” in *2015 European Conference on Networks and Communications (EuCNC)*, June 2015, pp. 190–194.
- [4] V. Y. Borodakiy, K. E. Samouylov, I. A. Gudkova, D. Y. Ostrikova, A. A. Ponomarenko-Timofeev, A. M. Turlikov, and S. D. Andreev, “Modeling Unreliable LSA Operation in 3GPP LTE Cellular Networks,” in *2014 6th International Congress on Ultra Modern Telecommunications and Control Systems and Workshops (ICUMT)*, Oct 2014, pp. 390–396.
- [5] J. Holis and P. Pechac, “Elevation Dependent Shadowing Model for Mobile Communications via High Altitude Platforms in Built-Up Areas,” *IEEE Transactions on Antennas and Propagation*, vol. 56, no. 4, pp. 1078–1084, April 2008.
- [6] “Ericsson Mobility Report,” June 2020.
- [7] “Ericsson Mobility Report,” November 2018.
- [8] ITU-R, “IMT Traffic Estimates for the Years 2020 to 2030-Report ITU-R M.2370-0,” International Telecommunication Union, July 2015.
- [9] G. Staple and K. Werbach, “The End of Spectrum Scarcity [Spectrum Allocation and Utilization],” *IEEE Spectrum*, vol. 41, no. 3, pp. 48–52, 2004.
- [10] M. H. Islam, C. L. Koh, S. W. Oh, X. Qing, Y. Y. Lai, C. Wang, Y. Liang, B. E. Toh, F. Chin, G. L. Tan, and W. Toh, “Spectrum Survey in Singapore: Occupancy Measurements and Analyses,” in *2008 3rd International Conference on Cognitive Radio Oriented Wireless Networks and Communications (CrownCom 2008)*, 2008, pp. 1–7.
- [11] M. Lopez-Benitez, A. Umbert, and F. Casadevall, “Evaluation of Spectrum Occupancy in Spain for Cognitive Radio Applications,” in *VTC Spring 2009 - IEEE 69th Vehicular Technology Conference*, 2009, pp. 1–5.

- [12] T. M. Taher, R. B. Bacchus, K. J. Zdunek, and D. A. Roberson, "Long-Term Spectral Occupancy Findings in Chicago," in *2011 IEEE International Symposium on Dynamic Spectrum Access Networks (DySPAN)*, 2011, pp. 100–107.
- [13] "Final RSPG Report on Collective Use of Spectrum and Other Sharing Approaches," November 2011.
- [14] ITU-R, "IMT Vision – Framework and Overall Objectives of the Future Development of IMT for 2020 and Beyond (REC-M.2083-0)," International Telecommunication Union, September 2015.
- [15] GSMA, "Understanding 5G: Perspectives on Future Technological Advancements in Mobile," GSMA Intelligence Technical Report, December 2014.
- [16] B. Lannoo, C. B. Lannoo, S. Lambert, W. V. Heddeghem, M. P. (iminds, O. K. (tudelft, G. Koutitas, H. Niavis, A. S. (certh, M. Till, A. Fischer, H. D. M. (uni Passau, P. A. (ulanc, N. H. Viet, T. P. (uio, J. A. (uam, and R. T. Certh, "D8.1: Overview of ICT Energy Consumption," 2012.
- [17] M. Pickavet, W. Vereecken, S. Demeyer, P. Audenaert, B. Vermeulen, C. Develder, D. Colle, B. Dhoedt, and P. Demeester, "Worldwide Energy Needs for ICT: The Rise of Power-Aware Networking," in *2008 2nd International Symposium on Advanced Networks and Telecommunication Systems*, Dec 2008, pp. 1–3.
- [18] Smart2020, "Enabling the Low Carbon Economy in the Information Age," The Climate Group, London, U.K., Tech. Rep., 2008.
- [19] C. Hepburn and N. Stern, "A New Global Deal on Climate Change," *Oxford Review of Economic Policy*, vol. 24, no. 2, pp. 369–395, Apr 2008.
- [20] K. Lahiri, A. Raghunathan, S. Dey, and D. Panigrahi, "Battery-Driven System Design: A New Frontier in Low Power Design," in *Proceedings of ASP-DAC/VLSI Design 2002. 7th Asia and South Pacific Design Automation Conference and 15th International Conference on VLSI Design*, Jan 2002, pp. 261–267.
- [21] Cisco, "Cisco Visual Networking Index: Forecast and Methodology, 2016 – 2021," "White Paper", Tech. Rep., June, 2017.
- [22] R. Shubair and F. Al-Ogaili, "Millimeter-Wave Mobile Communications for 5G: Challenges and Opportunities," in *2016 IEEE International Symposium on Antennas and Propagation (APSURSI)*, 06 2016.
- [23] J. Karjalainen, M. Nekovee, H. Benn, W. Kim, J. Park, and H. Sungsoo, "Challenges and Opportunities of mm-Wave Communication in 5G Networks," in *2014 9th International Conference on Cognitive Radio Oriented Wireless Networks and Communications (CROWNCOM)*, 2014, pp. 372–376.
- [24] M. Cheffena, "Industrial Wireless Communications Over the Millimeter Wave Spectrum: Opportunities and Challenges," *IEEE Communications Magazine*, vol. 54, no. 9, pp. 66–72, 2016.

- [25] A. V. Lopez, A. Chervyakov, G. Chance, S. Verma, and Y. Tang, "Opportunities and Challenges of mmWave NR," *IEEE Wireless Communications*, vol. 26, no. 2, pp. 4–6, 2019.
- [26] T. S. Rappaport, Y. Xing, O. Kanhere, S. Ju, A. Madanayake, S. Mandal, A. Alkhateeb, and G. C. Trichopoulos, "Wireless Communications and Applications Above 100 GHz: Opportunities and Challenges for 6G and Beyond," *IEEE Access*, vol. 7, pp. 78 729–78 757, 2019.
- [27] V. Frascolla, M. Faerber, L. Dussopt, E. Calvanese-Strinati, R. Sauleau, V. Kotsch, G. Romano, K. Ranta-aho, J. Putkonen, and J. Valiño, "Challenges and opportunities for Millimeter-Wave Mobile Access Standardisation," in *2014 IEEE Globecom Workshops (GC Wkshps)*, Dec 2014, pp. 553–558.
- [28] ETSI, "TR 103 113 - V1.1.1 - Electromagnetic Compatibility and Radio Spectrum Matters (ERM); System Reference Document (SRdoc); Mobile Broadband Services in the 2300 MHz - 2400 MHz Frequency Band Under Licensed Shared Access Regime," European Telecommunications Standards Institute, Tech. Rep., July, 2013.
- [29] M. Matinmikko, M. Palola, H. Saarnisaari, M. Heikkilä, J. Prokkola, T. Kippola, T. Hänninen, M. Jokinen, and S. Yrjölä, "Cognitive Radio Trial Environment: First Live Authorized Shared Access-Based Spectrum-Sharing Demonstration," *IEEE Vehicular Technology Magazine*, vol. 8, no. 3, pp. 30–37, 2013.
- [30] M. Palola, M. Matinmikko, J. Prokkola, M. Mustonen, M. Heikkilä, T. Kippola, S. Yrjölä, V. Hartikainen, L. Tudose, A. Kivinen, J. Paavola, K. Heiska, T. Hänninen, and J. Okkonen, "Description of Finnish Licensed Shared Access (LSA) Field Trial Using TD-LTE in 2.3 GHz Band," in *2014 IEEE International Symposium on Dynamic Spectrum Access Networks (DYSPAN)*, 2014, pp. 374–375.
- [31] M. Palola, M. Matinmikko, J. Prokkola, M. Mustonen, M. Heikkilä, T. Kippola, S. Yrjölä, V. Hartikainen, L. Tudose, A. Kivinen, J. Paavola, and K. Heiska, "Live field trial of licensed shared access (lsa) concept using lte network in 2.3 ghz band," in *2014 IEEE International Symposium on Dynamic Spectrum Access Networks (DYSPAN)*, 2014, pp. 38–47.
- [32] C. W. Kim, J. Ryoo, and M. M. Buddhikot, "Design and Implementation of an End-to-End Architecture for 3.5 GHz Shared Spectrum," in *2015 IEEE International Symposium on Dynamic Spectrum Access Networks (DySPAN)*, 2015, pp. 23–34.
- [33] P. Masek, E. Mokrov, A. Pyattaev, K. Zeman, A. Ponomarenko-Timofeev, A. Samuylov, E. Sopin, J. Hosek, I. A. Gudkova, S. Andreev, V. Novotny, Y. Koucheryavy, and K. Samouylov, "Experimental Evaluation of Dynamic Licensed Shared Access Operation in Live 3GPP LTE System," in *2016 IEEE Global Communications Conference (GLOBECOM)*, Dec 2016, pp. 1–6.
- [34] M. Palola, T. Rautio, M. Matinmikko, J. Prokkola, M. Mustonen, M. Heikkilä, T. Kippola, S. Yrjölä, V. Hartikainen, L. Tudose, A. Kivinen, J. Paavola, J. Okkonen, M. Mäkeläinen, T. Hänninen, and H. Kokkinen, "Licensed Shared Access (LSA) Trial Demonstration using Real LTE Network," in *2014 9th International Conference on*

- Cognitive Radio Oriented Wireless Networks and Communications (CROWNCOM)*, June 2014, pp. 498–502.
- [35] M. Matinmikko, M. Palola, M. Mustonen, T. Rautio, M. Heikkilä, T. Kippola, S. Yrjölä, V. Hartikainen, L. Tudose, A. Kivinen, H. Kokkinen, and M. Mäkeläinen, “Field Trial of Licensed Shared Access (LSA) with Enhanced LTE Resource Optimization and Incumbent Protection,” in *2015 IEEE International Symposium on Dynamic Spectrum Access Networks (DySPAN)*, 2015, pp. 263–264.
- [36] J. Kalliovaara, T. Jokela, R. Ekman, J. Hallio, M. Jakobsson, T. Kippola, and M. Matinmikko, “Interference Measurements for Licensed Shared Access (LSA) Between LTE and Wireless Cameras in 2.3 GHz Band,” in *2015 IEEE International Symposium on Dynamic Spectrum Access Networks (DySPAN)*, 2015, pp. 123–129.
- [37] D. Guiducci, C. Carciofi, V. Petrini, S. Pompei, J. Llorente, V. Ferrer, J. Costa-Requena, E. Spina, G. D. Sipio, D. Massimi, D. Spoto, F. Amerighi, T. Magliocca, H. Kokkinen, P. Chawdhry, L. Ardito, S. Yrjölä, V. Hartikainen, L. Tudose, P. Muller, M. Gianesin, F. Grazioli, and D. Caggiati, “Sharing Under Licensed Shared Access in a Live LTE Network in the 2.3–2.4 GHz Band End-to-End Architecture and Compliance Results,” in *2017 IEEE International Symposium on Dynamic Spectrum Access Networks (DySPAN)*, March 2017, pp. 1–10.
- [38] “ECC Report 172: Broadband Wireless Systems Usage in 2300-2400 MHz,” March 2012.
- [39] A. Ponomarenko-Timofeev, A. Pyattaev, S. Andreev, Y. Koucheryavy, M. Mueck, and I. Karls, “Highly Dynamic Spectrum Management within Licensed Shared Access Regulatory Framework,” *IEEE Communications Magazine*, vol. 54, no. 3, pp. 100–109, March 2016.
- [40] Deloitte, “The Impacts of Licensed Shared Use-of-Spectrum”, Report for GSM Association,” January 2014.
- [41] I. Gudkova, E. Markova, P. Masek, S. Andreev, J. Hosek, N. Yarkina, K. Samouylov, and Y. Koucheryavy, “Modeling the Utilization of a Multi-Tenant Band in 3GPP LTE System With Licensed Shared Access,” in *2016 8th International Congress on Ultra Modern Telecommunications and Control Systems and Workshops (ICUMT)*, Oct 2016, pp. 119–123.
- [42] V. Frascolla, A. J. Morgado, A. Gomes, M. M. Butt, N. Marchetti, K. Voulgaris, and C. B. Papadias, “Dynamic Licensed Shared Access - A New Architecture and Spectrum Allocation Techniques,” in *2016 IEEE 84th Vehicular Technology Conference (VTC-Fall)*, 2016, pp. 1–5.
- [43] “Draft CEPT Report 56 (B.1),” March 2015.
- [44] B. A. Jayawickrama, E. Dutkiewicz, and M. Mueck, “Incumbent User Active Area Detection for Licensed Shared Access,” in *2015 IEEE 82nd Vehicular Technology Conference (VTC2015-Fall)*, Sep. 2015, pp. 1–5.

- [45] E. Mokrov, A. Ponomarenko-Timofeev, I. Gudkova, P. Masek, J. Hosek, S. Andreev, Y. Koucheryavy, and Y. Gaidamaka, "Modeling Transmit Power Reduction for a Typical Cell With Licensed Shared Access Capabilities," *IEEE Transactions on Vehicular Technology*, vol. 67, no. 6, pp. 5505–5509, June 2018.
- [46] ETSI, "TR 103 588 V1.1.1-Reconfigurable Radio Systems (RRS); Feasibility Study on Temporary Spectrum Access for Local High-Quality Wireless Networks." 2018.
- [47] ———, "TS 103 652-1 - V1.1.1 - Reconfigurable Radio Systems (RRS); Evolved Licensed Shared Access (eLSA); Part 1: System Requirements," 2019.
- [48] S. Zhan, S. Chang, C. Chou, and Z. Tsai, "Spectrum Sharing Auction Platform for Short-term Licensed Shared Access," in *2017 Wireless Days*, 2017, pp. 184–187.
- [49] H. Wang, E. Dutkiewicz, G. Fang, and M. D. Mueck, "An Auction Framework Based on Flexible Transmit Powers in the Licensed Shared Access Systems," in *2015 15th International Symposium on Communications and Information Technologies (ISCIT)*, 2015, pp. 269–272.
- [50] ———, "Framework of Joint Auction and Mixed Graph for Licensed Shared Access Systems," in *2015 IEEE International Symposium on Dynamic Spectrum Access Networks (DySPAN)*, 2015, pp. 154–163.
- [51] H. Wang, D. N. Nguyen, E. Dutkiewicz, G. Fang, and M. D. Mueck, "Negotiable Auction Based on Mixed Graph: A Novel Spectrum Sharing Framework," *IEEE Transactions on Cognitive Communications and Networking*, vol. 3, no. 3, pp. 390–403, 2017.
- [52] H. Wang, E. Dutkiewicz, G. Fang, and M. D. Mueck, "Spectrum Sharing Based on Truthful Auction in Licensed Shared Access Systems," in *2015 IEEE 82nd Vehicular Technology Conference (VTC2015-Fall)*, 2015, pp. 1–5.
- [53] M. M. Butt, C. Galiotto, and N. Marchetti, "Fair and Regulated Spectrum Allocation in Licensed Shared Access Networks," in *2016 IEEE 27th Annual International Symposium on Personal, Indoor, and Mobile Radio Communications (PIMRC)*, 2016, pp. 1–6.
- [54] M. J. Osborne and A. Rubinstein, "A course in game theory.pdf," MIT Press Books, 1999.
- [55] Q. Ni and C. C. Zarakovitis, "Nash Bargaining Game Theoretic Scheduling for Joint Channel and Power Allocation in Cognitive Radio Systems," *IEEE Journal on Selected Areas in Communications*, vol. 30, no. 1, pp. 70–81, January 2012.
- [56] Jianwei Huang and Berry, R.A. and Honig, M.L., "Distributed Interference Compensation for Wireless Networks," *IEEE Journal on Selected Areas in Communications*, vol. 24, no. 5, pp. 1074–1084, 2006.
- [57] Zhang, Huaging and Li, Fei and Niyato, Dusit and Song, Lingyang and Jiang, Tao and Han, Zhu, "Zero-Determinant Strategy for Power Control of Small Cell Network," in *2014 IEEE International Conference on Communication Systems*, 2014, pp. 41–45.

- [58] Y. Jin and G. Kesidis, "Distributed Contention Window Control for Selfish Users in IEEE 802.11 Wireless LANs," *IEEE Journal on Selected Areas in Communications*, vol. 25, no. 6, pp. 1113–1123, 2007.
- [59] Y. Jin and G. Kesidis and J. W. Jang, "A Channel Aware MAC Protocol in an ALOHA Network with Selfish Users," *IEEE Journal on Selected Areas in Communications*, vol. 30, no. 1, pp. 128–137, 2012.
- [60] A. Saadat, G. Fang, and W. Ni, "A Two-Tier Evolutionary Game Theoretic Approach to Dynamic Spectrum Sharing Through Licensed Shared Access," in *2015 IEEE International Conference on Computer and Information Technology; Ubiquitous Computing and Communications; Dependable, Autonomic and Secure Computing; Pervasive Intelligence and Computing*, 2015, pp. 6–11.
- [61] A. Al Daoud, G. Kesidis, and J. Liebeherr, "Zero-Determinant Strategies: A Game-Theoretic Approach for Sharing Licensed Spectrum Bands," *IEEE Journal on Selected Areas in Communications*, vol. 32, no. 11, pp. 2297–2308, 2014.
- [62] D. Guiducci, C. Carciofi, V. Petrini, S. Pompei, M. Faccioli, E. Spina, G. De Sipio, D. Massimi, D. Spoto, F. Amerighi, T. Magliocca, P. Chawdhry, J. Chareau, J. Bishop, P. Viaud, T. Pinato, S. Yrjölä, V. Hartikainen, L. Tudose, J. Llorente, V. Ferrer, J. Costa-Requena, H. Kokkinen, L. Ardito, P. Muller, M. Gianesin, F. Grazioli, and D. Caggiati, "Regulatory Pilot on Licensed Shared Access in a Live LTE-TDD Network in IMT Band 40," *IEEE Transactions on Cognitive Communications and Networking*, vol. 3, no. 3, pp. 534–549, 2017.
- [63] I. Gudkova, K. Samouylov, D. Ostriko, E. Mokrov, A. Ponomarenko-Timofeev, S. Andreev, and Y. Koucheryavy, "Service Failure and Interruption Probability Analysis for Licensed Shared Access Regulatory Framework," in *2015 7th International Congress on Ultra Modern Telecommunications and Control Systems and Workshops (ICUMT)*, Oct 2015, pp. 123–131.
- [64] I. Gudkova, A. Korotyshcheva, A. Zeifman, G. Shilova, V. Korolev, S. Shorgin, and R. Razumchik, "Modeling and Analyzing Licensed Shared Access Operation for 5G network as an Inhomogeneous Queue with Catastrophes," in *2016 8th International Congress on Ultra Modern Telecommunications and Control Systems and Workshops (ICUMT)*, Oct 2016, pp. 282–287.
- [65] E. Pérez, K. Friederichs, I. Viering, and J. Diego Naranjo, "Optimization of Authorised/Licensed Shared Access Resources," in *2014 9th International Conference on Cognitive Radio Oriented Wireless Networks and Communications (CROWNCOM)*, June 2014, pp. 241–246.
- [66] T. Wirth, B. Holfeld, D. Wieruch, R. Halfmann, and K. Friederichs, "System Level Performance of Cellular Networks Utilizing ASA/LSA Mechanisms," in *2014 1st International Workshop on Cognitive Cellular Systems (CCS)*, 2014, pp. 1–5.
- [67] S. Yrjölä and E. Heikkinen, "Active Antenna System Enhancement for Supporting Licensed Shared Access (LSA) Concept," in *2014 9th International Conference on Cognitive Radio Oriented Wireless Networks and Communications (CROWNCOM)*, 2014, pp. 291–298.

- [68] E. V. Mokrov and I. A. Gudkova, "Performance Evaluation of Dynamic Licensed Shared Access Operation Through a Model of a Stand-Alone Cell," in *Peoples Friendship University of Russia*, Oct 2016, pp. 35–41.
- [69] E. Markova, I. Gudkova, A. Ometov, I. Dzantiev, S. Andreev, Y. Koucheryavy, and K. Samouylov, "Flexible Spectrum Management in a Smart City Within Licensed Shared Access Framework," *IEEE Access*, vol. 5, pp. 22 252–22 261, 2017.
- [70] K. Laetkangas, H. Saarnisaari, and A. Hulkkonen, "Licensed Shared Access System Development for Public Safety," in *European Wireless 2016; 22th European Wireless Conference*, May 2016, pp. 1–6.
- [71] G. K. Papageorgiou, K. Voulgaris, K. Ntougias, D. K. Ntaikos, M. M. Butt, C. Galiotto, N. Marchetti, V. Frascolla, H. Annouar, A. Gomes, A. J. Morgado, M. Pesavento, T. Ratnarajah, K. Gopala, F. Kaltenberger, D. T. M. Slock, F. A. Khan, and C. B. Papadias, "Advanced Dynamic Spectrum 5G Mobile Networks Employing Licensed Shared Access," *IEEE Communications Magazine*, vol. 58, no. 7, pp. 21–27, 2020.
- [72] C. Galiotto, G. K. Papageorgiou, K. Voulgaris, M. M. Butt, N. Marchetti, and C. B. Papadias, "Unlocking the Deployment of Spectrum Sharing With a Policy Enforcement Framework," *IEEE Access*, vol. 6, pp. 11 793–11 803, 2018.
- [73] K. Ntougias, C. B. Papadias, G. K. Papageorgiou, and G. Hasslinger, "Spectral Coexistence of 5G Networks and Satellite Communication Systems Enabled by Coordinated Caching and QoS-Aware Resource Allocation," in *2019 27th European Signal Processing Conference (EUSIPCO)*, 2019, pp. 1–5.
- [74] Z. Hasan, H. Boostanimehr, and V. K. Bhargava, "Green Cellular Networks: A Survey, Some Research Issues and Challenges," *IEEE Communications Surveys Tutorials*, vol. 13, no. 4, pp. 524–540, April 2011.
- [75] M. G. Khoshkholgh, *et. al.*, "Access Strategies for Spectrum Sharing in Fading Environment: Overlay, Underlay, and Mixed," *IEEE Transactions on Mobile Computing*, vol. 9, no. 12, pp. 1780–1793, Dec 2010.
- [76] G. Fettweis and E. Zimmermann, "ICT ENERGY CONSUMPTION – TRENDS AND CHALLENGES," in *The 11th International Symposium on Wireless Personal Multimedia Communications*, Sep 2008, pp. 1–4.
- [77] Y. Chen, S. Zhang, S. Xu, and G. Y. Li, "Fundamental Trade-offs on Green Wireless Networks," *IEEE Communications Magazine*, vol. 49, no. 6, pp. 30–37, June 2011.
- [78] Z. Song, Q. Ni, K. Navaie, S. Hou, S. Wu, and X. Sun, "On the Spectral-Energy Efficiency and Rate Fairness Tradeoff in Relay-Aided Cooperative OFDMA Systems," *IEEE Transactions on Wireless Communications*, vol. 15, no. 9, pp. 6342–6355, Sep. 2016.
- [79] A. Fotouhi, "Towards Intelligent Flying Base Stations in Future Wireless Network," in *2017 IEEE 18th International Symposium on A World of Wireless, Mobile and Multimedia Networks (WoWMoM)*, June 2017, pp. 1–3.

- [80] A. Al-Hourani, S. Kandeepan, and S. Lardner, "Optimal LAP Altitude for Maximum Coverage," *IEEE Wireless Communications Letters*, vol. 3, no. 6, pp. 569–572, Dec 2014.
- [81] Z. Xue, Q. Wu, Z. Feng, C. Zhong, and G. Ding, "Sum Rate Maximization in UAV-Enabled Mobile Relay Networks," in *2018 10th International Conference on Wireless Communications and Signal Processing (WCSP)*, 2018, pp. 1–6.
- [82] R. I. Bor-Yaliniz, A. El-Keyi, and H. Yanikomeroglu, "Efficient 3-D Placement of an Aerial Base Station in Next Generation Cellular Networks," in *2016 IEEE International Conference on Communications (ICC)*, May 2016, pp. 1–5.
- [83] M. Alzenad, A. El-Keyi, F. Lagum, and H. Yanikomeroglu, "3-D Placement of an Unmanned Aerial Vehicle Base Station (UAV-BS) for Energy-Efficient Maximal Coverage," *IEEE Wireless Communications Letters*, vol. 6, no. 4, pp. 434–437, Aug 2017.
- [84] E. Kalantari, M. Z. Shakir, H. Yanikomeroglu, and A. Yongacoglu, "Backhaul-Aware Robust 3D Drone Placement in 5G+ Wireless Networks," in *2017 IEEE International Conference on Communications Workshops (ICC Workshops)*, May 2017, pp. 109–114.
- [85] M. Alzenad, A. El-Keyi, and H. Yanikomeroglu, "3-D Placement of an Unmanned Aerial Vehicle Base Station for Maximum Coverage of Users With Different QoS Requirements," *IEEE Wireless Communications Letters*, vol. 7, no. 1, pp. 38–41, Feb 2018.
- [86] E. Kalantari, H. Yanikomeroglu, and A. Yongacoglu, "On the Number and 3D Placement of Drone Base Stations in Wireless Cellular Networks," in *2016 IEEE 84th Vehicular Technology Conference (VTC-Fall)*, Sept 2016, pp. 1–6.
- [87] M. Mozaffari, W. Saad, M. Bennis, and M. Debbah, "Drone Small Cells in the Clouds: Design, Deployment and Performance Analysis," in *2015 IEEE Global Communications Conference (GLOBECOM)*, Dec 2015, pp. 1–6.
- [88] C. Lai, C. Chen, and L. Wang, "On-Demand Density-Aware UAV Base Station 3D Placement for Arbitrarily Distributed Users With Guaranteed Data Rates," *IEEE Wireless Communications Letters*, vol. 8, no. 3, pp. 913–916, 2019.
- [89] L. Shen, Z. Zhu, N. Wang, X. Ji, X. Mu, and L. Cai, "Trajectory Optimization for Physical Layer Secure Buffer-Aided UAV Mobile Relaying," in *2019 IEEE 90th Vehicular Technology Conference (VTC2019-Fall)*, 2019, pp. 1–6.
- [90] L. Liu, S. Zhang, and R. Zhang, "Exploiting NOMA for Multi-Beam UAV Communication in Cellular Uplink," in *ICC 2019 - 2019 IEEE International Conference on Communications (ICC)*, 2019, pp. 1–6.
- [91] F. Ono, H. Ochiai, and R. Miura, "A Wireless Relay Network Based on Unmanned Aircraft System With Rate Optimization," *IEEE Transactions on Wireless Communications*, vol. 15, no. 11, pp. 7699–7708, Nov 2016.

- [92] I. Donevski and J. J. Nielsen, "Dynamic Standalone Drone-Mounted Small Cells," in *2020 European Conference on Networks and Communications (EuCNC)*, 2020, pp. 342–347.
- [93] A. Jaziri, R. Nasri, and T. Chahed, "Congestion Mitigation in 5G Networks Using Drone Relays," in *2016 International Wireless Communications and Mobile Computing Conference (IWCMC)*, Sept 2016, pp. 233–238.
- [94] S. A. R. Naqvi, S. A. Hassan, H. Pervaiz, and Q. Ni, "Drone-Aided Communication as a Key Enabler for 5G and Resilient Public Safety Networks," *IEEE Communications Magazine*, vol. 56, no. 1, pp. 36–42, 2018.
- [95] X. Li, D. Guo, H. Yin, and G. Wei, "Drone-Assisted Public Safety Wireless Broadband Network," in *2015 IEEE Wireless Communications and Networking Conference Workshops (WCNCW)*, March 2015, pp. 323–328.
- [96] S. Rohde and C. Wietfeld, "Interference Aware Positioning of Aerial Relays for Cell Overload and Outage Compensation," in *2012 IEEE Vehicular Technology Conference (VTC Fall)*, Sept 2012, pp. 1–5.
- [97] J. Lyu, Y. Zeng, R. Zhang, and T. J. Lim, "Placement Optimization of UAV-Mounted Mobile Base Stations," *IEEE Communications Letters*, vol. 21, no. 3, pp. 604–607, 2017.
- [98] J. Liu, M. Sheng, R. Lyu, and J. Li, "Performance Analysis and Optimization of UAV Integrated Terrestrial Cellular Network," *IEEE Internet of Things Journal*, vol. 6, no. 2, pp. 1841–1855, 2019.
- [99] H. Wang, H. Zhao, W. Wu, J. Xiong, D. Ma, and J. Wei, "Deployment Algorithms of Flying Base Stations: 5G and Beyond With UAVs," *IEEE Internet of Things Journal*, vol. 6, no. 6, pp. 10 009–10 027, 2019.
- [100] M. Mozaffari, W. Saad, M. Bennis, and M. Debbah, "Efficient Deployment of Multiple Unmanned Aerial Vehicles for Optimal Wireless Coverage," *IEEE Communications Letters*, vol. 20, no. 8, pp. 1647–1650, 2016.
- [101] A. A. Khuwaja, G. Zheng, Y. Chen, and W. Feng, "Optimum Deployment of Multiple UAVs for Coverage Area Maximization in the Presence of Co-Channel Interference," *IEEE Access*, vol. 7, pp. 85 203–85 212, 2019.
- [102] N. Taramas, G. C. Alexandropoulos, and C. B. Papadias, "Opportunistic Beamforming for Secondary Users in Licensed Shared Access Networks," in *2014 6th International Symposium on Communications, Control and Signal Processing (ISCCSP)*, May 2014, pp. 526–529.
- [103] M. Hafeez and J. M. H. Elmirghani, "Green Licensed-Shared Access," *IEEE Journal on Selected Areas in Communications*, vol. 33, no. 12, pp. 2579–2595, Dec 2015.
- [104] M. Haenggi and R. K. Ganti, "Interference in Large Wireless Networks," *Foundations and Trends in Networking*, vol. 3, no. 2, pp. 127–248, 2009.

- [105] M. Haenggi, *Stochastic Geometry for Wireless Networks*, 1st ed. New York, NY, USA: Cambridge University Press, 2012.
- [106] E. S. Sousa and J. A. Silvester, "Optimum Transmission Ranges in a Direct-Sequence Spread-Spectrum Multihop Packet Radio Network," *IEEE Journal on Selected Areas in Communications*, vol. 8, no. 5, pp. 762–771, Jun 1990.
- [107] S. R. Saunders and A. Argo-Zavala, "Antennas and Propagation for Wireless Communication Systems, 2nd Edition," New York: Wiley, 2007.
- [108] ITU-R, "Propagation Data and Prediction Methods Required for the Design of Terrestrial Broadband Millimetric Radio Access Systems Operating in a Frequency Range about 20 to 50 GHz," Recommendation P.1410-2, 2005, ITU.
- [109] E. Drocella, J. Richards, R. Sole, F. Najmy, A. Lundy, and P. McKenna, "3.5-GHz-Exclusion Zone Analyses and Methodology, NTIA report 15-517," March 2016.
- [110] C. Bettstetter, G. Resta, and P. Santi, "The Node Distribution of the Random Waypoint Mobility Model for Wireless Ad-Hoc Networks," *IEEE Transactions on Mobile Computing*, vol. 2, no. 3, pp. 257–269, July 2003.
- [111] C. Bettstetter, H. Hartenstein, and X. Pérez-Costa, "Stochastic Properties of the Random Waypoint Mobility Model: Epoch Length, Direction Distribution, and Cell Change Rate," in *Proceedings of the 5th ACM International Workshop on Modeling Analysis and Simulation of Wireless and Mobile Systems*. ACM, 2002, pp. 7–14.
- [112] X. Lin, R. K. Ganti, P. J. Fleming, and J. G. Andrews, "Towards understanding the fundamentals of mobility in cellular networks," *IEEE Transactions on Wireless Communications*, vol. 12, no. 4, pp. 1686–1698, 2013.
- [113] S. Chiu, D. Stoyan, W. Kendall, and J. Mecke, *Stochastic Geometry and Its Applications*, 3rd ed. West Sussex, United Kingdom: John Wiley and Sons, 2013.
- [114] Fp7 project adel. [Online]. Available: <http://www.fp7-adel.eu>
- [115] W. Yu, "Sum-Capacity Computation for the Gaussian Vector Broadcast Channel via Dual Decomposition," *IEEE Transactions on Information Theory*, vol. 52, no. 2, pp. 754–759, Feb 2006.
- [116] A. Zappone and E. Jorswieck, "Energy Efficiency in Wireless Networks via Fractional Programming Theory," *Foundations and Trends® in Communications and Information Theory*, vol. 11, pp. 185–396, 01 2015.
- [117] I. M. Stancu-Minasian, *Fractional Programming: Theory, Methods, and Applications*. Kluwer Academic Publishers, 1997.
- [118] S. Boyd and L. Vandenberghe, *Convex Optimization*. New York, NY, USA: Cambridge University Press, 2004.
- [119] I. Adan and J. Resing, *Queueing Systems*. Eindhoven, Netherlands: Eindhoven University of Technology, March 2015.

- [120] O. Amin, E. Bedeer, M. H. Ahmed, and O. A. Dobre, "Energy Efficiency–Spectral Efficiency Tradeoff: A Multiobjective Optimization Approach," *IEEE Transactions on Vehicular Technology*, vol. 65, no. 4, pp. 1975–1981, April 2016.
- [121] A. Ghasemi and E. S. Sousa, "Interference Aggregation in Spectrum-Sensing Cognitive Wireless Networks," *IEEE Journal of Selected Topics in Signal Processing*, vol. 2, no. 1, pp. 41–56, Feb 2008.
- [122] R. T. Marler and J. S. Arora, "Survey of Multi-objective Optimization Methods for Engineering," *Struct. Multidisciplinary Optim*, vol. 26, no. 6, pp. 369–395, Apr 2004.
- [123] S. Schaible, "Minimization of Ratios," *Journal of Optimization Theory and Applications*, vol. 19, no. 2, pp. 369–395, Jun 1976.
- [124] G. C. Deepak, K. Navaie, and Q. Ni, "Radio Resource Allocation in Collaborative Cognitive Radio Networks Based on Primary Sensing Profile," *IEEE Access*, vol. 6, pp. 50 344–50 357, 2018.
- [125] ECC, "(CEPT Report 58) Report B2 from CEPT to the European Commission in Response to the Mandate on 'Harmonised Technical Conditions for the 2300-2400 MHz ('2.3 GHz') Frequency Band in the EU for the Provision of Wireless Broadband Electronic Communications Services'." July 2015.
- [126] "TS 103 154 - V1.1.1 - Reconfigurable Radio Systems (RRS); System Requirements for Operation of Mobile Broadband Systems in the 2300 MHz - 2400 MHz Band Under Licensed Shared Access (LSA)," 2014.
- [127] B. Makki, T. Svensson, and M. Zorzi, "Finite Block-Length Analysis of Spectrum Sharing Networks Using Rate Adaptation," *IEEE Transactions on Communications*, vol. 63, no. 8, pp. 2823–2835, Aug 2015.
- [128] S. Onidare, K. Navaie, and Q. Ni, "On the Achievable Energy Efficiency in Dynamic Licensed Shared Access," in *2019 IEEE Globecom Workshops (GC Wkshps)*, 2019, pp. 1–6.
- [129] Onidare, Samuel O. and Navaie, Keivan and Ni, Qiang, "Spectral Efficiency of Dynamic Licensed Shared Access," *IEEE Transactions on Vehicular Technology*, vol. 69, no. 12, pp. 15 149–15 161, 2020.
- [130] S. O. Onidare, K. Navaie, and Q. Ni, "On the Spectrum and Energy Efficiency in Dynamic Licensed Shared Access Systems: A Multiobjective Optimization Approach," *IEEE Access*, vol. 7, pp. 164 517–164 532, 2019.
- [131] B. Thomas Jr. and J. Shruti and A. Usha and K. Taru, "Cisco Visual Networking Index (VNI) Complete Forecast Update, 2017–2022," APJC Cisco Knowledge Network (CKN) Presentation, December 2018.
- [132] M. M. Ahamed and S. Faruque, "5G Backhaul: Requirements, Challenges, and Emerging Technologies," in *Broadband Communications Networks*, A. Haidine and A. Aqqal, Eds. Rijeka: IntechOpen, 2018, ch. 4. [Online]. Available: <https://doi.org/10.5772/intechopen.78615>

- [133] D. Baron, M. A. Khojastepour, and R. G. Baraniuk, "How Quickly Can We Approach Channel Capacity?" in *Conference Record of the Thirty-Eighth Asilomar Conference on Signals, Systems and Computers, 2004.*, vol. 1, 2004, pp. 1096–1100.
- [134] J. Shi and R. D. Wesel, "A Study on Universal Codes With Finite Block Lengths," *IEEE Transactions on Information Theory*, vol. 53, no. 9, pp. 3066–3074, 2007.
- [135] P. Mary, J. Gorce, A. Unsal, and H. V. Poor, "Finite Blocklength Information Theory: What Is the Practical Impact on Wireless Communications?" in *2016 IEEE Globecom Workshops (GC Wkshps)*, 2016, pp. 1–6.
- [136] W. Yang, G. Durisi, T. Koch, and Y. Polyanskiy, "Quasi-Static SIMO Fading Channels at Finite Blocklength," in *2013 IEEE International Symposium on Information Theory*, 2013, pp. 1531–1535.
- [137] Y. Hu, M. C. Gursoy, and A. Schmeink, "Efficient Transmission Schemes for Low-Latency Networks: NOMA vs. Relaying," in *2017 IEEE 28th Annual International Symposium on Personal, Indoor, and Mobile Radio Communications (PIMRC)*, 2017, pp. 1–6.
- [138] Y. Hu, Y. Zhu, and A. Schmeink, "Simultaneous Wireless Information and Power Transfer in Relay Networks with Finite Blocklength Codes," in *2017 23rd Asia-Pacific Conference on Communications (APCC)*, 2017, pp. 1–6.
- [139] J. Du, Z. Chen, Y. Jia, L. Liang, and D. Liu, "Maximum Throughput of Two-Hop Half-Duplex Relaying in Ultra-Reliable and Low-Latency Communications," in *ICC 2020 - 2020 IEEE International Conference on Communications (ICC)*, 2020, pp. 1–6.
- [140] W. Ning, Y. Wang, Y. Chen, and M. Liu, "Resource Allocation in Relay-Assisted Mission-Critical Industrial Internet of Things," in *2020 IEEE Wireless Communications and Networking Conference Workshops (WCNCW)*, 2020, pp. 1–6.
- [141] L. Liu and J. Chamberland, "On the Effective Capacities of Multiple-Antenna Gaussian Channels," in *2008 IEEE International Symposium on Information Theory*, 2008, pp. 2583–2587.
- [142] X. Chen, R. Q. Hu, G. Wu, and Q. C. Li, "Tradeoff Between Energy Efficiency and Spectral Efficiency in a Delay Constrained Wireless System," *Wireless Communications and Mobile Computing*, vol. 15, pp. 1945–1956, 2015.
- [143] E. A. Jorswieck, R. Mochaourab, and M. Mittelbach, "Effective Capacity Maximization in Multi-Antenna Channels with Covariance Feedback," *IEEE Transactions on Wireless Communications*, vol. 9, no. 10, pp. 2988–2993, 2010.
- [144] M. Al-Saedy, H. Al-Raweshidy, H. Al-Hmood, and F. Haider, "Coverage and Effective Capacity in Downlink MIMO Multicell Networks With Power Control: Stochastic Geometry Modelling," *IEEE Access*, vol. 6, pp. 9173–9185, 2018.
- [145] Z. Ding, X. Lei, G. K. Karagiannidis, R. Schober, J. Yuan, and V. K. Bhargava, "A Survey on Non-Orthogonal Multiple Access for 5G Networks: Research Challenges and Future Trends," *IEEE Journal on Selected Areas in Communications*, vol. 35, no. 10, pp. 2181–2195, 2017.

- [146] Y. Saito, A. Benjebbour, Y. Kishiyama, and T. Nakamura, "System-Level Performance Evaluation of Downlink Non-Orthogonal Multiple Access (NOMA)," in *2013 IEEE 24th Annual International Symposium on Personal, Indoor, and Mobile Radio Communications (PIMRC)*, 2013, pp. 611–615.
- [147] J. Choi, "Power Allocation for Max-Sum Rate and Max-Min Rate Proportional Fairness in NOMA," *IEEE Communications Letters*, vol. 20, no. 10, pp. 2055–2058, 2016.
- [148] S. Timotheou and I. Krikidis, "Fairness for Non-Orthogonal Multiple Access in 5G Systems," *IEEE Signal Processing Letters*, vol. 22, no. 10, pp. 1647–1651, 2015.
- [149] Z. Ding, P. Fan, and H. V. Poor, "Impact of User Pairing on 5G Nonorthogonal Multiple-Access Downlink Transmissions," *IEEE Transactions on Vehicular Technology*, vol. 65, no. 8, pp. 6010–6023, 2016.
- [150] Y. Zhang, Q. Yang, T. Zheng, H. Wang, Y. Ju, and Y. Meng, "Energy Efficiency Optimization in Cognitive Radio Inspired Non-Orthogonal Multiple Access," in *2016 IEEE 27th Annual International Symposium on Personal, Indoor, and Mobile Radio Communications (PIMRC)*, 2016, pp. 1–6.
- [151] Z. Yang, Z. Ding, P. Fan, and N. Al-Dhahir, "A General Power Allocation Scheme to Guarantee Quality of Service in Downlink and Uplink NOMA Systems," *IEEE Transactions on Wireless Communications*, vol. 15, no. 11, pp. 7244–7257, 2016.
- [152] W. K. New, C. Y. Leow, K. Navaie, and Z. Ding, "Robust Non-Orthogonal Multiple Access for Aerial and Ground Users," *IEEE Transactions on Wireless Communications*, vol. 19, no. 7, pp. 4793–4805, 2020.
- [153] GSMA, "An-Introduction-to-Network-Slicing," Tech. Report, November 2017.
- [154] B. Yang, L. Zhang, O. Onireti, P. Xiao, M. A. Imran, and R. Tafazolli, "Mixed-Numerology Signals Transmission and Interference Cancellation for Radio Access Network Slicing," *IEEE Transactions on Wireless Communications*, vol. 19, no. 8, pp. 5132–5147, 2020.

